# Ridge subduction and crustal growth in the Central Asian Orogenic Belt: Evidence from Late Carboniferous adakites and high-Mg diorites in the western Junggar region, northern Xinjiang (west China)

Gongjian Tang[a, b], Qiang Wang[a*, c], Derek A. Wyman[d], Zheng-Xiang Li[c], Zhen-Hua Zhao[a], Xiao-Hui Jia[a, b], Zi-Qi Jiang[a, b]

[a] Key Laboratory of Isotope Geochronology and Geochemistry, Guangzhou Institute of Geochemistry, Chinese Academy of Sciences, Guangzhou 510640, P. R. China

[b] Graduate School of Chinese Academy of Sciences, Beijing 100049, China

[c] The Institute for Geoscience Research (TIGeR), Department of Applied Geology, Curtin University of Technology, GPO Box U1987, Perth, WA 6845, Australia

[d] School of Geosciences, Division of Geology and Geophysics, The University of Sydney, NSW 2006, Australia

***Corresponding authors**

E-mail address: wqiang@gig.ac.cn (Q. Wang)

**ABSTRACT:** The Central Asian Orogenic Belt (CAOB) is a natural laboratory for the study of accretionary tectonics and crustal growth owing to its massive generation of juvenile crust in the Paleozoic. There is a debate, however, on the mechanism of this growth. In the Baogutu area of the western Junggar region, northern Xinjiang (west China), diorite-granodiorite porphyry plutons and dikes are widely associated with Cu-Au mineralization. In this study, we present new results of zircon U-Pb geochronology, major and trace elements, and Sr-Nd-Pb-Hf isotope analyses for two diorite-granodiorite porphyry plutons and two dikes from this area. LA-ICPMS zircon U-Pb analyses of four plutonic and dike samples yield Late Carboniferous ages of 315 -310 Ma. The Baogutu diorite-granodiorite porphyries exhibit low-Fe and calc-alkaline compositions. They are also geochemically characterized by high Sr (346-841 ppm) contents, low Y (9.18-16.5 ppm) and Yb (0.95-1.60 ppm) contents, and relatively high Sr/Y (31-67) ratios, which are similar to those of typical adakites. In addition, some samples have relatively high MgO (2.35-8.32 wt.%) and $Mg^{\#}$ (48-75) values, and Cr (22.7-291 ppm) and Ni (32.0-132 ppm) contents, which are similar to those of high-Mg andesites. All rock samples exhibit mid-oceanic ridge basalt (MORB)-like Nd-Sr-Pb-Hf isotope features: high $\varepsilon_{Nd}(t)$ (+5.8-+8.3) and $\varepsilon_{Hf}(t)$ (+13.1-+15.7) values, and relatively low $(^{87}Sr/^{86}Sr)_i$ (0.7033 to 0.7054) and $(^{206}Pb/^{204}Pb)_i$ (17.842-18.055). The Baogutu adakitic rocks also contain reversely zoned clinopyroxene phenocrysts, which have low MgO cores and relatively high MgO rims. Geochemical modeling indicates that the Baogutu adakitic rocks could have been derived by mixing ~95% altered oceanic crust-derived melts with ~5% sediment-derived melts. Taking into account the regional geology, I- and A-type granitoids and Cu-Au mineralization, and the presence of Carboniferous ophiolite m[illegible]anges in northern Xinjiang, we suggest that the Baogutu adakitic rocks were most probably generated by partial melting of a slab edge close to a subducting spreading ridge

in the Late Carboniferous. Ridge subduction and the resultant slab window probably caused strong extension in the overlying lithosphere, extensive melting of subducting oceanic crust, mantle and juvenile lower crust, and interaction between slab-derived melts and the mantle. Thus, events associated with ridge subduction are likely to have played an important role in crustal growth in the CAOB in addition to previously recognized accretion of subduction and arc complexes and post-collisional crustal melting.

**Key words:** Ridge subduction; slab window; adakite; crustal growth; Central Asian Orogenic Belt; western Junggar; Xinjiang

## 1. Introduction

A common tectonic feature in accretionary orogens is ridge subduction accompanied by ridge-trench interaction (Windley et al., 2007). Ridge subduction has been documented at a number of places along the modern Pacific Rim (Sisson et al., 2003; McCrory and Wilson, 2009). However, only a few cases have been well-documented in the pre-Cenozoic geologic record, indicating that this process is grossly underrepresented in tectonic syntheses of plate margins in the ancient geologic record (Sisson et al., 2003).

Ridge subduction and ridge-trench interaction may impact strongly on magmatic activity, metamorphism and mineralization near convergent plate margins (Cole and Basu, 1992; Haeussler et al., 1995; Sisson et al., 2003; Chadwick et al., 2009; McCrory and Wilson, 2009). When a ridge intersects with the subduction zone, a “slab window” may form between the subducted parts of the diverging oceanic plates (Dickinson and Snyder, 1979, Thorkelson, 1996). The “Blowtorch effect” (Delong et al., 1979) resulting from the upwelling of asthenospheric mantle through the slab window can produce a wide variety

of magmas. Typical magmatic rocks resulting from the subduction of slab windows include adakites, tholeiite, high-Mg andesites (e.g., Hole et al., 1991; Abratis and Worner, 2001; Rogers et al., 1985; Guivel et al., 1999; Breitsprecher et al., 2003). The upwelling of asthenospheric mantle through the slab window not only provides high heat flow that can induce partial melting of the slab edge, overlying mantle wedge and/or upwelling asthenospheric mantle and crustal rocks (e.g., Yogodzinski et al., 2001; Thorkelson and Breitsprecher, 2005), but also causes an extensional stress field above the slab window, leading to the formation of alkaline magmatic rocks or A-type granites (Mortimer et al., 2006; Hung et al., 2007; Anma et al., 2009).

The Central Asian Orogenic Belt (CAOB) (Fig. 1a) is one of the largest orogens in the world and comprises island arcs, seamounts, accretionary wedges, oceanic plateaus and, possibly, microcontinents accreted during the closure of the Paleo-Asian Ocean (Sengör et al., 1993; Jahn et al., 2000, 2004; Xiao et al., 2008; Windley et al., 2007). There is evidence for possible ridge subduction events resulting from the Paleo-Asian Ocean closure. Windley et al. (2007) suggested that the CAOB contains many key features (e.g., adakites, boninites, near-trench magmatism, Alaskan-type mafic–ultramafic complexes and high-temperature metamorphic belts) that are explicable by ridge-trench interactions and that this new perspective may provide a promising approach for resolving many aspects of the orogenic belt's evolution. Based on data for Paleozoic ophiolites, tectonics and magmatism, several possible cases of ridge subduction have been proposed in the CAOB. Windley et al. (2007) focused mainly on the broad diagnostic features of ridge-trench interaction in the CAOB and suggested that gold deposits in eastern Tianshan may be related to slab window subduction. Based on geochronological data for ophiolites, Jian et al. (2008) suggested that a ca. 430-415 Ma ridge subduction event was recorded in

Inner Mongolia in the southeastern CAOB. Sun et al. (2009) suggested Early Paleozoic ridge subduction in the Altai area, CAOB. Geng et al. (2009) and Yin et al. (2010) proposed that a ridge subduction model could account for the geochemical characteristics of granitoids and coeval mafic rocks from the western Junggar region. Here, we further document such a case in the western Junggar region based on Cu-Au mineralization-related adakites as well as regional geology and the presence of I- and A-type granitoids.

The mechanism of Paleozoic crustal growth in the CAOB has been the subject of dispute (e.g., Sengör et al., 1993; Gao et al., 1998; Jahn et al., 2000, 2004; Zhou et al., 2004; Liu and Fei, 2006). In the western Junggar region of northwestern Xinjiang, there are widespread Late Paleozoic magmatic rocks, typically I or A-type granite batholiths with highly depleted isotopic signatures ($\varepsilon_{Nd}(t)$ of +6.4 to +9.2) (Chen and Arakawa, 2005; Han et al., 2006; Su et al., 2006). They have been attributed to either subduction-related sources in an island arc setting (Zhang et al., 2006; Xiao et al., 2008) or to depleted mantle contributions in a post-collisional extensional setting (Chen and Arakawa, 2005; Han et al., 2006; Su et al., 2006). These models clearly have significantly different implications for both granite petrogenesis and crustal growth.

In this study, we report on late Carboniferous adakitic and high-Mg diorite-granodiorite porphyry plutons and dikes associated with Cu-Au mineralization in the Baogutu area of the western Junggar region (Fig. 1b and c). On the basis of these results and previous regional studies, we suggest that ridge subduction played an important role in the generation of the large late Carboniferous-Early Permian magmatic suite, contemporary Cu-Au mineralization, and crustal growth in the western Junggar region of the CAOB.

## 2. Geological backgroud

The CAOB, also known as the Altaid Tectonic Collage (Sengör et al., 1993; Jahn et al., 2000, 2004; Windley et al., 2007), extends from the Urals in the west, through Kazakhstan, northern China, Mongolia, and southern Siberia to the Okhotsk Sea along the eastern Russian coast (Fig. 1a) (Sengör et al., 1993; Xiao et al., 2004). It is located between the Siberian Craton to the north and the North China and Tarim Cratons to the south (Fig. 1a). The CAOB was mainly formed by the progressive subduction of the Paleo-Asian Ocean and the amalgamation of terranes of diverse origins (Coleman, 1989; Xiao et al., 2004; Windley et al., 2007). The most outstanding feature of the CAOB is the vast expanse of granitoids and volcanic rocks, which are characterized by positive $\varepsilon_{Nd}(t)$ and young $T_{DM}$ model ages (e.g., Jahn et al., 2000; Wu et al., 2000).

The western Junggar region is surrounded by the Altai orogen to the north, the Tianshan orogen to the south, the Kazakhstan plate to the west, and the Junggar basin to the east (Fig. 1a). No metamorphic basement has been documented in this area and the oldest rocks are ophiolitic mafic-ultramafic types of Cambrian-Ordovician age (Fig. 1b). Post-Cambrian (Ordovician-Quaternary) sedimentary rocks, particularly Devonian and Carboniferous volcanic-sedimentary rocks, are abundant in the region (Fig. 1b). The Devonian strata are mainly distributed in the northwest and the Carboniferous strata are mainly in the southeast; both contain extensive volcanic rocks (Fig. 1b). The Carboniferous strata are principally composed of the Tailegula Formation, the Baogutu Formation, and Xibeikulasi Formation, in an upward sequence (Fig. 1c) (Shen and Jin, 1993). Both Jin et al. (1987) and Song et al. (1996) reported Late Carboniferous deep-water sedimentary rocks close to the Baogutu area in the eastern part of the western

Junggar region (Fig.1b), and suggested that a deep-marine basin persisted there until that time. Based on paleogeographic data, Wang (2006) also suggested a late Carboniferous deep-marine environment in that region, in contrast to a contemporary shallow-marine environment to the west and northwest (Fig. 1d-f). During the early Carboniferous, however, a deep marine environment is believed to have existed across the entire region (Fig. 1d-f) (Wang, 2006). These observations suggest that the western Junggar might have been a growing accretionary prism during the Carboniferous, with a northwest (in present coordinates) directed subduction system (Fig. 1d-f).

Many ophiolitic mafic-ultramafic rocks occur in the western Junggar region, and their ages range from the Cambrian to late Carboniferous (Fig. 1b) (Beijing SHRIMP Unit, 2005; Xu et al., 2006a). Recently discovered ophiolites located to the northeast of Keramay city have a SHRIMP zircon U-Pb age of 332 ± 14 Ma and are the youngest known in the area (Xu et al., 2006a; Xiao et al., 2008).

Carboniferous to Early Permian magmatic rocks occur widely in the western Junggar region and are referred to here as the Keramay arc magmatic rocks (Fig. 1b) (see discussion in part 6). Carboniferous to early Permian granitoid intrusions show systematic changes in both compositions and ages from north to south (Fig. 1b).

In the north of the western Junggar region (Hebukesaier region) (Fig. 1b), the intrusions mainly consist of I-type granitoids, which have an age range of 338 Ma to 313 Ma (Han et al., 2006; Zhou et al., 2008). They are characterized by the enrichment of light rare earth elements (LREE) and depletion of high field strength elements (HFSE) (e.g., Nb, Ta and Ti) (Zhou et al., 2008).

In the central part of the magmatic province (i.e., the Keramay-Hatu-Tuoli area), large batholiths and relatively small stocks intrude Paleozoic strata (Fig. 1b). These are predominantly 315-300 Ma A-type intrusions and minor 300-290 Ma I-type granitoids (Fig. 1) (Chen and Jahn, 2004; Chen and Arakawa, 2005; Han et al., 2006; Su et al., 2006). The I-type granitoids are characterized by enrichment of large ion lithophile elements (LILE) and LREE, depletion of HFSE and relatively high $Mg^{\#}$ ($100\times Mg^{2+}/(Fe^{2+}+Mg^{2+})$) (41-63) (Chen and Jahn, 2004; Chen and Arakawa, 2005), i.e., geochemical characteristics similar to typical arc magmatic rocks. The more voluminous A-type granites are characterized by high $SiO_2$ (71-75 wt.%), alkalis and Fe/(Fe+Mg) values, low $Al_2O_3$ and CaO contents, enrichment in LILEs (Rb, Th and K) and HFSEs (Nb, Ta, Zr and Hf), and obvious negative anomalies in Eu, Ba and Sr (Chen and Jahn, 2004; Chen and Arakawa, 2005; Su et al., 2006; Geng et al., 2009), similar to typical A-type granites (Loiselle and Wones, 1979).

In the southern part of the region (Tangbale-Mayle area), there are fewer scattered intrusions, which mainly consist of quartz monzonite, biotite granite and diorite, similar to I-type granitoids (Fig. 1b). They are considered to have formed in the late Early Carboniferous (Xinjiang Bureau of Geology and Mineral Resources (XBGMR), 1993). Thus, granitoids in the central part of the area are slightly younger than those in the northern and southern areas. Almost all these granitoids exhibit high $\varepsilon_{Nd}(t)$ (+5.4 to +9.2) but the central A-type granites have slightly higher $\varepsilon_{Nd}(t)$ (+6.4 to +8.4) (Chen and Jahn, 2004; Chen and Arakawa, 2005; Su et al., 2006).

Volcanic rocks and dikes are also abundant in the central part of the magmatic province

(Fig. 1b). The volcanic rocks consist of andesitic basalt, andesite, felsic tuff and minor quartz or olivine tholeiite and occur as part of the Carboniferous Tailegula Formation (Shen and Jin, 1993). A U-Pb zircon SHRIMP age of 328 ± 2 Ma has been reported for felsic tuffs in the Baobei gold deposit from the western Junggar region (Wang and Zhu, 2007). Several hundred intermediate-basic dikes in this area mainly strike NW (280°–300°), and cut both granitoid intrusions and Carboniferous strata (Li et al., 2004; Yin et al., 2010).

The western Junggar region is one of the most important copper and gold producing areas in northwestern China (Shen and Jin, 1993; Rui et al., 2002; Zhu et al., 2007). Our study area (Baogutu) is located in the centre of the western Junggar region, and is 40 km southeast of the Keramay city (Fig. 1). Porphyry Cu-Au deposits and orogenic (vein) Au deposits in the area (Fig. 1b-c) are hosted in about twenty small plutons and many NW and NE-trending dikes, including the Wudehe No. 2 (outcrop area of ~3 $km^2$) and No. 5 (outcrop area of ~0.84 $km^2$) plutons in the north, and the Kuogeshaye dikes in the south (Fig. 1c). The plutons intrude the Xibeikulasi and Baogutu formations, which consist mainly of tuffaceous breccias and siltstone (Fig. 1c). The Wudehe No. 5 porphyry copper deposit, containing about $1.115 \times 10^6$ ton resource averaging 0.28% Cu, >0.01% Mo, and 0.25 ppm Au (Shen et al., 2009), is the second largest porphyry copper deposit in Xinjiang following the Tuwu-Yandong deposit in eastern Tianshan. The Wudehe Cu (Cu-Mo) mineralization is generally hosted in, or occurs around, small plutons (Fig. 1b). The eastern Kuogeshaye orogenic gold deposit (Rui et al., 2002) is the largest gold deposit in the western Junggar area, with an estimated total reserve of 4.2 tons. The eastern and western Kuogeshaye gold deposits are located in the southern part of the Baogutu area (Fig. 1b), with lensoid or ribbon-like gold-bearing veins generally hosted in

wall rocks (tuff and tuffaceous siltstone) close to the dioritic porphyrite dikes (Fig. 1b).

## 3. Petrography

The Wudehe plutons mainly consist of quartz diorite and granodiorite or corresponding porphyries whereas the Kuogeshaye dikes are mainly dioritic porphyrite. The intrusive rocks in the Wudehe No. 2 pluton exhibit fine-medium and medium-coarse-grained inequigranular or porphyry texture and mainly contain plagioclase (30-40 vol. %), hornblende (15-20 vol. %), biotite (5-15 vol. %) and quartz (<5 vol. %). Accessory minerals include pyroxene, magnetite, titanite, zircon and apatite. Plagioclase, up to 3mm in size, is the most abundant phenocryst phase in all of the Wudehe No.2 intrusive rocks. They are generally euhedral and lath-shaped, and some of them show polysynthetic twinning. Hornblende occurs as euhedral phenocrysts with 300-600 μm in size, but some crystals are altered. Biotite phenocrysts, 100-500 μm in size, are transparent brown and subhedral. The intrusive rocks contain minor quartz, which has a round shape caused by resorption. Pyroxene is rare in the intrusive rocks. Fe-Ti oxides appear as microphenocrysts and microlites in the matrix, or as inclusions in other phases (e.g., hornblende).

The porphyries in the Wudehe No.5 pluton contain phenocrysts up to 2 mm. They contain plagioclase (30-45 vol. %), hornblende (15-20 vol. %), biotite (10-15 vol. %), pyroxene (3-6 vol. %), quartz (<5 vol. %), and minor titanite, rutile, apatite, magnetite, and zircon. Plagioclase phenocrysts are generally euhedral with polysynthetic twinning. Horblende commonly occurs as transparent euhedral phenocrysts. Brown biotite occurs as euhedral phenocryts. Some biotite granules are altered to chlorites and epidote. Pyroxene phenocrysts are sometimes altered to hornblende along grain boundaries.

The Kuogeshaye dioritic porphyrites consist of plagioclase (15-30 vol. %), hornblende (10-20 vol. %), biotite (5-15 vol. %), pyroxene (5-15 vol. %), and accessory minerals similar to those in the Wudehe intrusive rocks. Pyroxene phenocrysts in the Kuogeshaye dioritic porphyries are abundant relative to those of the Wudehe intrusive rocks. They occur as transparent and euhedral phenocrysts that have diameters of 50-300 μm.

## 4. Analytical methods

Zircons were separated using conventional heavy liquid and magnetic separation techniques. Cathodoluminescence (CL) images were obtained for zircons prior to analysis, using a JEOL JXA-8100 Superprobe at the Guangzhou Institute of Geochemistry, Chinese Academy of Sciences (GIGCAS), in order to characterize internal structures and choose potential target sites for U-Pb dating. LA-ICP-MS zircon U–Pb analyses were conducted on an Agilent 7500 ICP-MS equipped with a 193-nm laser, housed at the National Key Laboratory of Geological Processes and Mineral Resources, Faculty of Earth Sciences, China University of Geosciences (Wuhan). Zircon 91500 was used as the standard (Wiedenbeck et al., 1995) and the standard silicate glass NIST 610 was used to optimize the machine, with a beam diameter of 30μm. Raw count rates for $^{29}Si$, $^{204}Pb$, $^{206}Pb$, $^{207}Pb$, $^{208}Pb$, $^{232}Th$ and $^{238}U$ were collected and U, Th and Pb concentrations were calibrated using $^{29}Si$ as the internal calibrant and NIST 610 as the reference material. $^{207}Pb/^{206}Pb$ and $^{206}Pb/^{238}U$ ratios were calculated using the GLITTER program (Jackson et al., 2004). Measured $^{207}Pb/^{206}Pb$, $^{206}Pb/^{238}U$ and $^{208}Pb/^{232}Th$ ratios in zircon 91500 were averaged over the course of the analytical session and used to calculate correction factors. These correction factors were then applied to each sample to correct for both instrumental mass bias and depth-dependent elemental and isotopic fractionation. Common Pb was corrected by ComPbCorr#3 151 (Andersen, 2002) for those with common $^{206}Pb$ > 1%.

Further detailed descriptions of the instrumentation and analytical procedure for the LA-ICP-MS zircon U-Pb technique can be found in Gao et al. et al. (2002) and Liu et al. (2008, 2009). Uncertainties in the ages listed in Appendix 1 are cited as 1σ, and the weighted mean ages are quoted at the 95% confidence level. The age calculations and concordia plots were made using Isoplot (ver 3.0) (Ludwig, 2003). LA-ICP-MS U–Pb zircon data are presented in Appendix 1.

Major element analysis and back-scattered-electron imaging for clinopyroxene and plagioclase were carried out at Guangzhou Institute of Geochemistry, Chinese Academy of Sciences (GIG-CAS) using a JXA-8100 electron microprobe. An accelerating voltage of 15 kV, a specimen current of $3.0 \times 10^{-8}$ A, and a beam size of 1-2 μm were employed. The analytical errors are generally less than 2%. The analytical procedures were described in detail in Huang et al. (2007). The results are listed in Appendix 2.

Rock samples were examined by optical microscopy and unaltered or least-altered samples were selected for geochemical analysis. Major element oxides were determined using the standard X-ray fluorescence (XRF) method (Li et al., 2006). Trace elements were analyzed by inductively coupled plasma mass spectrometry (ICP-MS), using a Perkin-Elmer Sciex ELAN 6000 instrument at GIGCAS. Analytical procedures are the same as those described by Li et al. (2006). Analytical precision for most elements is better than 3%. The results are listed in Appendix 3.

Sr and Nd isotopic analyses were performed on a Micromass Isoprobe multi-collector ICPMS at the GIGCAS, using analytical procedures described by Li et al. (2006). Sr and REE were separated using cation columns, and Nd fractions were further separated by

HDEHP-coated Kef columns. Measured $^{87}Sr/^{86}Sr$ and $^{143}Nd/^{144}Nd$ ratios were normalized to $^{86}Sr/^{88}Sr$= 0.1194 and $^{146}Nd/^{144}Nd$=0.7219, respectively. The reported $^{87}Sr/^{86}Sr$ and $^{143}Nd/^{144}Nd$ ratios were respectively adjusted to the NBS SRM 987 standard $^{87}Sr/^{86}Sr$=0.71025 and the Shin Etsu JNdi-1 standard $^{143}Nd/^{144}Nd$=0.512115.

For Pb isotopic determination, about 100 mg powder was weighed into the Teflon beaker, spiked and dissolved in concentrated HF at 180 ℃ for 7 h. Lead was separated and purified by conventional cation-exchange technique (AG1×8, 200–400 resin) with diluted HBr as an eluant. Total procedural blanks were less than 50pg Pb. Isotopic ratios were measured using a VG-354 mass-spectrometer at the GIGCAS following procedures described by Zhu et al. (2001). Repeated analyses of SRM 981 yielded average values of $^{206}Pb/^{204}Pb = 16.9 \pm 4(2\sigma)$, $^{207}Pb/^{204}Pb = 15.498 \pm 4(2\sigma)$ and $^{208}Pb/^{204}Pb = 36.728 \pm 9(2\sigma)$.

Hf isotopic analyses were conducted using a multicollector Thermo Electron Neptune MC-ICP-MS system in the Institute of Geology and Geophysics, Chinese Academy of Sciences (Beijing). The analytical methods are similar to those of Li et al. (2006). $^{176}Hf/^{177}Hf$ measurements were normalized to $^{179}Hf/^{177}Hf$=0.7325. During the period of data acquisition, standard BCR-2 was also processed for Hf isotopes, which gave a ratio of 0.282881±8 (2σm) for $^{176}Hf/^{177}Hf$, in agreement with the recommended value (Bizzarro et al., 2003). The analyzed results, with the calculated initial isotopic values and model ages, are listed in Appendix 4.

## 5. Results

### 5.1 Zircon geochronology

To determine the emplacement ages of the ore-related porphyries, 4 representative

samples were chosen for LA-ICPMS zircon U-Pb dating, one each from the Wudehe No. 2 and No. 5 plutons, and the eastern and western Kuogeshaye dikes. Zircons have a size range of 30–150 μm with a length/width ratio of 1:1–3:1. Cathodoluminescence images of zircon grains used for LA-ICP-MS analysis show micro-scale oscillatory zoning (Fig. 2). These zircon grains also exhibit high Th/U ratios (0.31–1.46), suggesting a magmatic origin (Belousova et al., 2002). Tera-Wasserburg diagrams and representative CL images of analyzed zircon are shown in Fig. 2, and the U-Pb age data are given in Appendix 1.

Twenty-one analyses of zircons from the dominant rock type, quartz dioritic porphyry, were obtained for sample 06XJ145 from the Wudehe No. 2 pluton (84°27'10"N, 45°29'57"E) give a weighted mean $^{206}Pb/^{238}U$ age of 315 ± 4 Ma (2σ) (Mean square weighted deviation (MSWD) = 0.76) (Appendix 1; Fig. 2a). The remaining five analyzes give $^{206}Pb/^{238}U$ ages ranging from 361 Ma to 375 Ma, with a weighted mean $^{206}Pb/^{238}U$ age of 367 ± 9 Ma (2σ; MSWD = 1.08) (Fig. 2a), interpreted as the age of inherited zircons.

The twenty-two analyses of zircons from sample 06XJ147, a quartz dioritic porphyry typical of the Wudehe No. 5 pluton (Fig. 1c, 84°32'28"N, 45°28'27"E), result in a single age population with a weighted mean $^{206}Pb/^{238}U$ age of 311 ± 4 Ma (2σ; MSWD = 0.38) (Fig. 2b). This age is interpreted to be the best estimate of the crystallization age of the Wudehe No. 5 porphyritic intrusion.

Seventeen of the twenty zircons analyses from the dioritic porphyry dike sample (06XJ-153) in the east Kuogeshaye area (Fig. 1c, 84°26'25"N, 45°23'54"E) give a weighted mean $^{206}Pb/^{238}U$ age of 314 ± 4 Ma (2σ; MSWD = 1.4) (Fig. 2c). This age is

interpreted to be the best estimate of the crystallization age of the east Kuogeshaye dike. Analysis number 4 gives the oldest $^{206}Pb/^{238}U$ age of ~761 Ma (Appendix 1). Moreover, two other analyses give $^{206}Pb/^{238}U$ ages of 344 Ma and 364 Ma, respectively. The old (~761-344 Ma) zircons were likely inherited or entrained from the wall rocks during dike emplacement. Minor 761 Ma zircons were most probably derived from shallow-level sedimentary wall rocks because no Archean-Proterozoic metamorphic rocks have been found in the western Jungger and southern Altay areas (Hu et al., 2000; Sun et al., 2008; 2009).

All 30 analyses zircons from for the west Kuogeshaye dioritic porphyry (06XJ-156, 84°26'14"N, 45°23'24"E) share similar $^{206}Pb/^{238}U$ ratios and give a weighted mean $^{206}Pb/^{238}U$ age of 310 ± 3 Ma (2σ; (MSWD = 0.46) (Appendix 1; Fig. 2d). This age is regarded as the age of crystallization.

**5.2 Mineral compositions**

Clinopyroxenes from the Baogutu porphyries exhibit variable $SiO_2$ (49.4 – 53.3 wt.%), $Al_2O_3$ (0.85-3.42 wt%) and MgO (13.9 -15.5 wt.%) contents and $Mg^{\#}$ (69 – 85). Most clinopyroxene crystals are augite and diopside (Fig. 3). A prominent feature of the porphyries is the presence of simple reversely zoned clinopyroxene phenocrysts, which have low MgO and $Mg^{\#}$ cores and relatively high MgO and $Mg^{\#}$ rims (Fig. 4; Appendix 2). The cores also have high FeO and $Na_2O$ contents compared to the rims (Fig. 4e and f). No multiply zoned clinopyroxene has been observed in the Baogutu samples. Plagioclase phenocrysts occur as euhedral weakly zoned crystals, with An (anorthite) contents of 46-60 % in the core and An contents of 33-52 % in the rim. Plagioclases in the matrix show a large variation in An contents (3-46 %) (Appendix 5). Large plagioclase crystals

may occasionally partly enclose or contain some clinopyroxene grains (Appendix 5), indicating that the crystallization of clinopyroxene occurred prior to that of plagioclase.

### 5.3 Major and trace elements

All of the studied porphyries share similar major element contents. The samples all plot within the calc-alkaline and low-Fe fields on a $SiO_2$ vs $FeO_{total}$/MgO diagram (Fig. 5a), and conform to a medium-K calc-alkaline trend on a $SiO_2$ - $K_2O$ diagram (Fig. 5b). Most Baogutu porphyry samples plot in the field of gabbroic diorites, diorites and granodiorites (Fig. 5c) (Middlemost, 1994). Porphyries from the Wudehe plutons show a large range of $SiO_2$ contents from 50 to 70 wt.% and MgO contents from 0.47 wt.% to 8.70 wt.%, although they are dominantly dioritic (or andesitic) ($SiO_2$ 53.59–61.49 wt.%; MgO 3.39 wt%–7.79 wt.%) (see Appendix 3; Fig. 5c). The Kuogeshaye dikes show smaller ranges of $SiO_2$ (57.08 wt.%–67.88 wt.%) and MgO (1.48 wt%–4.14 w.t%) contents (see Appendix 3; Fig. 5c). The Wudehe plutons and the Kuogeshaye dikes have total alkali ($Na_2O+K_2O$) contents ranging from 4.17 to 8.52 wt.% and $Na_2O/K_2O$ ratios from 1.80 to 9.30 (see Appendix 3), indicating their sodium-rich compositions.

The Baogutu samples exhibit geochemical characteristics of typical adakites (Kay, 1978; Defant and Drummond, 1990; Martin et al., 2005). They are characterized by fractionated rare earth element (REE) patterns with La/Yb ratios (3.0 -17) higher than those of normal arc magmas (Fig. 6a), and negligible Eu and strongly positive Sr anomalies (Fig. 6b). They also show Nb, Ta and Ti depletions, however, which are similar to the Keramay I-type granitoids (Fig. 6b). They have high $Al_2O_3$ (14.98-18.32 wt.%) and Sr (346–841 ppm) contents (see Appendix 3). Except for sample 06XJ-143, all samples have low Y and Yb contents (9.18–16.5 ppm and 0.95–1.60 ppm, respectively), and high Sr/Y ratios

ranging from 31 to 67, and plot in the field of typical “adakites” (Fig. 5d).

In addition, some gabbroic diorite and diorite samples with $SiO_2$ contents less than 64 wt.% are characterized by elevated MgO (2.35–8.32 wt.%) and $Mg^{\#}$ (48–75) values (Fig. 5e-f), and higher Cr (22.7–291 ppm) and Ni (32.0–132 ppm) contents (Appendix 3). On $SiO_2$ versus MgO and $Mg^{\#}$ diagrams (Fig. 5e and f), they partially overlap with high-Mg andesites from the Setouchi Volcanic Belt, Japan (Shimoda et al., 1998; Tatsumi et al., 2006; Tatsumi, 2006, and reference therein). The Setouchi high-Mg andesites as a whole, however, are more magnesian and have significantly higher $Mg^{\#}$ values than the Baogutu intrusive rocks.

**5.4 Nd-Sr-Pb-Hf isotope compositions**

The Baogutu samples have isotopic features broadly similar to those of MORB. Both their initial $^{87}Sr/^{86}Sr$ isotopic ratios (0.7033 to 0.7054) and $\varepsilon_{Nd}(t)$ values (+5.8 – +8.3, average + 6.7) are comparable to those of the East Pacific Rise (EPR) basalts (Fig. 7a; Appendix 4). The Baogutu samples have slightly lower $\varepsilon_{Nd}(t)$ values than the Early Carboniferous (345 Ma) volcanic rocks in the Junggar Basin and late Carboniferous-Early Permian (315 – 290 Ma) granitoids in the western Junggar region (Fig. 7a). The Baogutu samples have high $\varepsilon_{Hf}(t)$ values (+13.5 to +15.7) and positive $\Delta\varepsilon_{Hf}(t)$ values (+0.9 to+4.3) [where $\Delta\varepsilon_{Hf}(t) = \varepsilon_{Hf}(t) - (1.59\varepsilon_{Nd}(t) + 1.28)$] and plot close to or above the mantle array [$\varepsilon_{Hf}(t)=1.59\varepsilon_{Nd}(t) + 1.28$] of Chauvel et al. (2008) in the $\varepsilon_{Hf}(t)$ versus $\varepsilon_{Nd}(t)$ diagram (Appendix 4; Fig. 7b). In addition, they have variable Pb isotopic compositions ($^{206}Pb/^{204}Pb_i$ = 17.842–18.055; $^{207}Pb/^{204}Pb_i$ = 15.411–15.466; $^{208}Pb/^{204}Pb_i$ = 37.316–37.313) (Appendix 4).

## 6. Discussion

### 6.1 Petrogenesis

Adakites were originally considered to form by melting of subducted young and hot oceanic crust (Mechanism A; Defant and Drummond, 1990). Later studies suggested that adakitic magmas could be produced by alternative mechanisms: (a) partial melting of thickened basaltic lower crust (Mechanism B; Atherton and Petford, 1993; Rudnick, 1995; Petford and Atherton, 1996; Chung et al., 2003; Condie, 2005; Wang et al., 2005, 2007a); (b) partial melting of delaminated lower crust (Mechanism C; Kay and Kay, 1993; Rudnick, 1995; Xu et al., 2002b; Gao et al., 2004; Wang et al., 2006a; Huang et al., 2008); (c) partial melting of subducting continental crust (Mechanism D; Wang et al., 2008); (d) assimilation–low-pressure fractional crystallization from parental basaltic magmas (Mechanism E; Castillo et al., 1999; Li et al., 2009); (e) high-pressure crystallization (involving garnet) of typical subduction-related magmas derived from melting of the mantle wedge (Mechanism F; Macpherson et al., 2006); (f) magma mixing, and combined assimilation–fractional crystallization of felsic and basaltic magmas (Mechanism G; Streck et al., 2007). We consider these alternative processes below with specific reference to the Baogutu adakitic porphyries.

#### 6.1.1 Mechanisms B-G

The geochemical characteristics of the Baogutu adakitic porphyries are inconsistent with partial melting of thickened or delaminated continental lower crust (Mechanisms B and G). Commonly, adakitic rocks derived by melting of thickened lower crust are characterized by relatively low MgO or $Mg^{\#}$ values (Fig. 5e and f), which are similar to those of experimental melts from metabasalts and eclogites (Sen and Dunn, 1994; Rapp and Watson, 1995; Rapp et al., 1999). In contrast, the Baogutu adakitic rocks possess

452 distinctly higher MgO contents and $Mg^{\#}$ values than those of experimental melts from
453 metabasalts and eclogites (Fig. 5e and f) (e.g., Rapp et al., 1999).
454
455 Recently, Wang et al. (2008) proposed that adakitic rocks in some collisional orogenic
456 belts (e.g., Tibet) could have been formed by partial melting of subducted continental
457 crust (Mechanism D). Adakitic rocks formed from subducted continental crust also
458 commonly have higher $K_2O$ contents (> 3 wt.%) than those of the Baogutu adakitic rocks
459 (<3 wt.%) (Fig. 5b). Moreover, adakitic rocks formed in this way have low $\varepsilon_{Nd}(t)$ values
460 (generally below -3) (Wang et al., 2008), whereas the Baogutu adakitc rocks have $\varepsilon_{Nd}(t)$
461 values of between +5.8 and +8.3. In addition, in the case of the Baogutu adakitic rocks,
462 sedimentary data suggest that an oceanic setting persisted into the late Carboniferous in
463 the western Junggar region (Jin et al., 1987; Song et al., 1996; Wang, 2006), indicating
464 that no continental collision took place at that time.
465
466 The Baogutu adakitic rocks are also difficult to explain by low-pressure
467 assimilation-fractional crystallization (AFC) from parental basaltic magmas (Mechanism
468 E). If AFC processes could account for the petrogenesis of the Baogutu adakitic rocks,
469 then the most probable candidate for a parental magma would be that of the 345 Ma
470 Kexia basalts with high $\varepsilon_{Nd}(t)$ (+6.8 – +9.6) in the western Junggar Basin (Zheng et al.,
471 2007). If olivine and pyroxene fractionated from the Kexia basalts, then the derived
472 magma would show a clear decrease in $Mg^{\#}$ values as well as MgO contents, but this does
473 not occur (Fig. 5e-f). In addition, fractionation of olivine and pyroxene is not consistent
474 with the depletion of HREE (e.g., Yb). These minerals are unable to incorporate HREE
475 elements, which generally leads to concave-upward HREE in the chondrite-normalized
476 REE concentration patterns (Castillo et al., 1999). Low pressure hornblende fractionation

may drive magmas toward adakitic Sr/Y ratios (Castillo et al., 1999) but even the most Mg-rich samples in the Baogutu suite display this feature (e.g., MgO = 8.7 – 7.4 ; $SiO_2$ = 51.7 – 54.0; Sr/Y = 23 - 39). The Sr/Y and La/Yb ratios can also not be associated with a crystal fractionation assemblage involving plagioclase, given that Eu anomalies are absent and Sr/Y remains high across the entire range of $SiO_2$ contents (Figs. 5d and 8b, d). Where differentiation of high-Mg adaktic rocks has been observed elsewhere, Sr/Y and La/Yb have been reported to increase with higher MgO content (Danyushevsky et al., 2008), but these trends are not present for the Baogutu rocks (Fig. 8b). Moreover, most of the Baogutu samples display lower $\varepsilon_{Nd}(t)$ than the Miaoergou and Keramy granite and Kexi basalt samples, which is inconsistent with a crust assimilation model (Fig. 8e). The relatively high MgO rims of reversely zoned clinopyroxene phenocrysts (Fig. 4) also argue against crustal contamination.

The Baogutu adakitic rocks are also unlikely to be the result of high-pressure crystallization (Mechanism F). The high Sr/Y and Dy/Yb ratios can only be achieved by extensive fractionation of amphibole (30–85%) and garnet (15–20%) from the parental basalt (Fig. 8a). However, this conflicts with experimental and natural evidence (Müntener et al., 2001), which suggests that amphibole and garnet only occur at higher degrees of crystallization, and high-pressure fractionation of hydrous basalts would essentially form pyroxene-rich lithologies. In addition, an important feature of high-pressure crystallization is that some key ratios, such as Sr/Y and Dy/Yb, would increase with increasing $SiO_2$ contents (Macpherson et al., 2006), because garnet is involved in crystallization. However, the data for the Baogutu adakitic rock do not show such trends (Fig. 8b-c).

It is also unlikely that magma mixing of felsic and basaltic magmas (Mechanism G) can account for the Baogutu adakitic rocks. Candidates for mantle-derived basaltic and crust-derived felsic end-members in the area are most plausibly represented by the ~ 345 Ma Kexia basalts (Zheng et al., 2007) and the ~ 290 Ma Miaoergou granites, which have high $SiO_2$ (71.39–78.81 wt.%) and low MgO contents (0.01–0.85 ppm) (Han et al., 2006; Su et al., 2006). The Baogutu adakitic rocks have an average $\varepsilon_{Nd}(t)$ value of +6.7, which is slightly lower than those of the Kexia basalts (average value = +7.9) and the Miaoergou granites (average value = +7.2) (Fig. 8e), suggesting that the adakitic rocks are not products of mixing between the felsic and basaltic end members. In addition, adakitic rocks formed by magma mixing generally have relatively uniform compositions with $SiO_2$ contents that span a narrow range (Streck et al., 2007). In contrast, the Baogutu adakitic rocks display a wide range of $SiO_2$ contents from 52.46 to 70.65 wt.% (Appendix 3). Magma mixing between felsic and basaltic magmas is also inconsistent with the petrographic evidence. Such a process should commonly be accompanied by multiply zoned phenocrysts (Troll and Schmincke, 2002), however, the clinopyroxenes from the Baogutu samples only display simple reverse zoning (Fig. 4). The normally zoned plagioclase (Appendix 5) also contrasts with the complex zoning caused by magma mixing (Troll and Schmincke, 2002). Although mafic microgranular enclaves (MMEs) were found in the Keramay plutons (Chen and Arakawa, 2005), no MMEs were discovered in the Baogutu adakitic rocks, implying that magma mixing between mantle- and crust-derived magmas is unlikely to have played an important role in the genesis of the Baogutu samples.

### 6.1.2 Partial melting of subducted oceanic crust (Mechanism A)

We suggest that the Baogutu adakitic rocks were generated by partial melting of

subducted oceanic crust based on both geological and geochemical evidence, as follows:

(1) The Baogutu adakitic rocks are geochemically similar to slab-derived adakites. They are medium-K calc-alkaline and have relatively low $K_2O$ contents (Fig. 5b), similar to slab-derived adakites in Pacific Cenozoic arcs (Stern and Kilian, 1996) and the North Tianshan ranges (Wang et al., 2006b, 2007b) formed by partial melting of young and hot subducted oceanic crust. They also have high MgO, $Mg^{\#}$, Cr and Ni values, similar to metabasaltic and eclogite melts hybridized by assimilation of 10-20% peridotite (Fig. 5e-f). Moreover, on the discrimination diagrams for low-$SiO_2$-adakites (LSA) and high-$SiO_2$-adakites (HSA) of Martin et al. (2005) (Fig. 9), the Baogutu adakitic rock samples mainly plot in the field of the HSA derived from the interaction between slab-derived melts and mantle peridotites. Therefore, the Baogutu adakitic rocks likely resulted from interactions between mantle peridotite and slab melts during their ascent (e.g., Rapp et al., 1999; Martin et al., 2005).

(2) There is growing evidence for the existence and subduction of a Carboniferous ocean in the Junggar area. Huang et al. (1990) proposed that a “Carboniferous Asian Ocean” or “North Tianshan Ocean” existed in the south Junggar region in the Carboniferous. Xiao et al. (1992) also suggested that a Carboniferous ocean existed here, which they named the “North Tianshan Ocean”. Recently, several Carboniferous ophiolites have been confirmed in the area, such as the Keramay ophiolites in which gabbro samples yield SHRIMP zircon ages of 332 ± 14 Ma (Xu et al., 2006a). The Darbut ophiolite formed at 346–347 Ma as dated by the SHRIMP zircon U-Pb method (Beijing SHRIMP Unit 2005 annual report). The Bayingou ophiolites, from which a gabbro sample yielded a zircon U-Pb age of 344.0 ± 3.4 Ma (Xu et al., 2006b), developed in response to the opening of the

552 Carboniferous Ocean (Huang et al., 1990). Wang (2006) also argued that there was a
553 Carboniferous shallow to deep ocean setting in the western Junggar region, based on a
554 sedimentary and paleogeographic analysis. In addition, recently indentified Carboniferous
555 adakite, high-Mg andesite and Nb-enriched basalt suites in northern Tianshan (Wang et al.,
556 2006b; 2007b) suggest subduction of Carboniferous oceanic crust along the southern
557 margin of the Junggar Basin.
558
559 (3) The occurrence of the Early Carboniferous Darbut, Keramay and Bayingou ophiolites
560 (Fig. 1b) suggests the presence of young oceanic crust, the subduction of which could
561 produce the 315-310 Ma Baogutu adakitic rocks. The Nd-Sr isotopic compositions of the
562 Baogutu adakitic rocks are similar to those of the basaltic rocks from the Bayingou
563 ophiolites (Xu et al., 2006c), and also overlap those of the slab-derived adakites resulting
564 from subduction associated with the "Carboniferous North Tianshan ocean" in the North
565 Tianshan ranges (Wang et al., 2006b, 2007b). In addition, the Baogutu adakitic rocks
566 display a limited $\varepsilon_{Nd}(t)$-$\varepsilon_{Hf}(t)$ field overlapping with those of typical MORB (Fig. 7b).
567
568 (4) Reverse zoning in clinopyroxene phenocrysts in the Baogutu adakitic rocks (Fig. 4)
569 reflects a significant MgO or $Mg^{\#}$ increase and $Na_2O$ content decrease in the melt, which
570 is consistent with reaction between the melt and mantle peridotite (e.g., Yogodzinski and
571 Kelemen, 1998; Gao et al., 2004, 2008; Xiong et al., 2006). Therefore, the Baogutu
572 adakitic rocks are most probably derived by the interaction between ascending subducted
573 oceanic crust-derived adakitic melts and mantle wedge peridotites, based on the
574 petrographic evidence.
575
576 (5) It is well documented that subduction zone magmatism is controlled by contributions

from the subducted mafic oceanic crust, the overlying subducted sediments, and the mantle wedge (e.g., Kay, 1978; Defant and Drummond, 1990; Plank and Langmuir, 1993; Hawkesworth et al., 1997; Chauvel et al., 2008). Adakites are generally produced by partial melting of subducted mafic ocean crust, followed by the interaction of this melt with the mantle (Kay, 1978; Defant and Drummond, 1990). If subducted basaltic ocean crust begins to melt, however, then subducted sediments must also undergo partial melting (Kelemen et al., 2003).

In Fig. 10a, Th/Ce ratios are plotted against initial $^{143}Nd/^{144}Nd$ ratios for Baogutu adakitic rocks. This diagram is sensitive to the addition of a sediment-derived melt because the subducted sediments have low $^{143}Nd/^{144}Nd$ and high Th/Ce ratios relative to mantle wedge (Hawkesworth et al., 1997). The Baogutu adakitic rocks show a broad negative trend, which is consistent with the addition of a sediment melt. The Baogutu adakitic rocks have high Th/La ratios, although they do not show particularly high Th contents (Fig. 10b). They are similar to the high-Mg andesites from the Setouchi Volcanic Belt, Japan (Fig. 10b), which were generated by the partial melting of subducting sediments, and subsequent melt-mantle interaction (Shimoda et al., 1998; Tatsumi, 2001; Hanyu et al., 2006). Plots of Th/La versus Sm/La for arc volcanic rocks show mixing toward local sediments (Plank, 2005) and it is evident in Fig. 10c that the Baogutu adakitic rock compositions can be produced by a mixture of basalts from the Bayingou ophiolites and subducted sediments.

To model partial melting of subducted oceanic crust and its overlying sediment, we used a Kexia basalt sample (Zheng et al., 2007) and a Bayingou ophiolite gabbro sample (Xu et al., 2006c) as the subducted Carboniferous Junggar Altered Ocean basaltic crust (AOC),

and the average Global Subducting Sediment (GLOSS: Plank and Langmuir, 1998) composition as the overlying sediments. Based on these starting materials, the Baogutu samples can be modeled as 99:1 to 90:10 AOC melt:sediment melt mixture on Sr, Nd and Pb isotopic variation diagrams (Fig. 11a-c). An average composition of the Baogutu rocks can be derived by mixing at a 95:5 ratio of AOC and sediment melts (large red circles in Fig. 11a-c). Its primitive mantle-normalized trace element pattern can also be reproduced by this simple mixing scenario, except for the fluid-mobile elements (Rb, and Ba) (Fig. 11d). This suggests that these highly soluble elements were lost in a fluid phase prior to melting. Thus, the Baogutu adakitic rocks were most probably produced by partial melting of subducted oceanic crust and a thin veneer of overlying sediments (Fig. 11), and subsequent melt-mantle interaction (Fig. 5e-f).

### 6.2 Geodynamic processes

Two competing viewpoints for the tectonic evolution of the western Junggar area stress either island arc or post-collisional processes (Chen and Arakawa, 2005; Han et al., 2006; Su et al., 2006; Zhang et al., 2006; Xiao et al., 2008). The most appropriate tectonic model for the western Junggar area must account for the diverse compositional characteristics of the voluminous Carboniferous to Early Permian magmatic rocks, particularly granitoids.

#### 6.2.1 Three types of granitoids in the central western Junggar area

The central western Junggar area hosts many Late Carboniferous to Early Permian granitoids (ca. 315 to 290 Ma) (Fig. 12a). Distinct from the dominantly I-type granitoids of the northern and southern areas (Fig. 1b), the central area contains a diverse range of intrusive rocks, which can be classified into three groups based on their geochemical and

geochronological features (Figs. 5-7, 12). From the southeast to the northwest of the central area, these are the Baogutu adakitic rock group (Group 1), the Keramay I-type granitoid group (Group 2), and the Miaoergou A-type granite group (Group 3), respectively (Fig. 1b). Group 3 granitoids include the Miaoergou, Akbastao, Hongshan and Hatu plutons (Fig. 1b). The three groups exhibit systematic variations in terms of ages and geochemical characteristics (Fig. 12). Their ages decrease slightly from Group 1 to 3, although Groups 1 and 2 overlap significantly (Fig. 12a). $Mg^{\#}$ and Sr/Y values clearly decrease from Group 1 to 3 (Fig. 12c-d), whereas zircon saturation temperatures increase from southeast (Group 1) to northwest (Group 3; Fig. 12e). If the transition from high to low Sr/Y ratios relates to the presence of garnet and plagioclase in their respective sources, and the variation in $Mg^{\#}$s reflects the proportion of mantle component involved in their petrogenesis (e.g., Rapp et al., 1999), then the differing compositions suggest that granitoid source depths become shallower from Group 1 in the southeast to Group 3 in the northwest.

### 6.2.2 Ridge subduction and slab window model

During the early Carboniferous, the Paleo-Asia Ocean (the Carboniferous Junggar Ocean) may have been subducting beneath the Keramay arc (Fig. 13a). During this process, upwelling slab-derived fluids would have triggered partial melting of the mantle wedge (Fig. 13a). These 338 – 316 Ma volcanic rocks and I-type granitoids with "island arc-type" geochemical compositions likely originated from partial melting of fluid-metasomatized mantle wedge (Fig. 13a). Based on several lines of evidence, discussed below, we suggest that subduction of a spreading centre during the late Carboniferous resulted in a slab window, which led to the formation of 315 – 290 Ma magmatism in the central area of the Keramay arc.

Ridge subduction can readily provide enough heat for partial melting of a young oceanic crust (≤ 25 Ma) or old oceanic crust (> 25 Ma), generating adakitic rocks (Defant and Drummond, 1990; Aguillon-Robles et al., 2001; Kelemen et al., 2003). Such melting occurs because the resultant slab window permits the upwelling of hot asthenospheric mantle (e.g, Kay et al., 1993; Abratis and Worner, 2001; Breitsprecher et al., 2003; Kelemen et al., 2003; Windley et al., 2007). In this scenario, the Baogutu low Mg ($Mg^{\#}$ < 48 ) adakitic rocks resulted from partial melting of a slab edge and high-Mg ($Mg^{\#}$ > 48 ) gabbroic diorites and diorites originated from subsequent interaction between slab melts and the mantle (Fig. 13b).

The Baogutu samples generally have slightly lower Sr (346–841 ppm) contents, Sr/Y (31–67 ppm) values and higher HREE and Y contents relative to typical adakites derived from melting of subducted oceanic crust in non-ridge subduction settings (Kay, 1978; Defant and Drummond, 1990; Kay et al., 1993; Stern and Kilian, 1996) (Fig. 5d). This is similar to other adakites (e.g., Vizcaino Peninsula, Mexico) formed by ridge subduction (Aguillon-Robles et al., 2001). In addition, the Baogutu samples also show relatively low Nb/Ta ratios (10.7 to 18, with an average of 13.4). This feature, coupled with higher Zr/Sm ratios (16.9 to 75.7 and average 40.2; Appendix 3), is similar to Archean TTGs (Condie, 2005). These trace element patterns indicate that slab (AOC + sediments) melting took place at relatively shallow depths, but mainly with a garnet amphibolite residuum (Fig. 11d). These depth and source requirements further suggest that special circumstances, such as mantle upwelling by ridge subduction, provided the anomalous heat source for slab melting (e.g., Aguillon-Robles et al., 2001). Interestingly, the zircon saturation temperatures (Watson and Harrison 1983) (642 - 778 ℃) for the Baogutu

677 adakites are distinctly lower than those (729 - 976 ℃) of the Miaoergou A-type granites
678 (Fig. 12e), but similar to those (671 - 726 ℃) of the southern Costa Rica adakites formed
679 by subduction of the Cocos Ridge (Abratis and Worner, 2001). The temperatures may
680 reflect adakite formation by hydrous partial melting of slab edges saturated with water
681 (Martin, 1999) and generation of A-type granites under $H_2O$-absent conditions.
682
683 The Keramay I-type granitoids are characterized by relatively high MgO and Sr contents
684 (Fig. 5d-e), high $Mg^{\#}$, MORB-like Nd-Sr isotopic compositions and young Nd model
685 ages ($T_{2DM}$) of 300–550 Ma (Figs. 5f, 7a and 12b), indicating that they were derived from
686 a juvenile source (Chen and Arakawa, 2005). Experimental melts of basaltic rocks
687 generally exhibit $Mg^{\#}$ lower than 40, whereas the $Mg^{\#}$ of the Keramay series are
688 significantly higher than 40 (Figs. 5f and 11c). Accordingly, the melts were not directly
689 derived by partial melting of basaltic (or equivalent) rocks. The Keramay series are also
690 unlikely to have been generated by direct melting of a mantle source, given that their
691 silica contents are as high as 70 wt.% (Fig. 5). Chen and Arakawa (2005) proposed that
692 the parent magma to the Keramay rocks originated from a depleted lithospheric mantle
693 source that had been metasomatized by fluids released from a subducting slab. We
694 suggest that the asthenosphere ascending from the slab window as a result of ridge
695 subduction provided the heat for such partial melting (Fig. 13b). The mantle-derived
696 magma may then have evolved into the Keramay I-type granitoids by fractional
697 crystallization (Chen and Arakawa, 2005). Thus, the “island-arc type” characteristics of
698 the Keramay I-type granitoids were probably inherited from their mantle sources (Fig.
699 13a-b).
700
701 Geochemical and isotopic characteristics of the Miaoergou series A-type granites suggest

that they formed above a slab window (Fig. 13b). The granites have low initial Sr isotopic ratios and MgO contents and $Mg^{\#}$ values, positive $\varepsilon_{Nd}(t)$ values and young Nd model ages ($T_{2DM}$) (Figs. 5e-f, 7a and 12b-c). Their very high zircon saturation temperatures (729 – 976 ℃) are characteristic of A-type granites (Skjerlie and Johnston1993). Accordingly, it has been suggested that they were generated by partial melting of juvenile (oceanic?) lower crust (Chen and Arakawa, 2005; Geng et al., 2009). We propose that such partial melting occurred because of the upwelling asthenosphere through a slab window (Fig. 13b). In addition, the compositional variations of the Miaoergou series A-type granites suggests minor fractional crystallization after the A-type granite magmas were generated. The A-type granites have pronounced negative Eu, Sr and Ba anomalies (Fig. 6), indicating the possible fractionation of plagioclase or K-feldspar in the evolution of the A-type granite magmas (Wu et al., 2002). The A-type granites have relatively high Yb (1.96-6.56 ppm) and Y (16.3-80.4 ppm) contents, precluding heavy rare earth element-rich garnet in the residue and indicating partial melting under low pressure (< 15 kbar) conditions (Patiño Douce, 2005). In summary, we suggest that they were most likely derived from partial melting of juvenile lower crust above a slab window at low pressure (< 15 kbar), followed by minor fractional crystallization of plagioclase or K-feldspar.

There is additional evidence for ridge subduction in the region. First, charnockites occur as giant enclaves in the Miaoergou batholith, suggesting a hotter than normal geotherm at that time (Fig. 13b). Zhang et al. (2004) proposed that the charnockites were produced by partial melting of juvenile lower crust, heated by mantle upwelling. A slab window would facilitate this upwelling (Fig. 13b). Second, numerous NW-extending basic-intermediate

727 dikes intrude the granite batholiths and the Carboniferous strata. The dikes are only
728 slightly younger than the rocks that they intrude (Fig. 1b). They display typical
729 “subduction zone” characteristics and may have formed by partial melting of
730 metasomatized lithosphere mantle in an extensional environment. Intrusion of mafic dikes
731 into the accretionary prism is a typical feature of ridge subduction and slab window
732 scenarios (Sisson et al., 2003; Windley et al., 2007), and the trend of these dikes may be
733 parallel to that of the subducted oceanic ridge (Fig. 13b). Third, other recent studies also
734 document Late Carboniferous adakitic diorites (Geng et al., 2009) and high Mg diorite (or
735 sanukitoid) dikes (Yin et al., 2009) in the west Junggar Basin outside of our study area
736 and also suggest the possible subduction of oceanic ridge (Geng et al., 2009; Yin et al.,
737 2009). Fourth, there are Carboniferous primitive tholeiitic basalts in the Hatu area with
738 typical N-MORB geochemical characteristics (Shen and Jin, 1993). Such magmas are a
739 common manifestation of spreading ridge subduction (Guivel et al., 1999), and the Hatu
740 basalts were probably derived from partial melting of upwelling mid-ocean-ridge-like
741 depleted mantle above a slab window.
742
743 The rock suite in the Keramay arc area is similar to those known to be associated with
744 ridge subduction and slab window formation elsewhere. For example, in the south-central
745 Alaska Range, broadly contemporaneous adakites, I-type granitoids, and A-type granite
746 suites are associated with ridge subduction and slab window formation (Cole et al., 2007;
747 Hung et al., 2007). Adakites there (e.g., the Jack River pluton) were generated at 62.7 ±
748 0.4 Ma (Cole et al., 2007), I type granitoids (e.g., the Composite plutons) at 67 – 69 Ma,
749 and A-type granites (e.g, the McKinley pluton) at 51 ± 1 Ma (Hung et al., 2007).
750 Moreover, these A-type granites are considered to have been generated through partial
751 melting of lower crust by upwelling asthenosphere above a slab window (Mortimer et al.,

752 2006; Hung et al., 2007; Anma et al., 2009). In this case, the A-type granites are ca.
753 10–20 Ma younger than the adakites, which is a similar relationship to that found in the
754 Keramay arc (Fig. 12a).
755
756 The short duration (315-290 Ma) of magmatism in the Keramay arc area is also
757 similar to that known to be associated with ridge subduction and slab window formation
758 elsewhere. Cole et al., (2006) suggested the Caribou Creek volcanic rocks from the
759 southern Talkeetna Mountains were related to a slab window, which existed between 59
760 Ma and 35 Ma. Kinoshita (2002) also documented a similar period of magmatism (~ 20
761 Ma) above a slab window that formed in response to spreading ridge subduction beneath
762 southwest Japan. The Princeton Group in south-central British Columbia formed by
763 remelting of arc basalt above a slab window, and geochronological results indicate that
764 they were erupted between approximately 53 and 47 Ma (Ickert et al., 2009). Anma et al.
765 (2009) demonstrated that the Taitao granites were related to the subduction of a short
766 segment of the Chile ridge spreading center that started ~ 6 Ma ago. Therefore, one of the
767 most distinctive features of ridge-subduction is the short duration of magmatism (~20
768 m.y.) above the resulting slab windows, which is consistent with a ridge subduction
769 model for the 315-290 Ma magmatism in the Keramay arc area.
770
771 In addition, some plutons in the western Junggar area are rounded to ellipse-shaped,
772 indicating that they are likely to have undergone little or no deformation. Many ridge
773 subduction-related plutons exhibit similar characteristics. For example, the McKinley
774 Sequence and associated Plutons (62-50 Ma) in the Central Alaska Range, which are also
775 related to ridge-subduction (Hung et al., 2007), show no deformation and are mostly
776 rounded to ellipse-shaped. The Taitao granite pluton (southern Chile) formed due to

777 subduction of the Chile ridge and is undeformed and ellipse-shaped (Anma et. al.， 2009).
778 In fact, in the ridge-subduction model, the upwelling of asthenosphere through a slab
779 window would cause widespread crustal extension (Wilson et al., 2005; Cole et al., 2006;
780 Cole and Stewart, 2009), generally resulting in undeformed plutons, in contrast to those
781 found in a normal (i.e., non-ridge) subduction setting.
782
783 **6.3 Implications for crustal growth in the CAOB**
784 The most remarkable feature of the three groups of magmatic rocks in the central area of
785 the western Junggar region is the fact that they are characterized by positive $\varepsilon_{Nd}(t)$ values
786 (+5.4–+9.2) and very young Nd model ages ($T_{2DM}$) of 300–600 Ma (Fig. 7a and 12b),
787 which is also a common feature of the CAOB. These features indicate that the CAOB
788 crust is made up of young mantle derived material (Jahn et al., 2004). Two competing
789 viewpoints of CAOB crust growth (arc and post-collision related) have frequently caused
790 dispute (Sengör et al., 1993; Jahn et al., 2000, 2004). Sengör et al. (1993) hypothesized
791 that nearly half of the CAOB was derived from the mantle by successive accretion of arc
792 complexes and subduction accretion during the Palaeozoic. Conversely, many researchers
793 suggest that Phanerozoic CAOB granitoids were generated by basalt underplating in a
794 post-collisional setting (Jahn et al., 2000; Wu et al., 2000). More recently, Jahn et al.
795 (2004) argued that both processes probably played equally important roles.
796
797 We suggest that ridge subduction and slab window formation also played an important
798 role in the growth of CAOB crust. Figure 13 illustrates the most plausible geodynamic
799 scenario: (1) Oceanic crust subduction and fluid release leading to mantle wedge partial
800 melting and resultant 338－316 Ma volcanic rocks and I-type granites in an arc setting
801 (Fig. 13a). (2) Direct partial melting of subducted basaltic slab (AOC+sediments),

802 generating adakitic magmas (Process 1: see caption in Fig. 13b). (3) Melting of
803 metasomatised mantle-wedge in the slab window to produce post-315 Ma I-type
804 granitoids (Process 2 of the Fig. 13b). Process 3 in Fig. 13b also illustrates crustal growth
805 via partial melting of the basaltic lower crust by underplating of mantle-derived magmas
806 or direct melting of depleted mantle to produce A-type granites and N-MORB type
807 basalts, respectively. These events were triggered by upwelling of asthenospheric mantle
808 in a ridge subduction setting (Fig. 13b).
809
810 Windley et al., (2007) proposed that diagnostic features of ridge subduction are abundant
811 throughout the geological record of the CAOB. Such processes probably accompanied the
812 successive closure of branches of the Paleo-Asian Ocean, given that most subduction
813 systems eventually interact with a spreading ridge (Sisson et al., 2003). Although our
814 study was confined to a relatively small area in the western part of the CAOB (Fig. 1), it
815 supports the view that ridge subduction was common during formation of the entire belt.
816 If so, then ridge subduction likely made major contributions to crustal growth in the
817 CAOB in addition to those made by accretion of subduction and arc complexes (Sengör et
818 al., 1993) and post-collisional crustal melting (Jahn et al., 2000, 2004).
819
820 **7. Conclusions**
821 (1) The Baogutu porphyries in the western Junggar region are calc-alkaline quartz
822 dioritic and granodioritic plutons and dioritic porphyrite dikes. They exhibit
823 geochemical and petrologic characteristics that are typical of adakites; some of them
824 also have the geochemical characteristics of high-Mg andesites.
825 (2) LA-ICPMS zircon U-Pb dating suggests that the Baogutu plutons and dikes have
826 similar crystallization ages of 315–311 Ma and 314–310 Ma, respectively, and were
827 generated in the late Carboniferous.

(3) The Baogutu adakitic rocks were most likely generated by partial melting of a slab edge (containing ca. 95% basaltic oceanic crust and ca. 5% overlying sediments) close to a subducting spreading ridge in the garnet amphibolite faces as a result of a ridge subduction, and subsequent interactions between mantle peridotite and slab melts during their ascent.

(4) Events associated with ridge subduction are likely to have played an important role in crustal growth in the CAOB in addition to previously recognized accretion of subduction and arc complexes and post-collisional crustal melting.

**Acknowledgements**

We sincerely thank Professors R. Rudnick and M. Sun and two anonymous reviewers for their constructive and helpful reviews on this manuscript. We are also grateful to Professor Liu Yongsheng, Chen Haihong, Liu Ying, Hu Guangqian, Ma Jinlong, Tu Xianglin and Xinjiang 305 Project Office for their help in the analytical and fieldwork. This study was jointly supported by the Major State Basic Research Program (973 Program) of People's Republic of China (No. 2007CB411308), the National Natural Science Foundation of China (Grant No. 40721063), the Knowledge Innovation Program of Chinese Academy of Sciences (KZCX2-YW-128), and the Institute for Geoscience Research (TIGeR) at Curtin University of Technology. This is contribution No. IS-XXXX from GIGCAS and TIGeR publication #xxx".

**References**

Abratis, M., Worner, G., 2001. Ridge collision, slab-window formation, and the flux of Pacific asthenosphere into the Caribbean realm. Geology 29, 127-130.

853 Aguillon-Robles, A., Calmus, T., Benoit, M., Bellon, H., Maury, R.C., Cotten, J., Bourgois, J.,
854 Michaud, F., 2001. Late Miocene adakites and Nb-enriched basalts from Vizcaino Peninsula,
855 Mexico: Indicators of East Pacific Rise subduction below southern Baja California? Geology
856 29, 531-534.
857 Andersen, T., 2002. Correction of common lead in U-Pb analyses that do not report $^{204}$Pb. Chemical
858 Geology 192, 59-79.
859 Anma, R., Armstrong, R., Orihashi, Y., Ike, S.i., Shin, K.C., Kon, Y., Komiya, T., Ota, T., Kagashima,
860 S.i., Shibuya, T., Yamamoto, S., Veloso, E.E., Fanning, M., and Hervé, F., 2009. Are the
861 Taitao granites formed due to subduction of the Chile ridge? Lithos 113 (1-2), 246-258.
862 Arculus, R.J., 2003. Use and abuse of the terms calcalkaline and calcalkalic. Journal of Petrology 44,
863 929-935.
864 Atherton, M.P., Petford, N., 1993. Generation of sodium-rich magmas from newly underplated
865 basaltic crust. Nature 362, 144-146.
866 Barth, M.G., Foley, S.F., Horn, I., 2002. Partial melting in Archean subduction zones: constraints from
867 experimentally determined trace element partition coefficients between eclogitic minerals and
868 tonalitic melts under upper mantle conditions. Precambrian Research 113, 323-340.
869 Belousova, E.A., Griffin, W.L., Suzanne, Y.O.R., Fisher, N.I., 2002. Igneous zircon: Trace element
870 composition as an indicator of source rock type. Contributions to Mineralogy and Petrology
871 143 (5), 602-622.
872 Bizzarro, M., Baker, J.A., Ulfbeck, D., 2003. A new digestion and chemical separation technique for
873 rapid and highly reproducible determination of Lu/Hf and Hf isotope ratios in geological
874 materials by MC-ICP-MS. Geostandards and Geoanalytical Research 27, 133-145.
875 Breitsprecher, K., Thorkelson, D.J., Groome, W.G., Dostal, J., 2003. Geochemical confirmation of the
876 Kula-Farallon slab window beneath the Pacific Northwest in Eocene time. Geology 31,
877 351-354.
878 Castillo, P.R., Janney, P.E., Solidum, R.U., 1999. Petrology and geochemistry of Camiguin Island,
879 southern Philippines: insights to the source of adakites and other lavas in a complex arc
880 setting. Contributions to Mineralogy and Petrology 134, 33-51.
881 Chadwick, J., M. Perfit, B. McInnes, G. Kamenov, T. Plank, I. Jonasson, C. Chadwick., 2009. Arc

882 lavas on both sides of a trench: Slab window effects at the Solomon Islands triple junction, SW
883 Pacific. Earth and Planetary Science Letters 279, 293-302.
884 Chauvel, C., Lewin, E., Carpentier, M., Arndt, N.T., Marini, J.C., 2008. Role of recycled oceanic
885 basalt and sediment in generating the Hf-Nd mantle array. Nature Geoscience 1, 64-67.
886 Chen, B., Arakawa, Y., 2005. Elemental and Nd-Sr isotopic geochemistry of granitoids from the West
887 Junggar foldbelt NW China., with implications for Phanerozoic continental growth.
888 Geochimica et Cosmochimica Acta 69, 1307-1320.
889 Chen, B., Jahn, B.M., 2004. Genesis of post-collisional granitoids and basement nature of the Junggar
890 Terrane, NW China: Nd-Sr isotope and trace element evidence. Journal of Asian Earth
891 Sciences 23, 691-703.
892 Cheng, Y., Zhang, R., 2006. Mineralization regularity of Cu-Au deposits in the Baogutu area, western
893 Junggar, Xinjiang. Geology Prospecting 42, 11-15 (in Chinese with English abstract).
894 Chung, S.L., Liu, D.Y., Ji, J.Q., Chu, M.F., Lee, H.Y., Wen, D.J., Lo, C.H., Lee, T.Y., Qian, Q.,
895 Zhang, Q., 2003. Adakites from continental collision zones: Melting of thickened lower crust
896 beneath southern Tibet. Geology 31, 1021-1024.
897 Cole, R.B., Basu, A.R., 1992. Middle Tertiary volcanism during ridge – trench interactions in western
898 California. Science 258, 793 – 796.
899 Cole, R.B., Layer, P.W., Hooks, B., Cyr, A., Turner, J., 2007. Magmatism and deformation in a
900 terrane suture zone south of the Denali fault, northern Talkeetna Mountains, Alaska. In
901 Tectonic Growth of a Collisional Continental Margin: Crustal Evolution of Southern Alaska
902 eds. K.D. Ridgway, J.M. Trop, J.M.G. Glen., J.M. O' Neill., Geological Society of America
903 Special Paper 431, pp. 477-506.
904 Cole, R.B., Nelson, S.W., Layer, P.W., Oswald, P.J., 2006. Eocene volcanism above a depleted mantle
905 slab window in southern Alaska. Geological Society of America Bulletin 118(1-2), 140-158.
906 Cole, R.B., Stewart, B.W., 2009. Continental margin volcanism at sites of spreading ridge subduction:
907 Examples from southern Alaska and western California. Tectonophysics 464(1-4), 118-136.
908 Coleman, R.G., 1989. Continental growth of Northwest China. Tectonics 8, 621-635.
909 Condie, K.C., 2005. TTGs and adakites: are they both slab melts? Lithos 80, 33-44.

910 Danyushevsky, L.V., Falloon, T.J., Crawford, A.J., Tetroeva, S.A., Leslie, R.L., and Verbeeten, A.,
911 2008. High-Mg adakites from Kadavu Island Group, Fiji, southwest Pacific: Evidence for the
912 mantle origin of adakite parental melts. Geology 36 (6), 499-502.
913 Defant, M.J., Drummond, M.S., 1990. Derivation of some modern arc magmas by melting of young
914 subducted lithosphere. Nature 347, 662-665.
915 Defant, M.J., Drummond, M.S., 1993. Mount St. Helens; potential example of the partial melting of
916 the subducted lithosphere in a volcanic arc. Geology 21, 547-550.
917 Delong, S.E., Schwarz, W.M., Anderson, R.N., 1979. Thermal effects of ridge subduction. Earth and
918 Planetary Science Letters 44, 239-246
919 Dickinson, W.R., Snyder, W.S., 1979. Geometry of subducted slabs related to San Andreas transform.
920 Journal of Geology 87, 609-627.
921 Gao, J., Li, M.S., Xiao, X.C., Tang, Y.Q., He, G.Q., 1998. Paleozoic tectonic evolution of the
922 Tianshan Orogen, northwestern China. Tectonophysics 287, 213-231.
923 Gao, S., Liu, X.M., Yuan, H.L., Hattendorf, B., Günther, D., Chen, L., Hu, S.H., 2002. Determination
924 of forty-two major and trace elements in USGS and NIST SRM glasses by laser
925 ablationinductively coupled plasma-mass spectrometry. Geostandards and Geoanalytical
926 Research 26 (2), 181-195.
927 Gao, S., Rudnick, R.L., Xu, W.L., Yuan, H.L., Liu, Y.S., Walker, R.J., Puchtel, I.S., Liu, X., Huang,
928 H., Wang, X.R., Yang, J., 2008. Recycling deep cratonic lithosphere and generation of
929 intraplate magmatism in the North China Craton. Earth And Planetary Science Letters
930 270(1-2), 41-53.
931 Gao, S., Rudnick, R.L., Yuan, H.L., Liu, X.M., Liu, Y.S., Xu, W.L., Ling, W.L., Ayers, J., Wang,
932 X.C., Wang, Q.H., 2004. Recycling lower continental crust in the North China Craton. Nature
933 432, 892-897.
934 Gao, S.L., He, Z.L., Zhou, Z.Y., 2006. Geochemical characteristics of the karamay granitoids and their
935 significance in west Junggar, Xinjiang. Xinjiang Geology 24, 125-130 (in Chinese with
936 English abstract).
937 Geng, H.Y., Sun, M., Yuan, C., Xiao, W.J., Xian, W.S., Zhao, G.C., Zhang, L.F., Wong, K., Wu, F.Y.,
938 2009. Geochemical, Sr-Nd and zircon U-Pb-Hf isotopic studies of Late Carboniferous

939 magmatism in the West Junggar, Xinjiang: implications for ridge subduction? Chemical
940 Geology 266 (3-4), 364-389.
941 Guivel, C., Lagabrielle, Y., Bourgois, J., Maury, R.C., Fourcade, S., Martin, H., Arnaud, N., 1999. New
942 geochemical constraints for the origin of ridge-subduction-related plutonic and volcanic suites
943 from the Chile Triple Junction Taitao Peninsula and Site 862, LEG ODP141 on the Taitao
944 Ridge. Tectonophysics 311, 83-111.
945 Haeussler, P.J., Bradley, D.C., Goldfarb, R.J., Snee, L.W., Taylor, C.D., 1995. Link between ridge
946 subduction and gold mineralization in Southern Alaska. Geology 23, 995-998.
947 Han, B.F., Ji, J.Q., Song, B., Chen, L.H., Zhang, L., 2006. Late Paleozoic vertical growth of
948 continental crust around the Junggar Basin, Xinjiang, China Part I.: Timing of post-collisional
949 plutonism. Acta Petrologica Sinica 22, 1077-1086 (in Chinese with English abstract).
950 Hanyu, T., Tatsumi, Y., Nakai, S., Chang, Q., Miyazaki, T., Sato, K., Tani, K., Shibata, T., Yoshida,
951 T., 2006. Contribution of slab melting and slab dehydration to magmatism in the NE Japan arc
952 for the last 25 Myr: Constraints from geochemistry. Geochemistry Geophysics and
953 Geosystems 78, Q08002, doi:10.1029/2005GC001220
954 Hawkesworth, C.J., Turner, S.P., McDermott, F., Peate, D.W., van Calsteren, P., 1997. U-Th isotopes
955 in arc magmas: Implications for element transfer from the subducted crust. Science 276, 551.
956 Hole, M.J., Rogers, G., Saunders, A.D., Storey, M., 1991. Relation between alkalic volcanism and
957 slab-window formation. Geology 19, 657-660.
958 Hu, A.Q., Jahn, B.M., Zhang, G.X., Chen, Y.B., Zhang, Q.F., 2000. Crustal evolution and Phanerozoic
959 crustal growth in northern Xinjiang: Nd isotopic evidence. Part I. Isotopic characterization of
960 basement rocks. Tectonophysics 328(1-2), 15-51.
961 Huang, J.J., Qiang, C.F., Wang, Z.X., 1990. Plate tectonics and accordion-style of Xinjiang and its
962 adjacent area. Xinjiang Geology Science 1, 3-16 (in Chinese).
963 Hung, C., Chung, S., Cole, R., Iizuka, Y., Chiu, H., Chu, C., Gallet, S., 2007. Zircon U-Pb ages for the
964 McKinley sequence and associated plutons, Central Alaska Range. American Geophysical
965 Union, Fall Meeting 2007, abstract #T11B-0574.
966 Huang, X.L., Xu, Y.G., Lo, C.H., Wang R.C., Lin C.Y., 2007. Exsolution Lamellae in a
967 Clinopyroxene Megacryst Aggregate from Cenozoic Basalt, Leizhou Peninsula, South China:

968 Petrography and Chemical Evolution, Contributions to Mineralogy and Petrology 154,
969 691–705.
970 Ickert, R.B., Thorkelson, D.J., Marshall, D.D., Ullrich, T.D., 2009. Eocene adakitic volcanism in
971 southern British Columbia: Remelting of arc basalt above a slab window. Tectonophysics,
972 164(1-4): 164-185.
973 Jackson, S.E., Pearson, N.J., Belousova, E., Griffin, W.L., 2004. The application of laser
974 ablation-inductively coupled plasma-mass spectrometry (LA-ICP-MS). to in situ U-Pb
975 geochronology. Chemical Geology 211, 47-69.
976 Jahn, B.M., Windley, B., Natal'in, B., Dobretsov, N., 2004. Phanerozoic continental growth in Central
977 Asia. Journal of Asian Earth Sciences 23, 599-603.
978 Jahn, B.M., Wu, F.Y., Chen, B., 2000. Massive granitoid generation in Central Asia: Ndisotope
979 evidence and implication for continental growth in the Phanerozoic. Episodes 23, 82-92.
980 Jian, P., Liu, D.Y., Kroner, A., Windley, B.F., Shi, Y., Zhang, F., Shi, G., Miao, L., Zhang, W., Zhang,
981 Q., Zhang, L., Ren, J., 2008. Time scale of an early to mid-Paleozoic orogenic cycle of the
982 long-lived Central Asian Orogenic Belt, Inner Mongolia of China: Implications for
983 continental growth. Lithos 101, 233-259.
984 Jin, H.J., Li, Y.C., Li, J.Y., 1987. Discovery and study of Carboniferous deepo-water sediments in the
985 northwest of Junggar Basin, Xinjiang. Acta Sedimentologica Sinica 5, 125-134 (in Chinese
986 with English abstract).
987 Johnson, M.C., Plank, T., 1999. Dehydration and melting experiments constrain the fate of subducted
988 sediments. Geochemistry Geophysics and Geosystems 1 (12), doi:10.1029/1999GC000014.
989 Kay, R.W., 1978. Aleutian magnesian andesites: Melts from subducted Pacific ocean crust. Journal of
990 Volcanology and Geothermal Research 4, 117-132.
991 Kay, R.W., Kay, S.M., 1993. Delamination and delamination magmatism. Tectonophysics 219 (1-3),
992 177-189.
993 Kay, S.M., Ramos, V.A., Marquez, M., 1993. Evidence in Cerro Pampa volcanic rocks for
994 slab-melting prior to ridge-trench collision in southern South America. Journal of Geology
995 101, 703-714.

996 Kelemen, P.B., Yogodzinski, G.M., Scholl, D.W., 2003. Along-strike variation in the Aleutian island
997 arc: Genesis of high $Mg^{\#}$ andesite and implications for continental crust. Geophysical
998 monograph American Geophysical Union, pp. 223-276.
999 Kessel, R., Schmidt, M.W., Ulmer, P., Pettke, T., 2005. Trace element signature of subduction-zone
1000 fluids, melts and supercritical liquids at 120-180km depth. Nature 437, 724-727.
1001 Kinoshita, O., 2002. Possible manifestations of slab window magmatisms in Cretaceous southwest
1002 Japan. Tectonophysics 344(1-2), 1-13.
1003 Klemme, S., Prowatke, S., Hametner, K., Gunther, D., 2005. Partitioning of trace elements between
1004 rutile and silicate melts: Implications for subduction zones. Geochimica et Cosmochimica
1005 Acta 69, 2361-2371.
1006 Li, J.W., Zhao, X.F., Zhou, M.F., Ma, C.Q., de Souza, Z., Vasconcelos, P., 2009. Late Mesozoic
1007 magmatism from the Daye region, eastern China: U-Pb ages, petrogenesis, and geodynamic
1008 implications. Contributions to Mineralogy and Petrology 157, 383-409.
1009 Li, X.H., Li, Z.X., Wingate, M.T.D., Chung, S.L., Liu, Y., Lin, G.C., Li, W.X., 2006. Geochemistry of
1010 the 755Ma Mundine Well dyke swarm, northwestern Australia: Part of a Neoproterozoic
1011 mantle superplume beneath Rodinia? Precambrian Research 146, 1-15.
1012 Li, X.Z., Han, B.F., Ji, J.Q., Li, Z.H., Liu, Z.Q., Yang, B., 2004. Geology, geochenistry and K-Ar ages
1013 of the Karamay basic-intermediate dyke swarm from Xinjiang, China. Geochimica 33,
1014 574-584 (in Chinese with English abstract).
1015 Liu, W., Fei, P.X., 2006. Methane-rich fluid inclusions from ophiolitic dunite and post-collisional
1016 mafic-ultramafic intrusion: The mantle dynamics underneath the Palaeo-Asian Ocean through
1017 to the post-collisional period. Earth and Planetary Science Letters 242, 286-301.
1018 Liu, Y.S., Gao, S., Gao, C.G., Wang, D.B., Zong, K.Q., Hu, Z.C., 2009. Timing of melt-peridotite
1019 interactions in xenoliths of the Trans-North China Orogen: U-Pb dating, Hf isotopes and trace
1020 elements in zircon. Journal of Petrology (in revision).
1021 Liu,Y.S., Hu, Z.C., Gao, S., Günther, D., Xu, J., Gao, C.G., Chen, H.H., 2008. In situ analysis of
1022 major and trace elements of anhydrous minerals by LA-ICP-MS without applying an internal
1023 standard. Chemical Geology 257, 34–43.

Loiselle, M.C. abd Wones, D.R., 1979. Characteristics and origin of anorogenic granites. Geological Society of America Bulletin (Abstracts with Programs) 11, 468.

Ludwig, K.R., 2003. User's manual for Isoplot 3.00: a geochronological toolkit for Microsoft Excel. Berkeley Geochronology Center Special Publication 4, 1–70.

Macpherson, C.G., Dreher, S.T., Thirlwall, M.F., 2006. Adakites without slab melting: High pressure differentiation of island arc magma, Mindanao, the Philippines. Earth and Planetary Science Letters 243, 581-593.

Martin, H., 1999. Adakitic magmas: modern analogues of Archaean granitoids. Lithos 46(3), 411-429.

Martin, H., Smithies, R.H., Rapp, R., Moyen, J.F., Champion, D., 2005. An overview of adakite, tonalite-trondhjemite-granodiorite TTG., and sanukitoid: relationships and some implications for crustal evolution. Lithos 79, 1-24.

McCrory, P.A., Wilson, D.S., 2009. Interpreting the tectonic evolution of Pacific Rim margins using plate kinematics and slab window volcanism. Tectonophysics 464, 1-2.

Middlemost, E.A.K., 1994. Naming materials in the magma/igneous rock system. Earth-Science Reviews 37, 215-224.

Miyashiro, A., 1974. Volcanic rock series in island arcs and active continental margins. American Journal of Science 274, 321-355.

Mori, L., Gomez-Tuena, A., Cai, Y., Goldstein, S.L., 2007. Effects of prolonged flat subduction on the Miocene magmatic record of the central Trans-Mexican Volcanic Belt. Chemical Geology 244, 452-473.

Morimoto, N., Fabries, J., Ferguson, A.K., Ginzburg, I.V., Ross, M., Seifert, F.A., Zussman, J., Aoki, K., Gottardi, G., 1988. Nomenclature of pyroxenes. American Mineralogist 73(9-10), 1123-1133.

Mortimer, N., Hoernle, K., Hauff, F., Palin, J.M., Dunlap, W.J., Werner, R., Faure, K., 2006. New constraints on the age and evolution of the Wishbone Ridge, southwest Pacific Cretaceous microplates, and Zealandia-West Antarctica breakup. Geology 34, 185-188.

1051 Müntener, O., Kelemen, P. ,Grove, T., 2001. The role of $H_2O$ during crystallization of primitive arc
1052 magmas under uppermost mantle conditions and genesis of igneous pyroxenites: an
1053 experimental study. Contributions to Mineralogy and Petrology 141 (6), 643-658.
1054 Patiño Douce, A.E., 2005. Vapor-absent melting of tonalite at 15–32kbar. Journal of Petrology 46,
1055 275–290.
1056 Peccerillo, A., Taylor, S.R., 1976. Geochemistry of Eocene calc-alkaline volcanic rocks from the
1057 Kastamonu area, Northern Turkey. Contributions to Mineralogy and Petrology 58, 63-81.
1058 Petford, N., Atherton, M., 1996. Na-rich partial melts from newly underplated basaltic crust: the
1059 Cordillera Blanca Batholith, Peru. Journal of Petrology 37, 1491-1521.
1060 Plank, T., 2005. Constraints from thorium/lanthanum on sediment recycling at subduction zones and
1061 the evolution of the continents. Journal of Petrology 46, 921-944.
1062 Plank, T., Langmuir, C.H., 1993. Tracing trace elements from sediment input to volcanic output at
1063 subduction zones. Nature 362, 739-743.
1064 Plank, T., Langmuir, C.H., 1998. The chemical composition of subducting sediment and its
1065 consequences for the crust and mantle. Chemical Geology 145, 325-394.
1066 Rapp, R.P., Shimizu, N., Norman, M.D., Applegate, G.S., 1999. Reaction between slab-derived melts
1067 and peridotite in the mantle wedge: experimental constraints at 3.8 GPa. Chemical Geology
1068 160, 335-356.
1069 Rapp, R.P., Watson, E.B., 1995. Dehydration Melting of Metabasalt at 8-32 kbar: Implications for
1070 Continental Growth and Crust-Mantle Recycling. Journal of Petrology 36, 891-931.
1071 Rogers, G., Saunders, A.D., Terrell, D.J., Verma, S.P., Marriner, G.F., 1985. Geochemistry of
1072 Holocene volcanic rocks associated with ridge subduction in Baja California, Mexico. Nature
1073 315, 389-392.
1074 Rollinson, H., 1993. Using Geochemical Data. Longman, London, p. 352.
1075 Rudnick, R.L., 1995. Making continental crust. Nature 378(6557), 571-578.
1076 Rui, Z. Y., Goldfarb, R. J., Qiu, Y. M., Zhou, T. H., Chen, R. Y., Pirajno, F., Yun, G., 2002.
1077 Paleozoic-early Mesozoic gold deposits of the Xinjiang Autonomous Region, northwestern
1078 China. Mineralium Deposita 37, 393-418.

1079 Sen, C., Dunn, T., 1994. Dehydration melting of a basaltic composition amphibolite at 1.5 and 2.0 GPa:
1080 implications for the origin of adakites. Contributions to Mineralogy and Petrology **117,**
1081 394-409.
1082 Sengör, A.M.C., Natal'in, B.A., Burtman, V.S., 1993. Evolution of the Altaid tectonic collage and
1083 Palaeozoic crustal growth in Eurasia. Nature 364, 299-307.
1084 Shen, P., Shen, Y., Liu, T., Meng, L., Dai, H., Yang, Y., 2009. Geochemical signature of porphyries in
1085 the Baogutu porphyry copper belt, western Junggar, NW China. Gondwana Research 16(2),
1086 227-242.
1087 Shen, Y.C., Jin, C.W., 1993. The relationships of magma activity and gold mineralization in west
1088 Junggar. In New developments of Solid Earth Sciences of Northern Xinjiang. ed. Tu. G.C.,
1089 Science Press, Beijing. P. 137-150 (in Chinese).
1090 Shimoda, G., Tatsumi, Y., Nohda, S., Ishizaka, K., Jahn, B.M., 1998. Setouchi high-Mg andesites
1091 revisited: geochemical evidence for melting of subducting sediments. Earth and Planetary
1092 Science Letters 160, 479-492.
1093 Sisson, V.B., Pavlis, T.L., Roeske, S.M., Thorkelson, D.J., 2003. Introduction: An overview of
1094 ridge-trench interactions in modern and ancient settings. In Geology of a transpressional
1095 orogen developed during ridge-trench interaction along the North Pacific margin. eds. V.B.
1096 Sisson, T.L. Pavlis, S.M. Roeske., D.J. Thorkelson., Geological Society of America Special
1097 Paper p. 1-18.
1098 Skjerlie, K.P., Johnston, A.D., 1993. Fluid-absent melting behavior of an F-rich tonalitic gneiss at
1099 mid-crustal pressures: Implications for the generation of anorogenic granites. Journal of
1100 Petrology 34 (4), 785-815.
1101 Song, C.H., Wang, J.R., Huang, F., 1996. Study of deep-water sediments of Tailegula formationon the
1102 north of Baijiantan, West of Junggar Basin. Journal of Lanzhou University-Natural Science 32,
1103 132-137(in Chinese with English abstract).
1104 Stern, C.R., Kilian, R., 1996. Role of the subducted slab, mantle wedge and continental crust in the
1105 generation of adakites from the Andean Austral Volcanic Zone. Contributions to Mineralogy
1106 and Petrology 123, 263-281.

1107 Streck, M.J., Leeman, W.P., Chesley, J., 2007. High-Mg andesite from Mount Shasta: A product of
1108 magma mixing and contamination, not a primitive mantle melt. Geology 35, 351-354.
1109 Su, Y.P., Tang, H.F., Hong, G.S., Liu, C.Q., 2006. Geochemistry of aluminous A-type granites along
1110 Darabut tectonic belt in West Junggar, Xinjiang. Geochima 35, 55-67 (in Chinese with
1111 English abstract).
1112 Sun, M., Long, X.P., Cai, K.D., Jiang, Y.D., Wang B.Y., Yuan, C., Zhao, G.C., Xiao, W.J., Wu, F.Y.,
1113 2009. Early Paleozoic ridge subduction in the Chinese Altai: insight from the abrupt change in
1114 zircon Hf isotopic compositions. Science in China (Series D) 39, 1-14.
1115 Sun, M., Yuan, C., Xiao, W.J., Long, X.P., Xia, X.P., Zhao, G.C., Lin, S.F., Wu, F.Y., Kroner, A.,
1116 2008. Zircon U-Pb and Hf isotopic study of gneissic rocks from the Chinese Altay: Progressive
1117 accretionary history in the early to middle Palaeozoic. Chemical Geology 247(3-4), 352-383.
1118 Sun, S.S., McDonough, W.F., 1989. Chemical and isotopic systematics of oceanic basalts:
1119 implications for mantle composition and processes. Geological Society London Special
1120 Publications 42, 313–345.
1121 Tatsumi, Y., 2001. Geochemical modeling of partial melting of subducting sediments and subsequent
1122 melt-mantle interaction: Generation of high-Mg andesites in the Setouchi volcanic belt,
1123 southwest Japan. Geology 29, 323-326.
1124 Tatsumi, Y., 2006. High-Mg andesites in the Setouchi volcanic belt, southwestern Japan: Analogy to
1125 Archean magmatism and continental crust formation? Annual Review of Earth and Planetary
1126 Sciences 34, 467-499.
1127 Tatsumi, Y., Suzuki, T., Kawabata, H., Sato, K., Miyazaki, T., Chang, Q., Takahashi, T., Tani, K.,
1128 Shibata, T., Yoshikawa, M., 2006. The petrology and geochemistry of Oto-Zan composite
1129 lava flow on Shodo-Shima Island, SW Japan: Remelting of a solidified high-mg andesite
1130 magma. Journal of Petrology 47, 595-629.
1131 Thorkelson, D.J., 1996. Subduction of diverging plates and the principles of slab window formation.
1132 Tectonophysics 255, 47–63.
1133 Thorkelson, D.J., Breitsprecher, K., 2005. Partial melting of slab window margins: genesis of adakitic
1134 and non-adakitic magmas. Lithos 79, 25-41.
1135 Troll, V.R., Schmincke, H.U., 2002. Magma mixing and crustal recycling recorded in ternary feldspar from
1136 compositionally zoned peralkaline Ignimbrite 'A', Gran Canaria, Canary Islands. Journal of
1137 Petrology 43(2), 243-270.

1138 Turner, S., Bourdon, B., Gill, J., 2003. Insights into Magma Genesis at Convergent Margins from
1139 U-series Isotopes. Reviews in Mineralogy and Geochemistry 52(1), 255-315.
1140 Wang, F.T., 2006. The Paleogeographic and Geo-ecological Atlas of Xinjiang Uygur Autonomous
1141 Region. SinoMaps Press, Beijing, p. 226 (in Chinese with English abstract).
1142 Wang, Q., McDermott, F., Xu, J.F., Bellon, H., Zhu, Y.T., 2005. Cenozoic K-rich adakitic volcanic
1143 rocks in the Hohxil area, northern Tibet: Lower-crustal melting in an intracontinental setting.
1144 Geology 33, 465-468.
1145 Wang, Q., Wyman, D.A., Xu, J., Dong, Y., Vasconcelos, P.M., Pearson, N., Wan, Y., Dong, H., Li, C.,
1146 Yu, Y., Zhu, T., Feng, X., Zhang, Q., Zi, F., Chu, Z., 2008. Eocene melting of subducting
1147 continental crust and early uplifting of central Tibet: Evidence from central-western
1148 Qiangtang high-K calc-alkaline andesites, dacites and rhyolites. Earth and Planetary Science
1149 Letters 272, 158-171.
1150 Wang, Q., Wyman, D.A., Xu, J.F., Jian, P., Zhao, Z.H., Li, C., Xu, W., Ma, J.L., He, B., 2007a. Early
1151 Cretaceous adakitic granites in the Northern Dabie Complex, central China: Implications for
1152 partial melting and delamination of thickened lower crust. Geochimica et Cosmochimica Acta
1153 71, 2609-2636.
1154 Wang, Q., Wyman, D.A., Zhao, Z.H., Xu, J.F., Bai, Z.H., Xiong, X.L., Dai, T.M., Li, C.F., Chu, Z.Y.,
1155 2007b. Petrogenesis of Carboniferous adakites and Nb-enriched arc basalts in the Alataw area,
1156 northern Tianshan Range (western China): Implications for Phanerozoic crustal growth in the
1157 Central Asia orogenic belt. Chemical Geology 236, 42-64.
1158 Wang, Q., Xu, J.F., Jian, P., Bao, Z.W., Zhao, Z.H., Li, C.F., Xiong, X.L., Ma, J.L., 2006a.
1159 Petrogenesis of adakitic porphyries in an extensional tectonic setting, dexing, South China:
1160 Implications for the genesis of porphyry copper mineralization. Journal of Petrology 47,
1161 119-144.
1162 Wang, Q., Zhao, Z.H., Xu, J.F., Wyman, D.A., Xiong, X.L., Zi, F., Bai, Z.H., 2006b. Carboniferous
1163 adakite-high-Mg andesite-Nb-enriched basaltic rock suites in the Northern Tianshan area:
1164 Implications for Phanerozoic crustal growth in the Central Asia Orogenic Belt and Cu-Au
1165 mineralization. Acta Petrologica Sinica 22, 11-30 (in Chinese with English abstract).

Wang, R., Zhu, Y.F., 2007. Geology of the Baobei gold deposit in Western Juggar and zircon SHRIMP age of its wall-rocks, Western Junggar (Xinjiang, NW China). Geological Journal of China Universities 13, 590-602 (in Chinese with English abstract).

Watson, E.B. and Harrison, T.M., 1983. Zircon saturation revisited: temperature and composition effects in a variety of crustal magma types. Earth And Planetary Science Letters, 64(2), 295-304.

Wiedenbeck, M., Allé, P., Corfu, F., Griffin, W.L., Meier, M., Oberli, F., von Quadt, A., Roddick, J.C., Spiegel, W., 1995. Three natural zircon standards for U–Th–Pb, Lu–Hf, trace element and REE analyses. Geostandards and Geoanalytical Research 19, 1 –23.

Wilson, D.S., McCrory, P.A., Stanley, R.G., 2005. Implications of volcanism in coastal California for the Neogene deformation history of western North America. Tectonics 24(3), TC3008.

Windley, B.F., Alexeiev, D., Xiao, W., Kroner, A., Badarch, G. 2007. Tectonic models for accretion of the Central Asian Orogenic Belt. Journal of the Geological Society 164, 31-47.

Wu, F.Y., Jahn, B.M., Wilde, S., Sun, D.Y., 2000. Phanerozoic crustal growth: U-Pb and Sr-Nd isotopic evidence from the granites in northeastern China. Tectonophysics 328, 89-113.

Wu, F.Y., Sun, D.Y., Li, H.M., Jahn, B.M., Wilde, S., 2002. A-type granites in northeastern China: age and geochemical constraints on their petrogenesis. Chemical Geology 187(1-2), 143-173.

XBGMR., 1993. Regional Geology of Xinjiang Uygur Autonomy Region. Geological Publishing House, Beijing, p. 841(in Chinese with English abstract).

Xiao, W.J., Han, C.M., Yuan, C., Sun, M., Lin, S.F., Chen, H.L., Li, Z.L., Li, J.L., Sun, S., 2008. Middle Cambrian to Permian subduction-related accretionary orogenesis of Northern Xinjiang, NW China: Implications for the tectonic evolution of central Asia. Journal of Asian Earth Sciences 32, 102-117.

Xiao, W.J., Windley, B.F., Badarch, G., Sun, S., Li, J., Qin, K., Wang, Z., 2004. Palaeozoic accretionary and convergent tectonics of the southern Altaids: implications for the growth of Central Asia. Journal of the Geological Society 161, 339-342.

Xiao, X.C., Tang, Y.Q., Feng, Y.M., Zhu, B.Q., Li, J.Y., Zhao, M., 1992. Tectonic evolution of the north Xinjiang and its adjacent region. Geological Publishing House, Beijing, p.80 (in Chinese).

Xu, J.F., Castillo, P.R., 2004. Geochemical and Nd-Pb isotopic characteristics of the Tethyan asthenosphere: implications for the origin of the Indian Ocean mantle domain. Tectonophysics 393, 9-27.

Xiong, X.L., Xia, B., Xu, J.F. Na depletion in modern adakites via melt/rock reaction within the sub-arc mantle. Chemical Geology, 2006, 229:273-292.

Xu, J.F., Castillo, P.R., Li, X.H., Yu, X.Y., Zhang, B.R., Han, Y.W., 2002a. MORB-type rocks from the Paleo-Tethyan Mian-Lueyang northern ophiolite in the Qinling Mountains, central China: implications for the source of the low $^{206}Pb/^{204}Pb$ and high $^{143}Nd/^{144}Nd$ mantle component in the Indian Ocean. Earth and Planetary Science Letters 198, 323-337.

Xu, J.F., Shinjo, R., Defant, M.J., Wang, Q., Rapp, R.P., 2002b. Origin of Mesozoic adakitic intrusive rocks in the Ningzhen area of east China: Partial melting of delaminated lower continental crust? Geology 30, 1111-1114.

Xu, X., He, G.Q., Li, H.Q., Ding, T.F., Liu, X.Y., Mei, S.W., 2006a. Basic characteristics of the Karamay ophiolitic mélange, Xinjiang, and its zircon SHRIMP dating. Geology in China 33 (3), 470-475 (in Chinese with English abstract).

Xu, X.Y., Li, X.M., Ma, Z.P., Xia, L.Q., Xia, Z.C., Peng, S.X., 2006b. LA-ICPMS Zircon U-Pb Dating of gabbro from the Bayingou ophiolite in the Northern Tianshan Mountains. Acta Geologica Sinica 80, 1168-1176 (in Chinese with English abstract).

Xu, X.Y., Xia, L.Q., Ma, Z.P., Wang, Y.B., Xia, Z.C., Li, X.M., Wang, L.S., 2006c. SHRIMP zircon U-Pb geochronology of the plagiogranites from Bayringou ophiolite in North Tianshan Mountains and the petrogenesis of the ophiolite. Acta Petrologica Sinica 22, 83-94 (in Chinese with English abstract)

Yin, J.Y., Yuan, C., Sun, M., Long, X.P., Zhao, G.C., Geng, H.Y., 2010. Late Carboniferous High-Mg dioritic dikes in Western Junggar, NW China: geochemical features, petrogenesis and tectonic implications. Gondwana Research, 17 (1), 145-152.

Yogodzinski, G.M. and Kelemen, P.B., 1998. Slab melting in the Aleutians: implications of an ion probe study of clinopyroxene in primitive adakite and basalt. Earth and Planetary Science Letters, 158(1-2): 53-65.

Yogodzinski, G.M., Lees, J.M., Churikova, T.G., Dorendorf, F., Woerner, G., Volynets, O.N., 2001. Geochemical evidence for the melting of subducting oceanic lithosphere at plate edges. Nature 409, 500-504.

Zhang, L.C., Wan, B., Jiao, X.J., Zhang, R., 2006. Characteristics and geological significance of adakitic rocks in copper-bearing porphyry in Baogutu, western Junggar. Geology in China 33, 626-631 (in Chinese with English abstract).

Zhang, L.F., Xian, W.S., Sun, M., 2004. Petrogenesis of charnockites from Western Junggar, Xingjiang, China. Xinjiang Geology 22, 36-42 (in Chinese with English abstract).

Zhang, S.Q., Mahoney, J.J., Mo, X.X., Ghazi, A.M., Milani, L., Crawford, A.J., Guo, T.Y., Zhao, Z.D., 2005. Evidence for a widespread Tethyan upper mantle with Indian-Ocean-type isotopic characteristics. Journal of Petrology 46, 829-858.

Zheng, J.P., Sun, M., Zhao, G.C., Robinson, P.T., Wang, F.Z., 2007. Elemental and Sr-Nd-Pb isotopic geochemistry of Late Paleozoic volcanic rocks beneath the Junggar basin, NW China: Implications for the formation and evolution of the basin basement. Journal of Asian Earth Sciences 29, 778-794.

Zhou, M.F., Michael Lesher, C., Yang, Z.G., Li, J.W., Sun, M., 2004. Geochemistry and petrogenesis of 270 Ma Ni-Cu-PGE. sulfide-bearing mafic intrusions in the Huangshan district, Eastern Xinjiang, Northwest China: implications for the tectonic evolution of the Central Asian orogenic belt. Chemical Geology 209, 233-257.

Zhou, T.F., Yuan, F., Fan, Y., Zhang, D.Y., Cooke, D., Zhao, G.C., 2008. Granites in the Sawuer region of the west Junggar, Xinjiang Province, China: Geochronological and geochemical characteristics and their geodynamic significance. Lithos 106, 191-206.

Zhu, B. Q., Chen, Y. W., Peng, J., H. 2001. Lead isotope geochemistry of the urban enviroment in the Pearl River Delta. Applied Geochemistry 16, 409-417.

Zhu, Y.F., He, G.Q., An, F., 2007. Geological evolution and metallogeny in the core part of the Central Asian metallogenic domain. Geological Bulletin of China 26 (9), 1167-1177 (in Chinese with English abstract).

## Figures

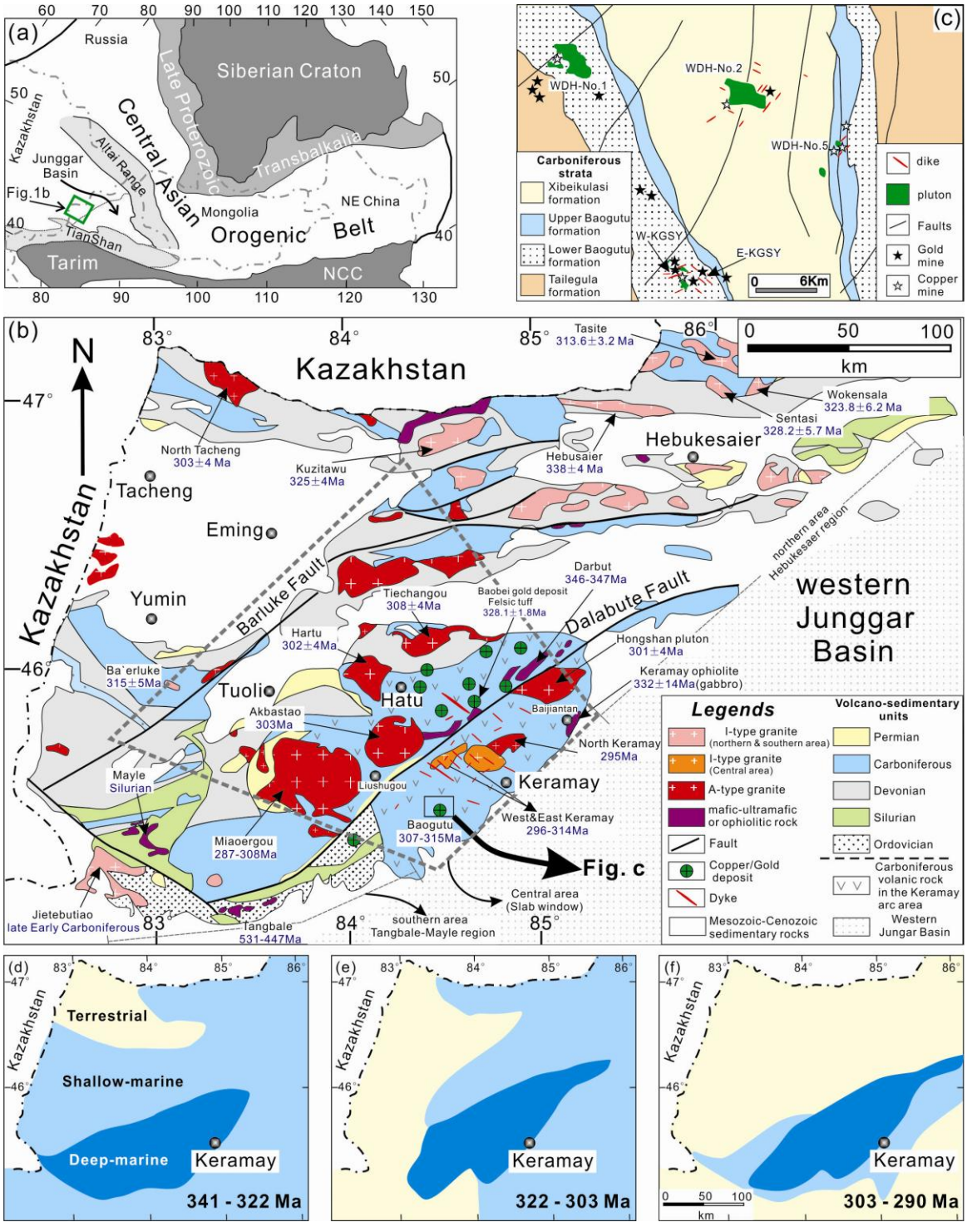


Fig. 1. (a) Simplified tectonic divisions of the CAOB (after Jahn et al., 2000). (b) Geological map of the western Junggar region (modified after XBGMR, 1993). (c) Simplified geological map of the Baogutu deposits (after Cheng and Zhang, 2006). WDH-Wudehe; E-KGSY-Eastern Kuogeshaye; W-KGSY-Western Kuogeshaye. Age

data for mafic-ultramafic or ophiolitic rocks are from Beijing SHRIMP Unit (2005), Xu et al. (2006a) and Xiao et al. (2008). Age data for granite intrusions and volcanic rocks are from Han et al. (2006), Su et al. (2006), Wang and Zhu (2007), (Zhou et al., 2008), Geng et al. (2009) and this study. Age data for Baogutu diorite-granodiorite porphyry plutons and dikes are from this study. (d-f) Paleogeographic maps of the western Junggar region during the Carboniferous to Early Permian (344 – 290 Ma) (from Wang, 2006): 344 - 323 Ma, turbidite facies pyroclastic rocks, tuffaceous sandstones, limestones, radiolarian cherts and tuff layers were deposited in the Liushugou area. Fusulinid, brachiopod, coral and gastropods fossils occur in ~ 400 m thick limestones. Marine clastic rocks including a ~ 2500m thick limestone sequence, occur in the Tuoli area and contain brachiopods, coral, gastropod and plant fossils. 323 - 303 Ma, bathyal facies pyroclastic rocks including ~ 1500 m of andesite, basalts and cherts, are abundant in the central area of the western Junggar region and radiolarian fossils are widespread. To the north, marine and continental facies sandstone, mudstone and shales with plant fossils occur and have a combined thickness of 3000 meters. 303 - 290 Ma, bathyal to deep-marine environments occurred in the Loushugou area where clastic sedimentary rocks contain cherts with radiolaria and have a combined thickness of ~ 750 meters. Contemporaneously, however, a continental environment was present in the northwest part of the western Junggar region.

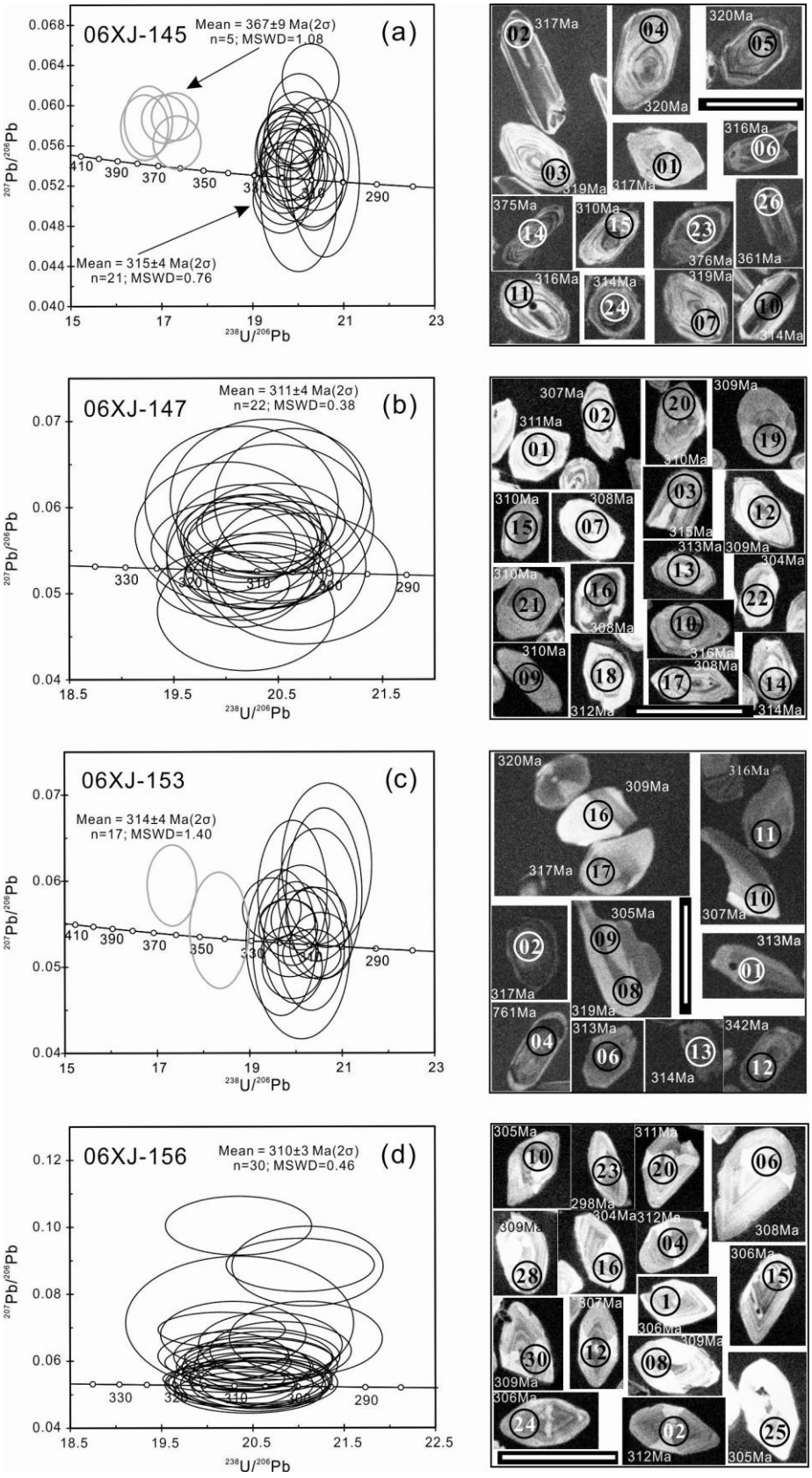


Fig. 2. LA-ICP-MS U-Pb zircon Tera-Wasserburg diagrams with CL images for (a) Quartz dioritic porphyry (06XJ-145), (b) Quartz dioritic porphyry (06XJ-147), (c) dioritic

porphyrite dike (06XJ-153) and (d) dioritic porphyrite dike (06XJ-156) from the Baogutu Cu-Au deposits, western Junggar, CAOB. Circles indicate locations of analyzed sites, with numbers in the circles representing spot numbers. The age for each spot is given. Scale bars all represent 100 μm.

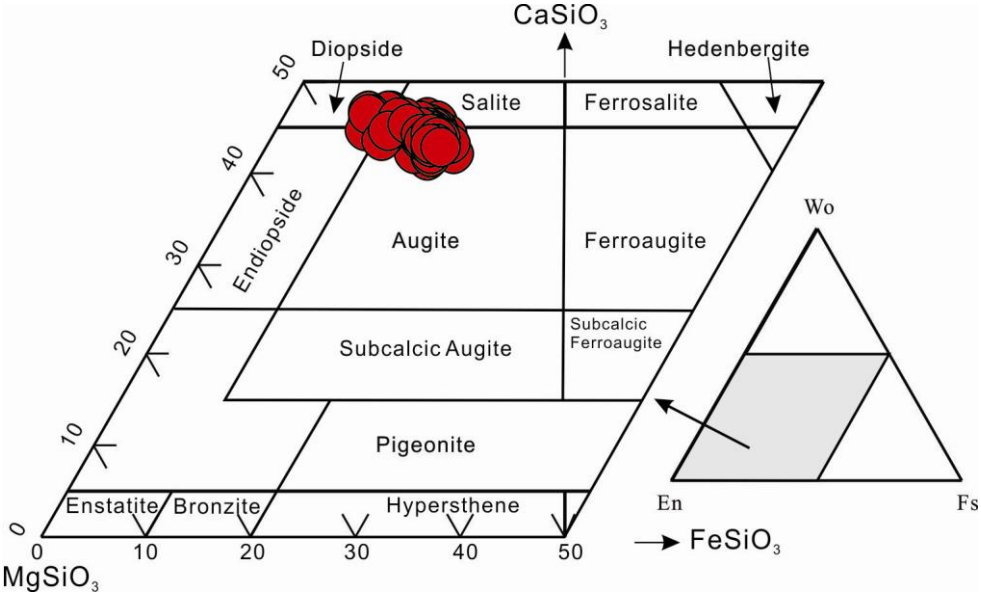


Fig. 3. $CaSiO_3$-$MgSiO_3$-$FeSiO_3$ diagram showing the compositions of pyroxene (Morimoto et al., 1988) from the Baogutu adakitic rocks in the western Junggar region, NW China.

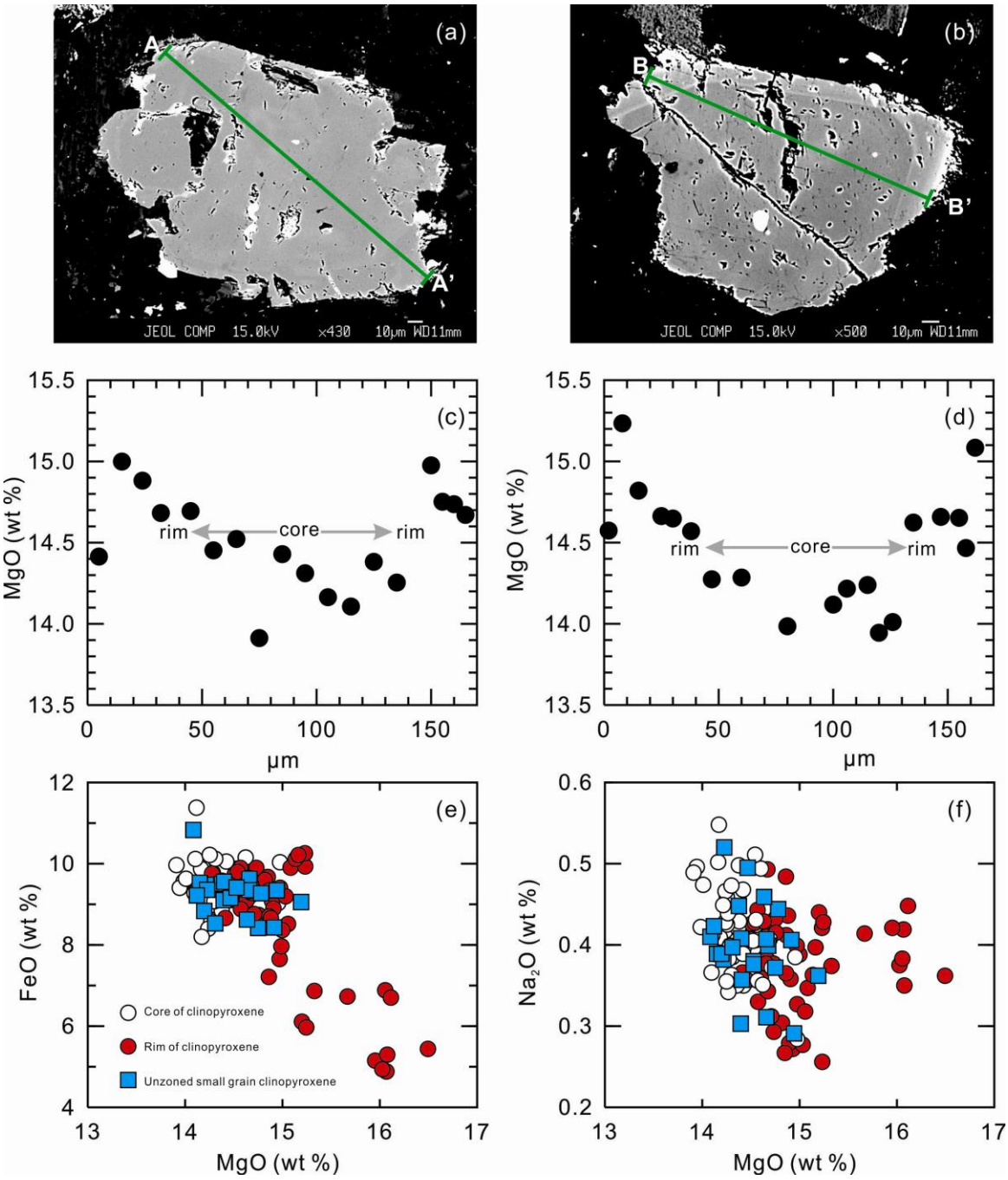


1288

1289 Fig. 4. (a-b) Two back-scattered electron images of typical cores and rims in reversely
1290 zoned clinopyroxene phenocrysts from the Baogutu adakitic rocks. (c-d) Composition
1291 variations (MgO) in clinopyroxene phenocrysts along the A-A' and B-B' sections from
1292 Fig. a and b, respectively. (e) FeO vs. MgO diagram for clinopyroxene phenocrysts. (f)
1293 $Na_2O$ vs. MgO diagram for clinopyroxene phenocrysts.

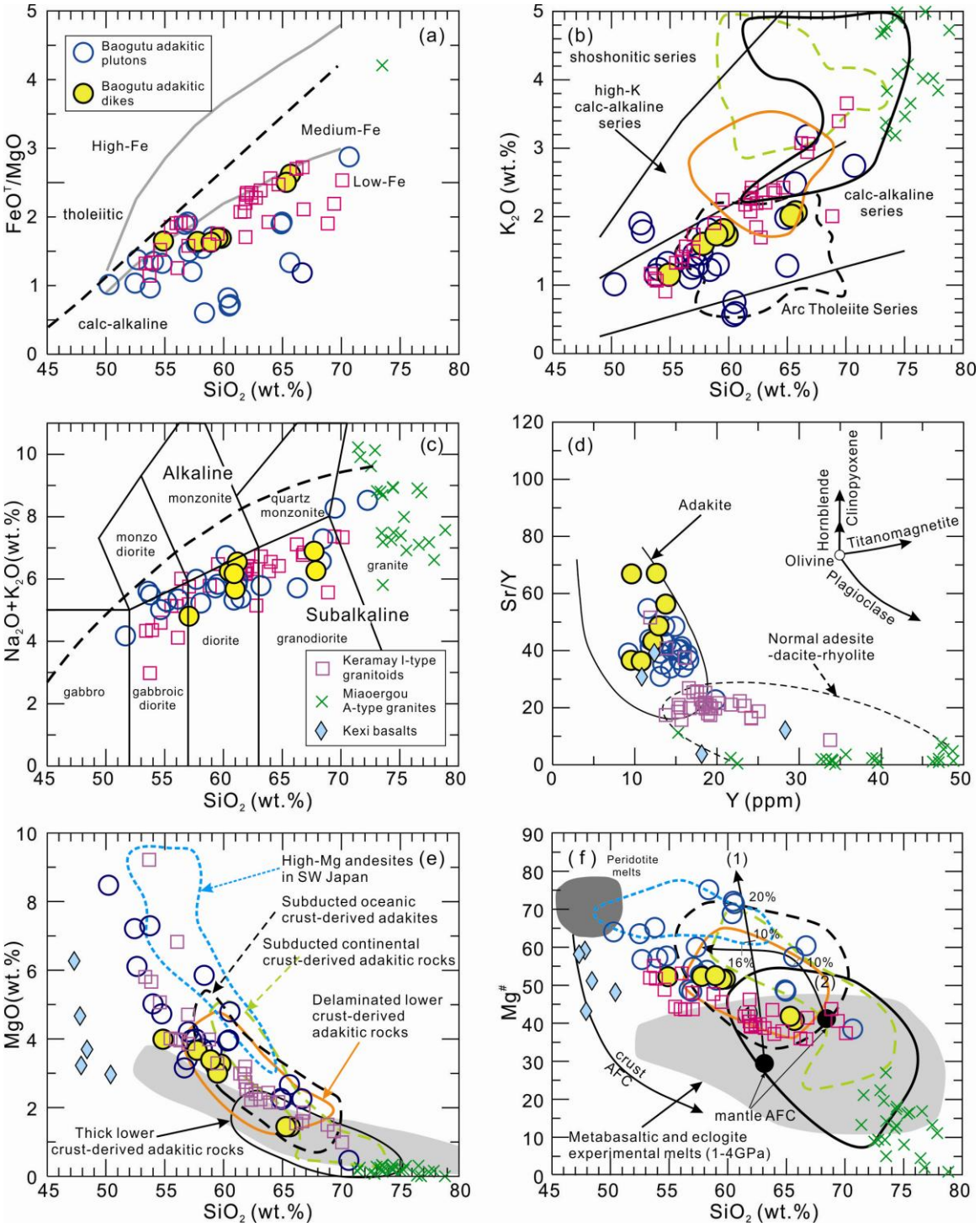


Fig. 5. (a) $SiO_2$ versus $FeO^T/MgO$ diagrams (Miyashiro, 1974). Dashed boundaries for the tholeiitic and calc-alkaline fields are after Miyashiro (1974). Discriminate boundaries (grey lines) between low-, medium-, and high-Fe suites are after Arculus (2003). (b) $SiO_2$ - $K_2O$ plot (Peccerillo and Taylor, 1976). (c) $SiO_2$ – $K_2O$ + $Na_2O$ plot (Middlemost, 1994). (d) Y versus Sr/Y diagram (after Defant and Drummond, 1993). Crystal fractionation

paths of the primary minerals are from Castillo et al. (1999). (e) $SiO_2$ versus MgO diagram. (f) $SiO_2$ versus $Mg^{\#}$ diagram. Mantle AFC curves, with proportions of assimilated peridotite indicated, are after Stern and Kilian (1996) (Curve 1) and Rapp et al. (1999) (Curve 2), peridotite melts and crust AFC curves from Stern and Kilian (1996). Data for metabasaltic and eclogite experimental melts (1-4.0 GPa), and peridotite-hybridized equivalents, are from Rapp et al. (1999) and references therein. Data for high-Mg andesites of SW Japan are from the following references: Shimoda et al. (1998), Tatsumi et al. (2006), Tatsumi et al. (2006), and references therein. Data for the Keramay I-type granitoids and Miaoergou series A-type granites are from Chen and Jahn (2004), Chen and Arakawa (2005), Gao et al. (2006) and Su et al. (2006). Data for the Kexi basalts are from Zheng et al. (2007). Data for the Baogutu samples are from Appendix 3. The fields of subducted oceanic crust-, delaminated lower crust-, and thickened lower crust-derived adakites are after Wang et al. (2006a).

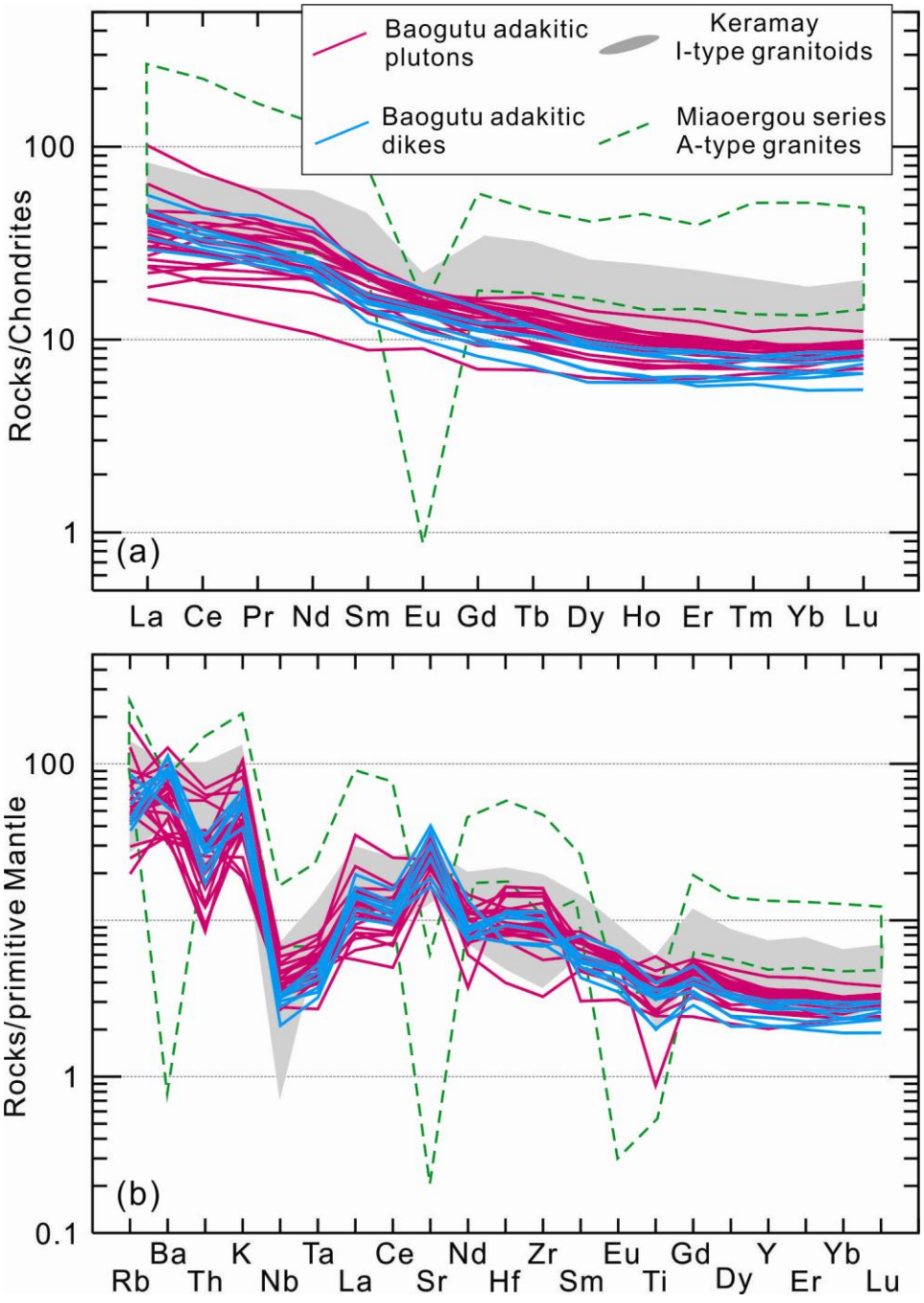


Fig. 6. Chondrite-normalized REE patterns (a) and primitive mantle normalized trace element diagrams (b) for Baogutu samples from the western Junggar compared with the Keramay I-type granitoids and Miaoergou series A-type granites (Data sources as for Fig. 5). Chondrite and primitive mantle normalized values are from Sun and McDonough (1989).

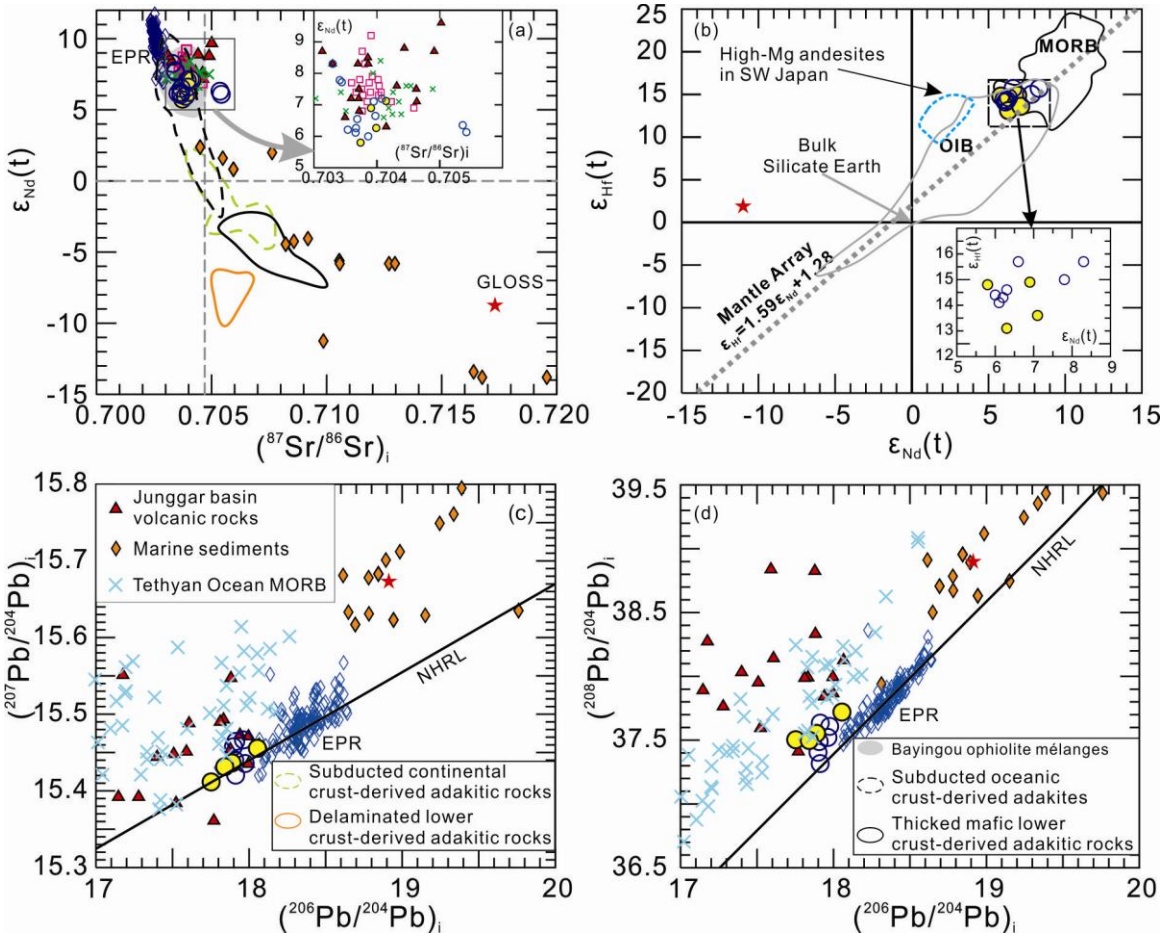


Fig. 7. (a) $\varepsilon_{Nd}(t)$ versus $(^{87}Sr/^{86}Sr)_i$, (b) $\varepsilon_{Hf}(t)$ versus $\varepsilon_{Nd}(t)$, $^{206}Pb/^{204}Pb_i$ versus $^{207}Pb/^{204}Pb_i$ (c) and $^{208}Pb/^{204}Pb_i$ (d) plotes. Data for marine sediments and global subducting sediment (GLOSS) are from Plank and Langmuir (1998) and Chauvel et al. (2008). Data for Tethyan Ocean MORB are from Xu et al. (2002a), Xu and Castillo (2004) and Zhang et al. (2005). Subducted oceanic crust-derived adakites, thickened and delaminated mafic lower crust-derived adakitic rocks are after Wang et al. (2006a, 2007a), Huang et al. (2008) and references therein. Subducted continental crust-derived adakites are after Wang et al. (2008). Basalts of the Bayingou ophiolite mélanges are after Xu et al. (2006c). Data for the Junggar basin volcanic rocks are from Zheng et al. (2007). The high-Mg andesites of SW Japan are from Hanyu et al. (2006) and reference therein. EPR: East Pacific Rise basalts, using the *Petdb* database (Petrological database of the ocean floor, www.petdb.org). The mantle array and fields for MORB and OIB are from Chauvel et al.

(2008). Data for the Baogutu samples are from Appendix 4. Other data sources and symbols are the same as for Fig. 5.

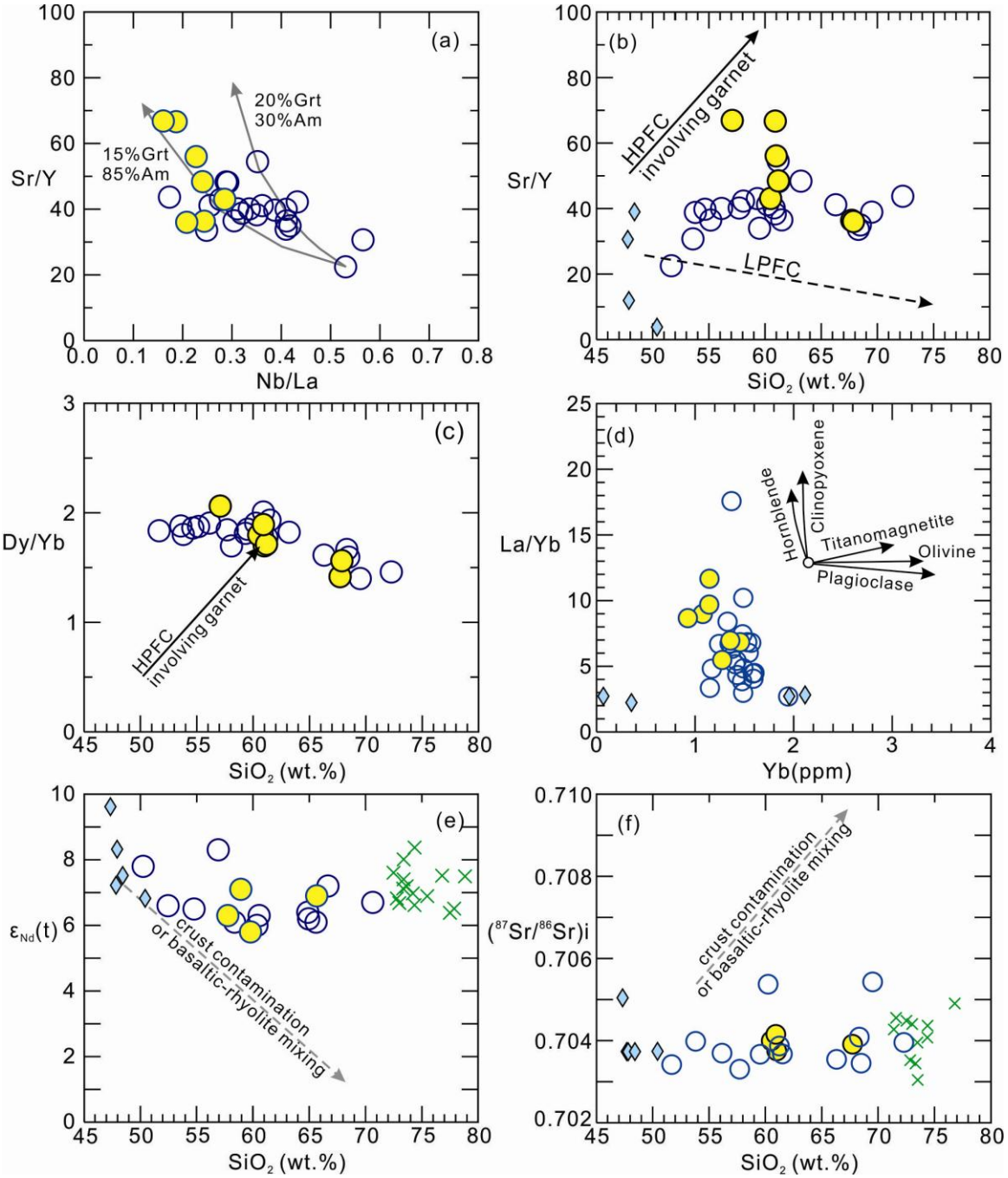


Fig. 8. (a) Nb/La versus Sr/Y; (b) $SiO_2$ versus Sr/Y; (c) $SiO_2$ versus Dy/Yb; (d) Yb versus La/Yb, crystal fractionation paths of the primary minerals are from Castillo et al. (1999). (e) $SiO_2$ versus $\varepsilon_{Nd}(t)$; and (f) $SiO_2$ versus $(^{87}Sr/^{86}Sr)_i$ plots. HPFC, high-pressure fractional crystallization involving garnet (Macpherson et al., 2006); LPFC: crystal

fractionation of an island arc tholeiite series basalt (Danyushevsky et al., 2008). Fractional crystallization models with different proportions of fractionating amphibole and garnet are shown in (b), using sample 06XJ143 as initial magma ($SiO_2$ = 50.24 wt.%; MgO = 8.46 wt.%). Partition coefficients are after Mori et al. (2007) and references therein: $D_{Nb}$ = 0.4945, $D_{La}$ = 0.0513, $D_{Sr}$ = 0.1095, $D_Y$=1.0291. Data sources and symbols are the same as in Fig. 5.

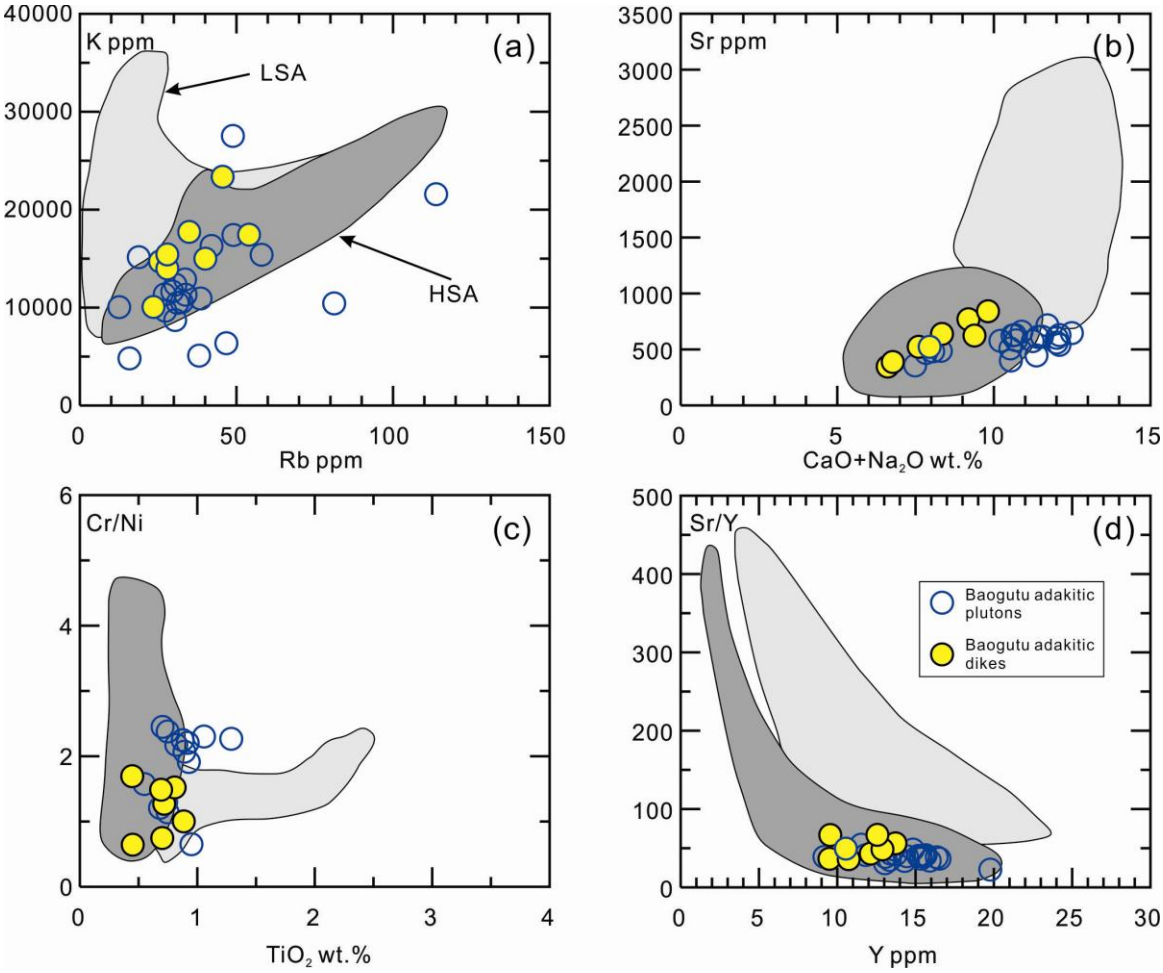


Fig. 9. Comparison between the geochemical characteristices of the Baogutu adakitic rocks and the key geochemical parameters used by Martin et al. (2005) to highlight the differences between high-$SiO_2$ (HSA) and low-$SiO_2$ (LSA) adakites., (a) K ppm vs Rb ppm; (b) Sr vs CaO+$Na_2O$; (c) Cr/Ni vs $TiO_2$; (d) Sr/Y vs Y.

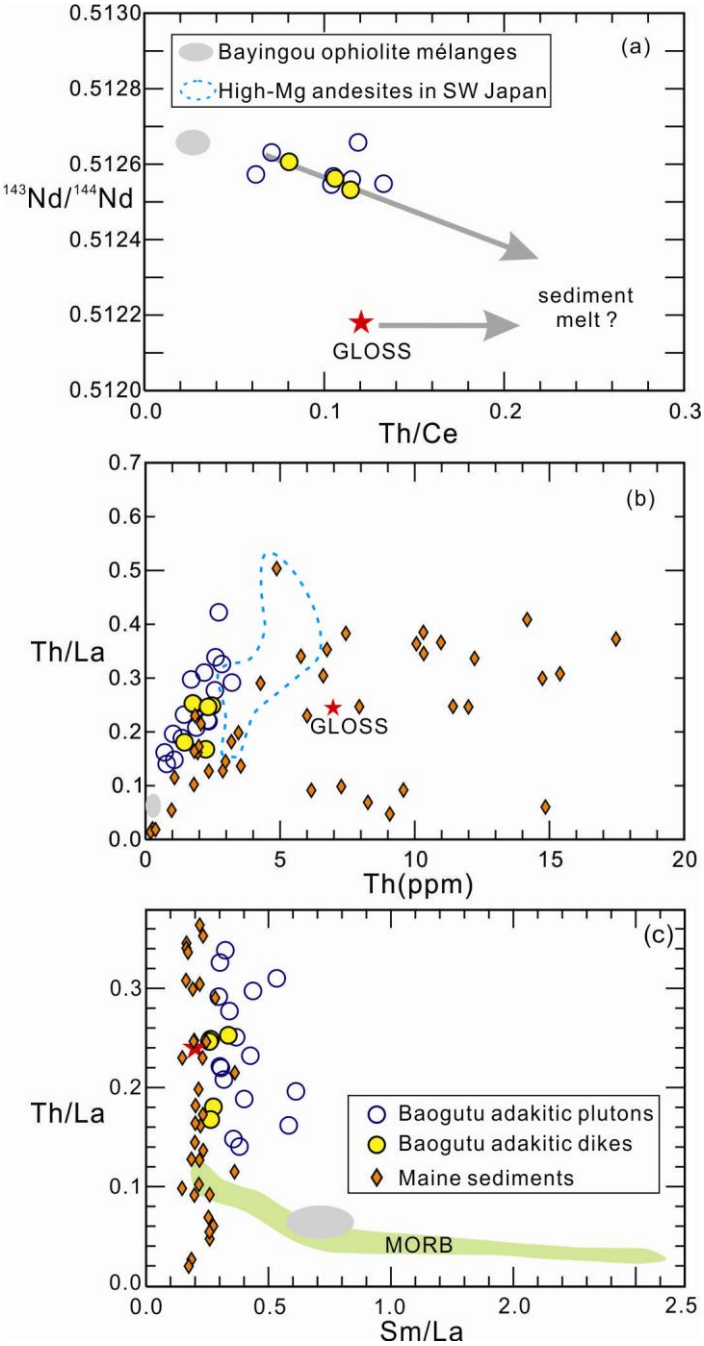


1350

1351 Fig. 10. (a) Th/Ce versus $^{143}Nd/^{144}Nd$ ratios diagram, illustrating a negative correlation
1352 for the Baogutu samples. The data set was first filtered to exclude all samples with $SiO_2$ >
1353 64 wt.%, in order to eliminate late possible AFC processes (Turner et al., 2003). (b) Plot
1354 of Th versus Th/La. (c) Sm/La versus Th/La plot after the concept of Plank (2005). Data
1355 sources of the Baogutu samples, Bayingou ophiolite mélanges, high-Mg andesites of SW
1356 Japan, marine sediments and GLOSS are the same as for Figs. 5 and 7.

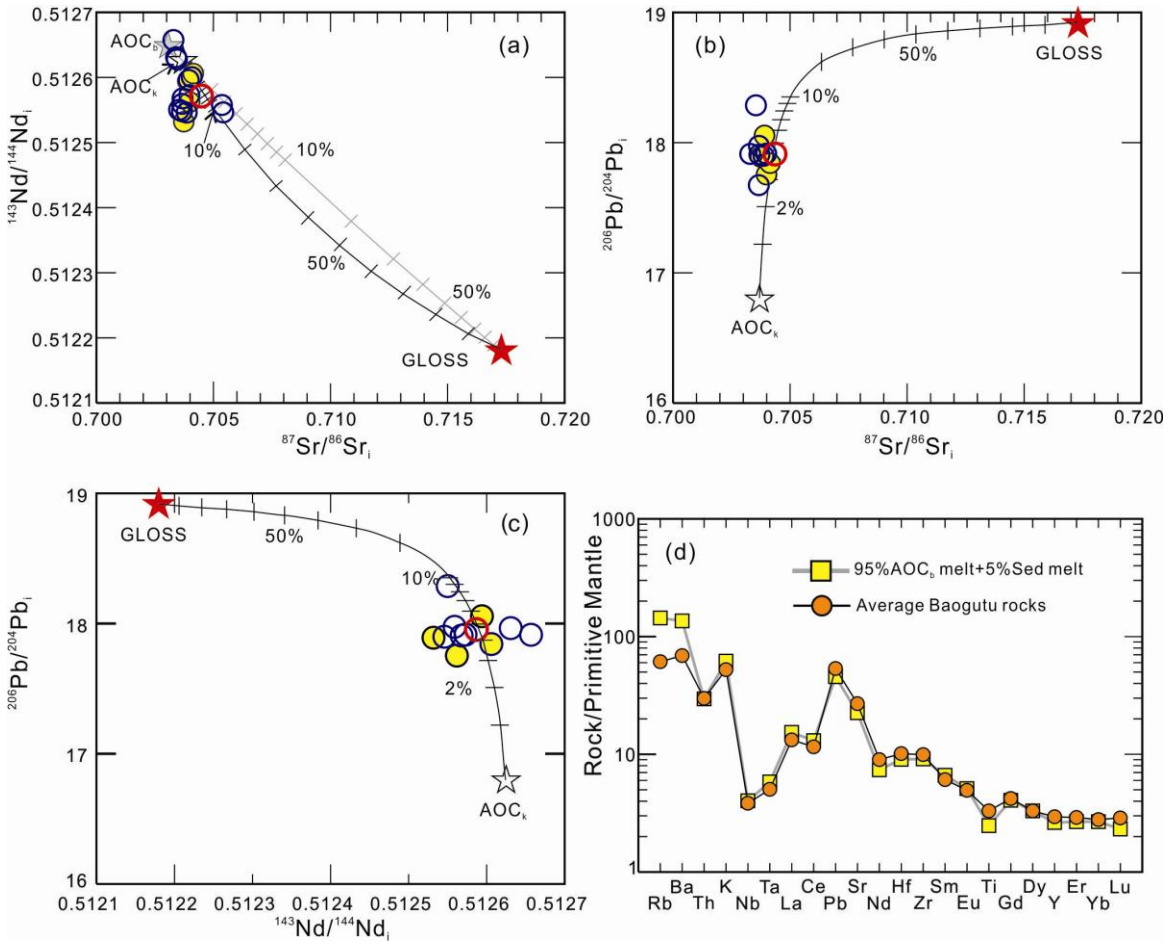


Fig. 11. Simple mixing modeling results of subducted oceanic crust and overlying sediments for the studied rock suites for (a) Sr-Nd, (b) Sr-Pb and (c) Nd-Pb isotopic spaces, and model primitive mantle normalized trace element pattern compared with an average Baogutu adakitc rock (d). The trace element pattern of an average Baogutu adakitc rock is closely matched by a mixture of 95% AOC melt and 5% sediment melt (red circles), except for the fluid mobile elements. $AOC_b$ = Bayingou ophiolite m danges in the North Tianshan (Xu et al., 2006c); $AOC_k$ = Kexi basalt in the western Junggar Basin from Zheng et al. (2007). Bulk solid/melt partition coefficients of andesitic-dacitic melts in equilibrium with a garnet amphibolite residuum (45% Cpx (clinopyroxene), 5% Gt (garnet), and 50% Amph (amphibolite)). Individual mineral $K_d$ values are from Rollinson (1993) and references therein, Barth et al. (2002), Klemme et al. (2005), and the Geochemical Earth Reference Model (GERM) (http://www.earthref.org). Bulk

solid/melt partition coefficients for sediment melting are from Johnson and Plank (1999). Composition of AOC and GLOSS melts are based on the assumption of 5% and 10% batch melting, respectively. The Baogutu samples and GLOSS are the same as in Fig. 5.

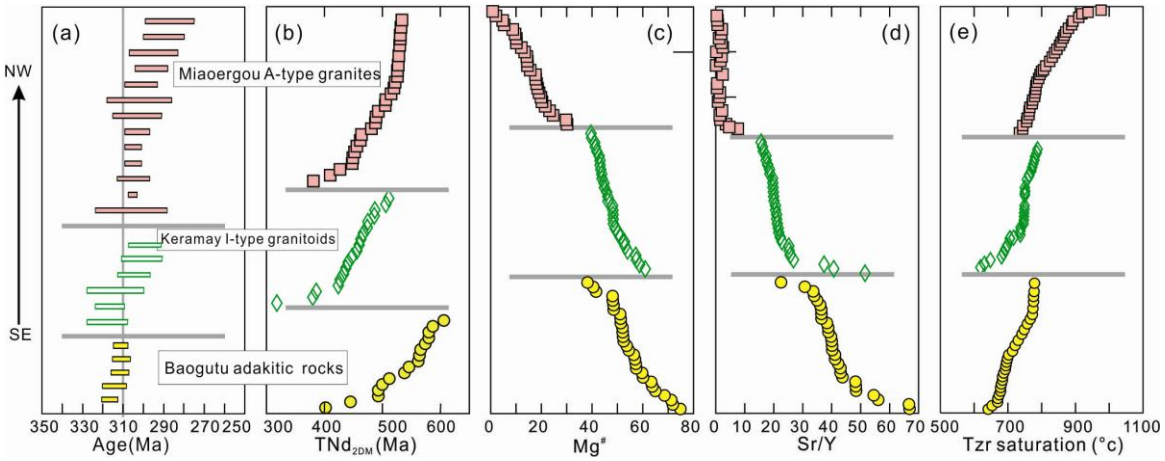


Fig. 12. Variation of zircon U-Pb ages (a), Nd isotopic model ages (b), $Mg^{\#}$, (c), Sr/Y (d), and zircon saturation temperatures (e) versus distance along a southeast to northwest traverse in the central zone of the western Junggar magmatic province. Zircon U-Pb ages are from Han et al. (2006), Su et al. (2006), Geng et al. (2009) and this study. Others data sources are the same as for Fig. 5.

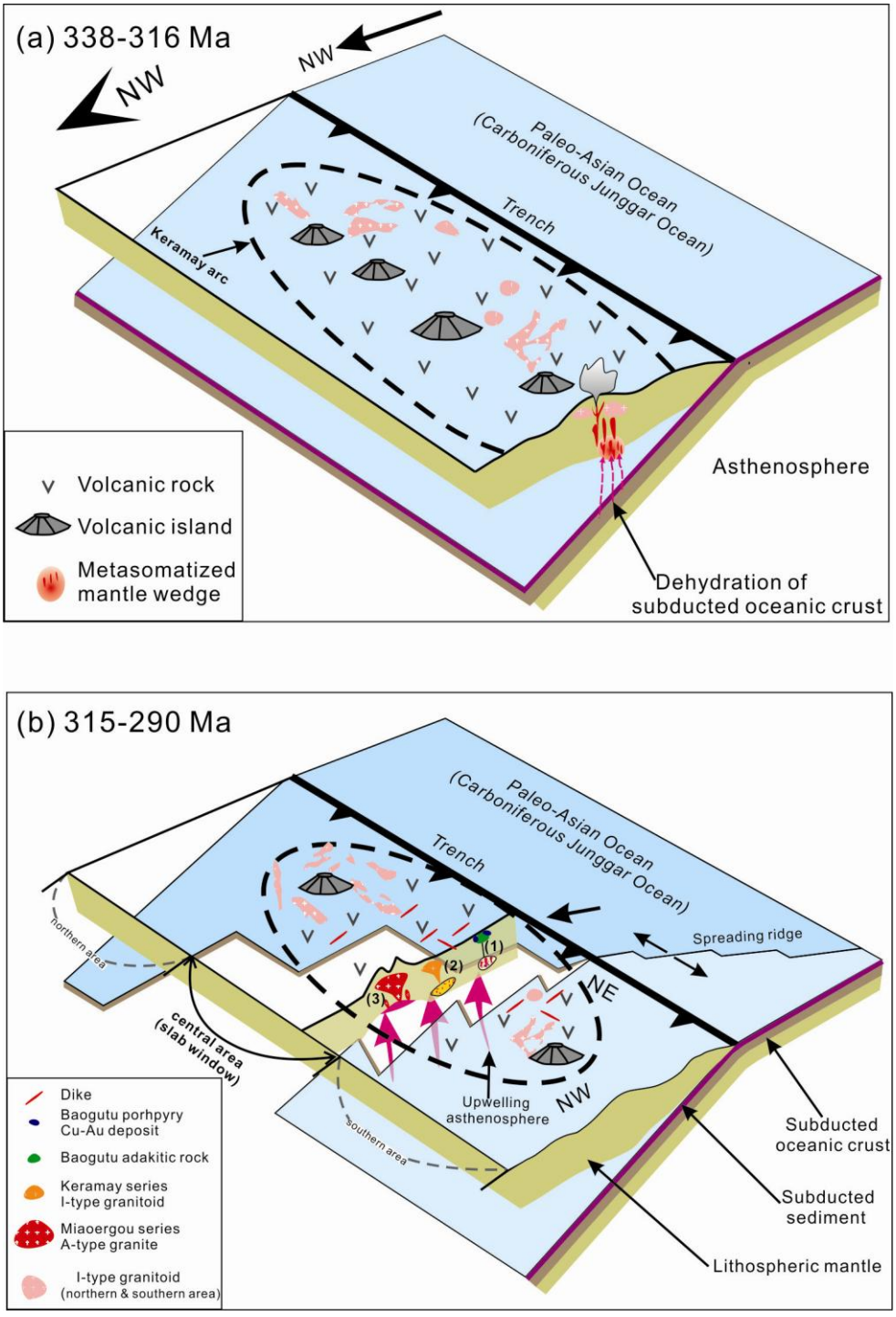


Fig. 13. Suggested tectonic model for the Carboniferous to Early Permian magmatic province in the western Junggar region. (a) 338-316 Ma: A Paleo-Asia Ocean plate subducting northwestward beneath the Keramay arc; fluids released from the subducted oceanic crust led to partial melting of mantle wedge and the formation of 338-316 Ma volcanic rocks and I-type granitoids. (b) 315-290 Ma: Formation of a slab window in the

central area of the Keramay due to a spreading ridge subduction. (1) Partial melting of subducted slab edge, and subsequent melt-mantle interaction, producing the Baogutu low Mg ($Mg^{\#}$ < 48) adakitic rocks and high Mg ($Mg^{\#}$ > 48) diorites, respectively. (2) Fractional crystallization of a mantle-derived magma, which was metasomatized by fluids released from subducted oceanic slab, to generate the I-type granitoids. (3) Partial melting of the juvenile lower crust triggered by upwelling asthenosphere through a slab window, to form the A-type granites. Other symbols are the same as in Fig. 1b.

1392 Appendix 1 LA-ICP-MS U-Pb isotopic analyses for zircons from the ore-porphyries in the West Junggar

| Analysis | Content (ppm) | | | Isotopic ratios | | | | | | Isotopic ages (Ma) | | | | | |
|---|---|---|---|---|---|---|---|---|---|---|---|---|---|---|---|
| | Th | U | Th/U | $^{207}Pb/^{206}Pb$ | ±1σ | $^{207}Pb/^{235}U$ | ±1σ | $^{206}Pb/^{238}U$ | ±1σ | $^{207}Pb/^{206}Pb$ | ±1σ | $^{207}Pb/^{235}U$ | ±1σ | $^{206}Pb/^{238}U$ | ±1σ |
| **06XJ145** | | | | | | | | | | | | | | | |
| 1 | 31 | 64 | 0.48 | 0.0541 | 0.0018 | 0.3763 | 0.0123 | 0.0505 | 0.0007 | 375 | 49 | 324 | 9 | 317 | 4 |
| 2 | 227 | 331 | 0.68 | 0.0565 | 0.0010 | 0.3933 | 0.0071 | 0.0504 | 0.0006 | 474 | 20 | 337 | 5 | 317 | 4 |
| 3 | 46 | 83 | 0.55 | 0.0551 | 0.0019 | 0.3854 | 0.0132 | 0.0507 | 0.0007 | 417 | 52 | 331 | 10 | 319 | 4 |
| 4 | 57 | 118 | 0.48 | 0.0522 | 0.0017 | 0.3660 | 0.0117 | 0.0508 | 0.0007 | 295 | 48 | 317 | 9 | 320 | 4 |
| 5 | 155 | 199 | 0.78 | 0.0506 | 0.0014 | 0.3558 | 0.0097 | 0.0510 | 0.0007 | 224 | 39 | 309 | 7 | 320 | 4 |
| 6 | 90 | 190 | 0.47 | 0.0540 | 0.0022 | 0.3734 | 0.0152 | 0.0502 | 0.0008 | 369 | 65 | 322 | 11 | 316 | 5 |
| 7 | 54 | 98 | 0.55 | 0.0558 | 0.0016 | 0.3894 | 0.0110 | 0.0507 | 0.0007 | 442 | 39 | 334 | 8 | 319 | 4 |
| 8 | 341 | 259 | 1.32 | 0.0542 | 0.0014 | 0.3701 | 0.0099 | 0.0495 | 0.0006 | 380 | 37 | 320 | 7 | 311 | 4 |
| 9 | 109 | 176 | 0.62 | 0.0580 | 0.0023 | 0.3912 | 0.0150 | 0.0489 | 0.0007 | 531 | 59 | 335 | 11 | 308 | 4 |
| 10 | 36 | 71 | 0.51 | 0.0506 | 0.0029 | 0.3483 | 0.0197 | 0.0500 | 0.0009 | 220 | 99 | 303 | 15 | 314 | 5 |
| 11 | 70 | 125 | 0.56 | 0.0544 | 0.0016 | 0.3766 | 0.0108 | 0.0502 | 0.0007 | 386 | 41 | 325 | 8 | 316 | 4 |
| 12 | 90 | 168 | 0.54 | 0.0526 | 0.0012 | 0.3558 | 0.0084 | 0.0491 | 0.0006 | 310 | 31 | 309 | 6 | 309 | 4 |
| 13 | 61 | 108 | 0.56 | 0.0532 | 0.0014 | 0.3674 | 0.0096 | 0.0501 | 0.0007 | 336 | 36 | 318 | 7 | 315 | 4 |
| 14 | 133 | 353 | 0.38 | 0.0584 | 0.0014 | 0.4820 | 0.0119 | 0.0598 | 0.0008 | 546 | 32 | 399 | 8 | 375 | 5 |
| 15 | 122 | 145 | 0.84 | 0.0627 | 0.0014 | 0.4264 | 0.0097 | 0.0493 | 0.0006 | 698 | 28 | 361 | 7 | 310 | 4 |
| 16 | 292 | 477 | 0.61 | 0.0589 | 0.0010 | 0.4695 | 0.0081 | 0.0578 | 0.0007 | 563 | 18 | 391 | 6 | 362 | 4 |
| 17 | 142 | 144 | 0.99 | 0.0568 | 0.0014 | 0.3943 | 0.0094 | 0.0503 | 0.0006 | 484 | 31 | 337 | 7 | 317 | 4 |
| 18 | 142 | 235 | 0.60 | 0.0563 | 0.0012 | 0.3834 | 0.0081 | 0.0494 | 0.0006 | 465 | 26 | 330 | 6 | 311 | 4 |
| 19 | 297 | 298 | 0.99 | 0.0552 | 0.0011 | 0.3851 | 0.0076 | 0.0506 | 0.0006 | 419 | 23 | 331 | 6 | 318 | 4 |
| 20 | 268 | 552 | 0.49 | 0.0586 | 0.0010 | 0.4736 | 0.0083 | 0.0586 | 0.0007 | 554 | 19 | 394 | 6 | 367 | 4 |
| 21 | 62 | 82 | 0.76 | 0.0543 | 0.0026 | 0.3687 | 0.0176 | 0.0492 | 0.0008 | 385 | 78 | 319 | 13 | 310 | 5 |
| 22 | 119 | 178 | 0.67 | 0.0578 | 0.0015 | 0.3991 | 0.0102 | 0.0501 | 0.0007 | 522 | 33 | 341 | 7 | 315 | 4 |
| 23 | 131 | 193 | 0.68 | 0.0578 | 0.0013 | 0.4793 | 0.0112 | 0.0601 | 0.0008 | 522 | 29 | 398 | 8 | 376 | 5 |
| 24 | 405 | 419 | 0.97 | 0.0585 | 0.0019 | 0.4026 | 0.0132 | 0.0500 | 0.0007 | 547 | 47 | 344 | 10 | 314 | 4 |
| 25 | 165 | 204 | 0.81 | 0.0525 | 0.0013 | 0.3677 | 0.0093 | 0.0508 | 0.0007 | 307 | 35 | 318 | 7 | 319 | 4 |
| 26 | 155 | 328 | 0.47 | 0.0563 | 0.0011 | 0.4477 | 0.0088 | 0.0577 | 0.0007 | 465 | 23 | 376 | 6 | 361 | 4 |

1393

1394 Appendix 1 Continued

| Analysis | Content (ppm) | | | Isotopic ratios | | | | | | Isotopic ages (Ma) | | | | | |
|---|---|---|---|---|---|---|---|---|---|---|---|---|---|---|---|
| | Th | U | Th/U | $^{207}Pb/^{206}Pb$ | ±1σ | $^{207}Pb/^{235}U$ | ±1σ | $^{206}Pb/^{238}U$ | ±1σ | $^{207}Pb/^{206}Pb$ | ±1σ | $^{207}Pb/^{235}U$ | ±1σ | $^{206}Pb/^{238}U$ | ±1σ |
| **06XJ147** | | | | | | | | | | | | | | | |
| 1 | 59 | 84 | 0.70 | 0.0566 | 0.0020 | 0.3856 | 0.0134 | 0.0494 | 0.0007 | 477 | 53 | 331 | 10 | 311 | 4 |
| 2 | 97 | 126 | 0.77 | 0.0582 | 0.0037 | 0.3923 | 0.0246 | 0.0488 | 0.0009 | 539 | 104 | 336 | 18 | 307 | 6 |
| 3 | 57 | 68 | 0.84 | 0.0554 | 0.0021 | 0.3820 | 0.0146 | 0.0501 | 0.0007 | 426 | 60 | 329 | 11 | 315 | 4 |
| 4 | 69 | 80 | 0.87 | 0.0511 | 0.0016 | 0.3526 | 0.0108 | 0.0501 | 0.0007 | 244 | 47 | 307 | 8 | 315 | 4 |
| 5 | 61 | 83 | 0.73 | 0.0564 | 0.0016 | 0.3845 | 0.0110 | 0.0494 | 0.0006 | 469 | 41 | 330 | 8 | 311 | 4 |
| 6 | 103 | 119 | 0.86 | 0.0562 | 0.0018 | 0.3819 | 0.0119 | 0.0493 | 0.0007 | 460 | 45 | 328 | 9 | 310 | 4 |
| 7 | 77 | 93 | 0.83 | 0.0530 | 0.0017 | 0.3572 | 0.0114 | 0.0489 | 0.0007 | 328 | 48 | 310 | 9 | 308 | 4 |
| 8 | 36 | 56 | 0.64 | 0.0479 | 0.0028 | 0.3274 | 0.0190 | 0.0495 | 0.0009 | 96 | 97 | 288 | 15 | 312 | 5 |
| 9 | 51 | 66 | 0.78 | 0.0525 | 0.0018 | 0.3571 | 0.0122 | 0.0493 | 0.0007 | 309 | 53 | 310 | 9 | 310 | 4 |
| 10 | 46 | 61 | 0.75 | 0.0622 | 0.0019 | 0.4309 | 0.0133 | 0.0502 | 0.0007 | 682 | 43 | 364 | 9 | 316 | 4 |
| 11 | 53 | 77 | 0.68 | 0.0612 | 0.0037 | 0.4139 | 0.0244 | 0.0490 | 0.0009 | 647 | 95 | 352 | 18 | 309 | 6 |
| 12 | 70 | 86 | 0.81 | 0.0578 | 0.0015 | 0.3915 | 0.0103 | 0.0491 | 0.0006 | 523 | 35 | 335 | 8 | 309 | 4 |
| 13 | 67 | 90 | 0.75 | 0.0585 | 0.0020 | 0.4022 | 0.0136 | 0.0498 | 0.0007 | 550 | 49 | 343 | 10 | 313 | 4 |
| 14 | 45 | 57 | 0.78 | 0.0570 | 0.0034 | 0.3926 | 0.0228 | 0.0499 | 0.0009 | 492 | 96 | 336 | 17 | 314 | 6 |
| 15 | 50 | 63 | 0.79 | 0.0550 | 0.0020 | 0.3733 | 0.0135 | 0.0493 | 0.0007 | 410 | 55 | 322 | 10 | 310 | 4 |
| 16 | 51 | 75 | 0.68 | 0.0597 | 0.0020 | 0.4028 | 0.0132 | 0.0489 | 0.0007 | 592 | 47 | 344 | 10 | 308 | 4 |
| 17 | 64 | 77 | 0.82 | 0.0582 | 0.0019 | 0.3922 | 0.0127 | 0.0489 | 0.0007 | 537 | 47 | 336 | 9 | 308 | 4 |
| 18 | 47 | 64 | 0.72 | 0.0604 | 0.0037 | 0.4130 | 0.0249 | 0.0496 | 0.0009 | 617 | 98 | 351 | 18 | 312 | 6 |
| 19 | 87 | 104 | 0.83 | 0.0521 | 0.0016 | 0.3528 | 0.0106 | 0.0491 | 0.0007 | 289 | 44 | 307 | 8 | 309 | 4 |
| 20 | 47 | 66 | 0.72 | 0.0744 | 0.0022 | 0.5058 | 0.0151 | 0.0493 | 0.0007 | 1052 | 38 | 416 | 10 | 310 | 4 |
| 21 | 53 | 72 | 0.73 | 0.0520 | 0.0016 | 0.3539 | 0.0105 | 0.0493 | 0.0007 | 286 | 43 | 308 | 8 | 310 | 4 |
| 22 | 60 | 86 | 0.70 | 0.0517 | 0.0031 | 0.3441 | 0.0203 | 0.0482 | 0.0009 | 274 | 102 | 300 | 15 | 304 | 5 |
| **06XJ153** | | | | | | | | | | | | | | | |
| 1 | 60 | 79 | 0.76 | 0.0554 | 0.0014 | 0.3800 | 0.0098 | 0.0498 | 0.0006 | 429 | 35 | 327 | 7 | 313 | 4 |
| 2 | 134 | 181 | 0.74 | 0.0604 | 0.0017 | 0.4203 | 0.0121 | 0.0505 | 0.0007 | 618 | 39 | 356 | 9 | 317 | 4 |
| 3 | 108 | 144 | 0.75 | 0.0524 | 0.0016 | 0.3518 | 0.0107 | 0.0487 | 0.0007 | 304 | 45 | 306 | 8 | 306 | 4 |

1395

1396 Appendix 1 Continued

| Analysis | Content (ppm) | | | Isotopic ratios | | | | | | Isotopic ages (Ma) | | | | | |
|---|---|---|---|---|---|---|---|---|---|---|---|---|---|---|---|
| | Th | U | Th/U | $^{207}Pb/^{206}Pb$ | ±1σ | $^{207}Pb/^{235}U$ | ±1σ | $^{206}Pb/^{238}U$ | ±1σ | $^{207}Pb/^{206}Pb$ | ±1σ | $^{207}Pb/^{235}U$ | ±1σ | $^{206}Pb/^{238}U$ | ±1σ |
| 4 | 184 | 600 | 0.31 | 0.1522 | 0.0021 | 2.6299 | 0.0382 | 0.1254 | 0.0015 | 2370 | 11 | 1309 | 11 | 761 | 9 |
| 5 | 140 | 378 | 0.37 | 0.0646 | 0.0013 | 0.5174 | 0.0103 | 0.0581 | 0.0007 | 761 | 22 | 423 | 7 | 364 | 4 |
| 6 | 53 | 60 | 0.88 | 0.0517 | 0.0041 | 0.3542 | 0.0278 | 0.0497 | 0.0011 | 272 | 140 | 308 | 21 | 313 | 6 |
| 7 | 55 | 129 | 0.43 | 0.0518 | 0.0012 | 0.3592 | 0.0085 | 0.0503 | 0.0006 | 274 | 31 | 312 | 6 | 317 | 4 |
| 8 | 27 | 44 | 0.61 | 0.0668 | 0.0024 | 0.4667 | 0.0168 | 0.0507 | 0.0007 | 830 | 51 | 389 | 12 | 319 | 5 |
| 9 | 22 | 34 | 0.65 | 0.0674 | 0.0030 | 0.4561 | 0.0200 | 0.0491 | 0.0008 | 850 | 65 | 382 | 14 | 309 | 5 |
| 10 | 37 | 51 | 0.72 | 0.0584 | 0.0032 | 0.3931 | 0.0209 | 0.0489 | 0.0008 | 544 | 86 | 337 | 15 | 307 | 5 |
| 11 | 47 | 95 | 0.49 | 0.0500 | 0.0015 | 0.3457 | 0.0105 | 0.0502 | 0.0007 | 193 | 45 | 301 | 8 | 316 | 4 |
| 12 | 111 | 167 | 0.66 | 0.0580 | 0.0017 | 0.4379 | 0.0127 | 0.0548 | 0.0007 | 529 | 40 | 369 | 9 | 344 | 5 |
| 13 | 128 | 195 | 0.66 | 0.0645 | 0.0019 | 0.4442 | 0.0129 | 0.0500 | 0.0007 | 757 | 39 | 373 | 9 | 314 | 4 |
| 14 | 741 | 506 | 1.46 | 0.0554 | 0.0010 | 0.3853 | 0.0071 | 0.0504 | 0.0006 | 429 | 21 | 331 | 5 | 317 | 4 |
| 15 | 63 | 91 | 0.69 | 0.0586 | 0.0024 | 0.4132 | 0.0164 | 0.0512 | 0.0008 | 550 | 60 | 351 | 12 | 322 | 5 |
| 16 | 87 | 183 | 0.47 | 0.0515 | 0.0012 | 0.3489 | 0.0080 | 0.0491 | 0.0006 | 263 | 30 | 304 | 6 | 309 | 4 |
| 17 | 825 | 1712 | 0.48 | 0.0545 | 0.0014 | 0.3788 | 0.0095 | 0.0504 | 0.0007 | 392 | 33 | 326 | 7 | 317 | 4 |
| 18 | 329 | 263 | 1.25 | 0.0559 | 0.0014 | 0.3772 | 0.0093 | 0.0489 | 0.0006 | 448 | 32 | 325 | 7 | 308 | 4 |
| 19 | 101 | 100 | 1.01 | 0.0618 | 0.0039 | 0.4124 | 0.0256 | 0.0484 | 0.0009 | 668 | 100 | 351 | 18 | 305 | 6 |
| 20 | 361 | 381 | 0.95 | 0.0567 | 0.0015 | 0.4014 | 0.0105 | 0.0513 | 0.0007 | 480 | 35 | 343 | 8 | 323 | 4 |
| **06XJ156** | | | | | | | | | | | | | | | |
| 1 | 44 | 85 | 0.52 | 0.0542 | 0.0028 | 0.3640 | 0.0181 | 0.0487 | 0.0007 | 380 | 120 | 315 | 13 | 306 | 4 |
| 2 | 41 | 79 | 0.52 | 0.0546 | 0.0016 | 0.3730 | 0.0110 | 0.0495 | 0.0007 | 396 | 42 | 322 | 8 | 312 | 4 |
| 3 | 36 | 67 | 0.54 | 0.0506 | 0.0025 | 0.3410 | 0.0167 | 0.0489 | 0.0008 | 222 | 83 | 298 | 13 | 308 | 5 |
| 4 | 51 | 98 | 0.52 | 0.0694 | 0.0021 | 0.4744 | 0.0144 | 0.0496 | 0.0007 | 909 | 39 | 394 | 10 | 312 | 4 |
| 5 | 30 | 56 | 0.53 | 0.0531 | 0.0029 | 0.3573 | 0.0190 | 0.0488 | 0.0008 | 331 | 89 | 310 | 14 | 307 | 5 |
| 6 | 37 | 67 | 0.55 | 0.0530 | 0.0028 | 0.3578 | 0.0183 | 0.0489 | 0.0007 | 330 | 124 | 311 | 14 | 308 | 4 |
| 7 | 45 | 84 | 0.53 | 0.0534 | 0.0030 | 0.3601 | 0.0199 | 0.0489 | 0.0009 | 348 | 93 | 312 | 15 | 308 | 5 |
| 8 | 42 | 75 | 0.57 | 0.1004 | 0.0036 | 0.6805 | 0.0237 | 0.0492 | 0.0008 | 1632 | 41 | 527 | 14 | 309 | 5 |
| 9 | 67 | 115 | 0.58 | 0.0614 | 0.0035 | 0.4118 | 0.0227 | 0.0487 | 0.0009 | 652 | 87 | 350 | 16 | 306 | 5 |

1397

1398 Appendix 1 Continued

| Analysis | Content (ppm) | | | Isotopic ratios | | | | | | Isotopic ages (Ma) | | | | | |
|---|---|---|---|---|---|---|---|---|---|---|---|---|---|---|---|
| | Th | U | Th/U | $^{207}Pb/^{206}Pb$ | ±1σ | $^{207}Pb/^{235}U$ | ±1σ | $^{206}Pb/^{238}U$ | ±1σ | $^{207}Pb/^{206}Pb$ | ±1σ | $^{207}Pb/^{235}U$ | ±1σ | $^{206}Pb/^{238}U$ | ±1σ |
| 10 | 36 | 69 | 0.52 | 0.0586 | 0.0033 | 0.3914 | 0.0211 | 0.0484 | 0.0008 | 553 | 125 | 335 | 15 | 305 | 5 |
| 11 | 51 | 87 | 0.58 | 0.0887 | 0.0032 | 0.5818 | 0.0208 | 0.0476 | 0.0008 | 1398 | 44 | 466 | 13 | 300 | 5 |
| 12 | 38 | 65 | 0.58 | 0.0546 | 0.0039 | 0.3669 | 0.0258 | 0.0488 | 0.0008 | 395 | 167 | 317 | 19 | 307 | 5 |
| 13 | 35 | 69 | 0.51 | 0.0595 | 0.0021 | 0.4056 | 0.0146 | 0.0494 | 0.0007 | 586 | 54 | 346 | 11 | 311 | 4 |
| 14 | 32 | 63 | 0.51 | 0.0631 | 0.0035 | 0.4182 | 0.0226 | 0.0481 | 0.0007 | 712 | 123 | 355 | 16 | 303 | 4 |
| 15 | 40 | 72 | 0.55 | 0.0529 | 0.0029 | 0.3544 | 0.0190 | 0.0486 | 0.0007 | 323 | 129 | 308 | 14 | 306 | 4 |
| 16 | 51 | 86 | 0.60 | 0.0535 | 0.0030 | 0.3567 | 0.0193 | 0.0484 | 0.0007 | 350 | 131 | 310 | 14 | 304 | 4 |
| 17 | 45 | 84 | 0.54 | 0.0533 | 0.0019 | 0.3624 | 0.0126 | 0.0494 | 0.0007 | 339 | 53 | 314 | 9 | 311 | 4 |
| 18 | 42 | 80 | 0.52 | 0.0615 | 0.0029 | 0.4199 | 0.0189 | 0.0496 | 0.0007 | 655 | 104 | 356 | 14 | 312 | 4 |
| 19 | 49 | 60 | 0.81 | 0.0649 | 0.0039 | 0.4327 | 0.0252 | 0.0483 | 0.0008 | 772 | 131 | 365 | 18 | 304 | 5 |
| 20 | 54 | 68 | 0.80 | 0.0679 | 0.0041 | 0.4612 | 0.0266 | 0.0493 | 0.0008 | 864 | 127 | 385 | 18 | 310 | 5 |
| 21 | 46 | 78 | 0.59 | 0.0531 | 0.0028 | 0.3615 | 0.0184 | 0.0494 | 0.0007 | 335 | 123 | 313 | 14 | 311 | 4 |
| 22 | 54 | 91 | 0.59 | 0.0583 | 0.0027 | 0.3932 | 0.0176 | 0.0489 | 0.0007 | 541 | 106 | 337 | 13 | 308 | 4 |
| 23 | 90 | 91 | 1.00 | 0.0884 | 0.0049 | 0.5773 | 0.0305 | 0.0474 | 0.0008 | 1390 | 109 | 463 | 20 | 298 | 5 |
| 24 | 51 | 81 | 0.63 | 0.0607 | 0.0027 | 0.4068 | 0.0177 | 0.0486 | 0.0008 | 628 | 66 | 347 | 13 | 306 | 5 |
| 25 | 49 | 84 | 0.58 | 0.0609 | 0.0033 | 0.4067 | 0.0209 | 0.0485 | 0.0007 | 635 | 118 | 346 | 15 | 305 | 4 |
| 26 | 45 | 82 | 0.54 | 0.0547 | 0.0032 | 0.3664 | 0.0205 | 0.0486 | 0.0008 | 399 | 134 | 317 | 15 | 306 | 5 |
| 27 | 51 | 82 | 0.62 | 0.0567 | 0.0024 | 0.3808 | 0.0162 | 0.0487 | 0.0008 | 478 | 66 | 328 | 12 | 307 | 5 |
| 28 | 47 | 82 | 0.58 | 0.0584 | 0.0030 | 0.3945 | 0.0191 | 0.0490 | 0.0007 | 544 | 114 | 338 | 14 | 309 | 4 |
| 29 | 51 | 71 | 0.72 | 0.0669 | 0.0045 | 0.4372 | 0.0285 | 0.0474 | 0.0008 | 833 | 144 | 368 | 20 | 299 | 5 |
| 30 | 26 | 41 | 0.65 | 0.0714 | 0.0081 | 0.4833 | 0.0538 | 0.0491 | 0.0012 | 968 | 244 | 400 | 37 | 309 | 8 |

1399

1400

Appendix 2 Major element compositions (wt %) of clinopyroxene and plagioclase from the Baogutu adakitic ore-porphyries

| Spot | Crystal | Zone | SiO2 | TiO2 | Al2O3 | Cr2O3 | FeO | MnO | MgO | CaO | Na2O | K2O | Total | Wo | En | Fs | Mg# |
|---|---|---|---|---|---|---|---|---|---|---|---|---|---|---|---|---|---|
| 1 | 1 | R | 51.53 | 0.27 | 1.70 | | 8.66 | 0.27 | 14.41 | 22.70 | 0.37 | 0.01 | 100.08 | 45.1 | 39.8 | 13.7 | 74.8 |
| 2 | 1 | R | 51.61 | 0.41 | 1.57 | 0.02 | 8.37 | 0.26 | 15.00 | 22.59 | 0.39 | 0.00 | 100.23 | 44.5 | 41.1 | 13.1 | 76.2 |
| 3 | 1 | R | 53.24 | 0.55 | 1.67 | 0.04 | 8.66 | 0.25 | 14.88 | 20.20 | 0.44 | | 99.94 | 41.5 | 42.6 | 14.3 | 75.4 |
| 4 | 1 | R | 51.20 | 0.48 | 1.57 | | 9.27 | 0.27 | 14.68 | 21.67 | 0.38 | 0.02 | 99.54 | 43.2 | 40.7 | 14.7 | 73.8 |
| 5 | 1 | C | 51.11 | 0.49 | 1.87 | 0.09 | 9.78 | 0.26 | 14.69 | 21.16 | 0.41 | 0.01 | 99.87 | 42.2 | 40.8 | 15.5 | 72.8 |
| 6 | 1 | C | 51.02 | 0.38 | 1.41 | | 9.54 | 0.31 | 14.45 | 21.66 | 0.32 | 0.03 | 99.11 | 43.4 | 40.3 | 15.3 | 73.0 |
| 7 | 1 | C | 50.42 | 0.56 | 2.32 | 0.10 | 9.88 | 0.23 | 14.52 | 21.22 | 0.41 | 0.02 | 99.67 | 42.5 | 40.4 | 15.6 | 72.4 |
| 8 | 1 | C | 49.92 | 0.62 | 3.18 | 0.30 | 9.97 | 0.22 | 13.91 | 21.67 | 0.49 | 0.01 | 100.28 | 43.5 | 38.9 | 15.8 | 71.3 |
| 9 | 1 | C | 51.21 | 0.48 | 1.54 | 0.02 | 9.27 | 0.24 | 14.43 | 21.69 | 0.40 | 0.00 | 99.28 | 43.5 | 40.3 | 14.8 | 73.5 |
| 10 | 1 | C | 50.70 | 0.56 | 1.88 | | 10.12 | 0.33 | 14.31 | 21.53 | 0.39 | 0.01 | 99.81 | 42.9 | 39.7 | 16.1 | 71.6 |
| 11 | 1 | C | 50.13 | 0.59 | 2.65 | 0.31 | 9.87 | 0.27 | 14.16 | 21.19 | 0.50 | | 99.68 | 42.7 | 39.7 | 15.8 | 71.9 |
| 12 | 1 | C | 50.05 | 0.58 | 2.77 | 0.43 | 10.12 | 0.27 | 14.11 | 21.00 | 0.41 | 0.02 | 99.74 | 42.5 | 39.7 | 16.2 | 71.3 |
| 13 | 1 | C | 50.50 | 0.49 | 2.69 | 0.45 | 9.58 | 0.25 | 14.38 | 20.91 | 0.43 | 0.02 | 99.71 | 42.4 | 40.6 | 15.4 | 72.8 |
| 14 | 1 | C | 50.28 | 0.54 | 2.42 | 0.10 | 10.22 | 0.27 | 14.25 | 21.18 | 0.46 | | 99.71 | 42.4 | 39.7 | 16.2 | 71.3 |
| 15 | 1 | R | 51.30 | 0.45 | 1.59 | 0.02 | 9.41 | 0.27 | 14.98 | 21.88 | 0.33 | 0.00 | 100.21 | 43.1 | 41.0 | 14.7 | 73.9 |
| 16 | 1 | R | 50.92 | 0.49 | 1.80 | 0.03 | 9.43 | 0.22 | 14.75 | 21.70 | 0.43 | | 99.78 | 43.0 | 40.7 | 14.8 | 73.6 |
| 17 | 1 | R | 51.45 | 0.46 | 1.63 | | 9.61 | 0.26 | 14.74 | 21.55 | 0.29 | 0.01 | 99.99 | 42.9 | 40.8 | 15.2 | 73.2 |
| 18 | 1 | R | 51.23 | 0.34 | 1.59 | 0.00 | 9.21 | 0.23 | 14.67 | 21.90 | 0.49 | 0.01 | 99.67 | 43.4 | 40.4 | 14.4 | 73.9 |
| 19 | 2 | R | 51.22 | 0.32 | 1.31 | | 8.88 | 0.28 | 14.57 | 22.73 | 0.33 | | 99.63 | 44.9 | 40.0 | 14.0 | 74.5 |
| 20 | 2 | R | 51.66 | 0.48 | 1.31 | 0.01 | 9.93 | 0.36 | 15.23 | 20.81 | 0.26 | 0.01 | 100.06 | 41.3 | 42.0 | 15.8 | 73.2 |
| 21 | 2 | R | 51.16 | 0.41 | 1.50 | | 9.60 | 0.25 | 14.82 | 21.72 | 0.30 | 0.00 | 99.77 | 43.0 | 40.8 | 15.1 | 73.3 |
| 22 | 2 | R | 51.17 | 0.30 | 1.29 | | 9.33 | 0.29 | 14.66 | 22.09 | 0.41 | 0.02 | 99.56 | 43.6 | 40.3 | 14.7 | 73.7 |
| 23 | 2 | C | 50.42 | 0.52 | 2.56 | 0.04 | 9.88 | 0.21 | 14.65 | 21.48 | 0.30 | 0.01 | 100.06 | 42.8 | 40.6 | 15.5 | 72.5 |
| 24 | 2 | C | 50.65 | 0.61 | 2.07 | 0.05 | 9.66 | 0.30 | 14.57 | 21.54 | 0.36 | 0.01 | 99.79 | 43.0 | 40.4 | 15.3 | 72.9 |
| 25 | 2 | C | 51.49 | 0.20 | 1.28 | 0.01 | 8.98 | 0.28 | 14.27 | 22.62 | 0.38 | | 99.53 | 44.9 | 39.5 | 14.2 | 73.9 |
| 26 | 2 | C | 50.94 | 0.42 | 1.51 | 0.02 | 9.77 | 0.33 | 14.29 | 21.96 | 0.40 | 0.01 | 99.64 | 43.6 | 39.5 | 15.5 | 72.2 |
| 27 | 2 | C | 50.63 | 0.64 | 2.36 | 0.01 | 9.57 | 0.27 | 13.99 | 22.16 | 0.42 | | 100.05 | 44.3 | 38.9 | 15.2 | 72.3 |
| 28 | 2 | C | 51.72 | 0.27 | 0.85 | 0.04 | 11.38 | 0.44 | 14.12 | 20.99 | 0.23 | 0.00 | 100.03 | 41.8 | 39.1 | 18.3 | 68.8 |
| 29 | 2 | C | 50.57 | 0.54 | 2.51 | 0.02 | 9.43 | 0.25 | 14.22 | 22.29 | 0.45 | | 100.27 | 44.3 | 39.3 | 14.8 | 72.9 |
| 30 | 2 | C | 51.47 | 0.60 | 1.87 | | 9.43 | 0.29 | 14.24 | 22.30 | 0.47 | | 100.67 | 44.2 | 39.3 | 14.9 | 72.9 |
| 31 | 2 | C | 50.81 | 0.56 | 2.33 | 0.00 | 9.41 | 0.30 | 13.95 | 22.05 | 0.50 | 0.02 | 99.92 | 44.2 | 38.9 | 15.1 | 72.5 |
| 32 | 2 | C | 50.88 | 0.64 | 2.43 | | 9.63 | 0.30 | 14.01 | 22.03 | 0.47 | | 100.39 | 44.0 | 38.9 | 15.3 | 72.2 |
| 33 | 2 | R | 51.59 | 0.28 | 0.98 | | 10.15 | 0.41 | 14.62 | 21.15 | 0.35 | 0.01 | 99.55 | 42.0 | 40.4 | 16.3 | 72.0 |
| 34 | 2 | R | 51.99 | 0.22 | 1.25 | | 9.32 | 0.27 | 14.66 | 21.90 | 0.41 | | 100.02 | 43.4 | 40.4 | 14.7 | 73.7 |
| 35 | 2 | R | 51.43 | 0.37 | 1.54 | | 9.66 | 0.30 | 14.65 | 22.02 | 0.39 | | 100.34 | 43.4 | 40.1 | 15.1 | 73.0 |
| 36 | 2 | R | 51.48 | 0.46 | 1.65 | 0.03 | 9.49 | 0.30 | 14.47 | 22.16 | 0.36 | 0.01 | 100.40 | 43.9 | 39.9 | 15.0 | 73.1 |
| 37 | 2 | R | 50.03 | 0.39 | 1.24 | 0.02 | 9.90 | 0.33 | 15.08 | 21.86 | 0.35 | | 99.20 | 42.6 | 40.9 | 15.3 | 73.1 |
| 38 | 3 | R | 51.28 | 0.41 | 1.64 | 0.02 | 10.11 | 0.40 | 15.14 | 21.24 | 0.36 | 0.01 | 100.61 | 41.6 | 41.2 | 15.9 | 72.7 |

Appendix 2 Continued

| | | | | | | | | | | | | | | | | | |
|---|---|---|---|---|---|---|---|---|---|---|---|---|---|---|---|---|---|
| 39 | 3 | R | 51.33 | 0.28 | 1.44 | 0.00 | 9.35 | 0.30 | 14.86 | 22.14 | 0.41 | 0.01 | 100.12 | 43.4 | 40.5 | 14.6 | 73.9 |
| 40 | 3 | R | 51.64 | 0.34 | 1.36 | 0.03 | 9.73 | 0.35 | 14.51 | 22.11 | 0.41 | 0.00 | 100.46 | 43.5 | 39.7 | 15.3 | 72.7 |
| 41 | 3 | R | 51.45 | 0.35 | 1.41 | | 9.33 | 0.28 | 14.51 | 22.09 | 0.43 | 0.02 | 99.85 | 43.8 | 40.0 | 14.7 | 73.5 |
| 42 | 3 | C | 51.53 | 0.20 | 1.29 | 0.01 | 8.58 | 0.31 | 14.27 | 22.94 | 0.34 | | 99.47 | 45.6 | 39.5 | 13.7 | 74.8 |
| 43 | 3 | C | 51.70 | 0.31 | 1.44 | 0.04 | 9.14 | 0.26 | 14.25 | 22.62 | 0.36 | 0.00 | 100.11 | 44.9 | 39.4 | 14.4 | 73.5 |
| 44 | 3 | C | 51.67 | 0.30 | 1.30 | | 9.27 | 0.29 | 14.10 | 22.87 | 0.37 | 0.00 | 100.18 | 45.3 | 38.8 | 14.6 | 73.0 |
| 45 | 3 | C | 51.53 | 0.48 | 1.34 | 0.03 | 9.42 | 0.30 | 14.42 | 22.48 | 0.39 | | 100.38 | 44.3 | 39.5 | 14.8 | 73.2 |
| 46 | 3 | C | 50.87 | 0.36 | 1.62 | 0.02 | 9.94 | 0.44 | 14.26 | 22.20 | 0.43 | 0.01 | 100.13 | 43.7 | 39.0 | 15.8 | 71.9 |
| 47 | 3 | C | 51.85 | 0.48 | 1.48 | 0.05 | 9.65 | 0.33 | 14.56 | 22.07 | 0.41 | 0.01 | 100.87 | 43.5 | 39.9 | 15.2 | 72.9 |
| 48 | 3 | C | 50.73 | 0.48 | 1.58 | 0.02 | 10.04 | 0.32 | 14.98 | 21.34 | 0.28 | | 99.77 | 42.1 | 41.1 | 15.8 | 72.7 |
| 49 | 3 | R | 51.33 | 0.40 | 1.48 | 0.01 | 9.80 | 0.30 | 14.54 | 22.00 | 0.43 | | 100.28 | 43.3 | 39.8 | 15.4 | 72.6 |
| 50 | 3 | R | 50.98 | 0.43 | 1.43 | | 10.26 | 0.37 | 15.23 | 21.26 | 0.42 | 0.01 | 100.37 | 41.4 | 41.2 | 15.9 | 72.6 |
| 51 | 3 | R | 51.23 | 0.47 | 1.52 | 0.03 | 10.21 | 0.33 | 15.17 | 21.34 | 0.40 | 0.01 | 100.71 | 41.6 | 41.1 | 15.9 | 72.6 |
| 52 | 3 | R | 50.92 | 0.20 | 2.63 | 0.68 | 6.11 | 0.14 | 15.20 | 23.13 | 0.44 | 0.01 | 99.46 | 46.4 | 42.4 | 9.7 | 81.6 |
| 53 | 3 | C | 51.18 | 0.39 | 1.44 | 0.03 | 9.37 | 0.32 | 14.42 | 22.07 | 0.47 | 0.02 | 99.70 | 43.7 | 39.8 | 14.8 | 73.3 |
| 54 | 3 | C | 50.99 | 0.25 | 1.65 | 0.05 | 9.37 | 0.35 | 14.30 | 21.88 | 0.47 | 0.01 | 99.33 | 43.6 | 39.7 | 15.0 | 73.1 |
| 55 | 3 | C | 50.00 | 0.68 | 3.42 | 0.33 | 8.20 | 0.22 | 14.17 | 22.24 | 0.55 | 0.01 | 99.81 | 45.0 | 39.9 | 13.2 | 75.5 |
| 56 | 3 | R | 51.04 | 0.39 | 2.64 | 0.76 | 5.97 | 0.17 | 15.25 | 22.83 | 0.43 | 0.01 | 99.49 | 46.1 | 42.8 | 9.6 | 82.0 |
| 57 | 4 | U | 51.01 | 0.41 | 1.52 | | 9.06 | 0.32 | 15.19 | 22.06 | 0.36 | | 99.92 | 43.2 | 41.4 | 14.2 | 74.9 |
| 58 | 4 | U | 51.28 | 0.29 | 1.50 | | 9.48 | 0.26 | 14.22 | 22.53 | 0.38 | | 99.93 | 44.6 | 39.2 | 14.9 | 72.8 |
| 59 | 4 | U | 51.74 | 0.28 | 1.39 | 0.04 | 9.53 | 0.33 | 14.15 | 22.67 | 0.39 | | 100.52 | 44.7 | 38.9 | 15.0 | 72.6 |
| 60 | 5 | U | 51.40 | 0.35 | 1.42 | 0.05 | 9.51 | 0.28 | 14.38 | 22.14 | 0.45 | 0.02 | 99.98 | 43.8 | 39.6 | 15.0 | 72.9 |
| 61 | 5 | U | 51.43 | 0.31 | 1.31 | | 9.55 | 0.28 | 14.40 | 22.01 | 0.41 | 0.02 | 99.71 | 43.7 | 39.8 | 15.1 | 72.9 |
| 62 | 5 | U | 51.68 | 0.37 | 1.30 | 0.00 | 9.11 | 0.26 | 14.41 | 22.15 | 0.36 | 0.01 | 99.64 | 44.2 | 40.0 | 14.5 | 73.8 |
| 63 | 6 | U | 51.14 | 0.28 | 1.37 | 0.03 | 9.41 | 0.29 | 14.53 | 22.12 | 0.38 | | 99.55 | 43.8 | 40.0 | 14.8 | 73.3 |
| 64 | 6 | U | 51.88 | 0.30 | 1.07 | 0.04 | 9.10 | 0.26 | 14.40 | 22.69 | 0.30 | | 100.03 | 44.9 | 39.7 | 14.4 | 73.8 |
| 65 | 6 | U | 51.63 | 0.39 | 1.50 | | 9.37 | 0.25 | 14.68 | 21.99 | 0.40 | 0.00 | 100.20 | 43.5 | 40.4 | 14.7 | 73.6 |
| 66 | 6 | U | 51.50 | 0.45 | 1.50 | 0.03 | 9.63 | 0.30 | 14.66 | 22.07 | 0.31 | 0.01 | 100.46 | 43.5 | 40.2 | 15.1 | 73.1 |
| 67 | 8 | U | 51.25 | 0.54 | 1.68 | 0.03 | 9.35 | 0.27 | 14.66 | 21.62 | 0.41 | 0.00 | 99.81 | 43.1 | 40.6 | 14.8 | 73.6 |
| 68 | 9 | R | 51.22 | 0.36 | 2.64 | 0.63 | 5.30 | 0.14 | 16.08 | 22.40 | 0.35 | 0.01 | 99.13 | 45.2 | 45.1 | 8.5 | 84.4 |
| 69 | 9 | C | 51.56 | 0.42 | 1.88 | 0.03 | 8.69 | 0.28 | 14.72 | 21.99 | 0.37 | | 99.93 | 43.9 | 40.9 | 13.9 | 75.1 |
| 70 | 9 | C | 50.46 | 0.47 | 2.94 | 0.03 | 8.40 | 0.28 | 14.24 | 22.25 | 0.43 | | 99.50 | 44.9 | 40.0 | 13.5 | 75.1 |
| 71 | 9 | C | 51.52 | 0.21 | 1.47 | 0.01 | 9.35 | 0.26 | 14.27 | 22.19 | 0.44 | | 99.71 | 44.1 | 39.5 | 14.8 | 73.1 |
| 72 | 9 | R | 51.13 | 0.43 | 1.67 | 0.04 | 8.76 | 0.29 | 14.71 | 21.80 | 0.31 | 0.04 | 99.19 | 43.7 | 41.1 | 14.1 | 74.9 |
| 73 | 10 | U | 51.66 | 0.36 | 1.53 | | 8.43 | 0.28 | 14.92 | 22.01 | 0.41 | | 99.59 | 43.8 | 41.3 | 13.4 | 75.9 |
| 74 | 10 | U | 51.92 | 0.35 | 1.43 | 0.05 | 9.16 | 0.30 | 14.47 | 22.30 | 0.50 | | 100.46 | 44.0 | 39.8 | 14.4 | 73.8 |
| 75 | 11 | U | 51.96 | 0.13 | 1.30 | 0.02 | 8.42 | 0.27 | 14.75 | 22.57 | 0.37 | | 99.78 | 44.7 | 40.7 | 13.3 | 75.7 |
| 76 | 11 | U | 51.60 | 0.27 | 1.12 | 0.05 | 10.83 | 0.30 | 14.09 | 21.54 | 0.41 | 0.02 | 100.21 | 42.7 | 38.8 | 17.0 | 69.9 |

Appendix 2 Continued

| | | | | | | | | | | | | | | | | | |
|---|---|---|---|---|---|---|---|---|---|---|---|---|---|---|---|---|---|
| 77 | 12 | U | 50.70 | 0.52 | 2.60 | 0.06 | 9.36 | 0.21 | 14.23 | 22.32 | 0.52 | | 100.52 | 44.3 | 39.3 | 14.6 | 73.0 |
| 78 | 12 | U | 50.93 | 0.43 | 1.91 | 0.02 | 9.22 | 0.28 | 14.12 | 22.30 | 0.42 | 0.00 | 99.63 | 44.6 | 39.3 | 14.7 | 73.2 |
| 79 | 13 | U | 50.43 | 0.58 | 2.57 | | 8.84 | 0.29 | 14.20 | 22.15 | 0.39 | | 99.45 | 44.6 | 39.8 | 14.2 | 74.1 |
| 80 | 13 | U | 51.51 | 0.38 | 1.75 | | 8.53 | 0.30 | 14.31 | 22.31 | 0.40 | 0.01 | 99.49 | 44.8 | 40.0 | 13.8 | 74.9 |
| 81 | 14 | R | 51.19 | 0.40 | 2.47 | 0.69 | 4.88 | 0.08 | 16.07 | 23.04 | 0.42 | | 99.23 | 46.1 | 44.7 | 7.7 | 85.4 |
| 82 | 14 | R | 51.10 | 0.37 | 2.68 | 0.67 | 5.44 | 0.11 | 16.50 | 22.20 | 0.36 | 0.02 | 99.45 | 44.3 | 45.8 | 8.6 | 84.4 |
| 83 | 14 | R | 51.52 | 0.38 | 2.42 | 0.79 | 5.15 | 0.14 | 15.95 | 22.83 | 0.42 | 0.00 | 99.60 | 45.8 | 44.5 | 8.2 | 84.7 |
| 84 | 14 | R | 51.34 | 0.24 | 2.40 | 0.69 | 4.94 | 0.12 | 16.03 | 22.93 | 0.38 | 0.01 | 99.07 | 46.0 | 44.8 | 7.9 | 85.3 |
| 85 | 14 | R | 50.79 | 0.47 | 2.82 | 0.38 | 7.21 | 0.19 | 14.86 | 22.75 | 0.48 | | 99.95 | 45.5 | 41.3 | 11.4 | 78.6 |
| 86 | 14 | C | 51.39 | 0.18 | 1.52 | | 8.84 | 0.32 | 14.38 | 22.24 | 0.50 | 0.02 | 99.38 | 44.3 | 39.8 | 14.1 | 74.3 |
| 87 | 14 | C | 51.56 | 0.19 | 1.47 | | 9.32 | 0.26 | 14.38 | 22.30 | 0.46 | 0.01 | 99.96 | 44.1 | 39.6 | 14.7 | 73.3 |
| 88 | 14 | R | 51.32 | 0.23 | 1.51 | 0.02 | 7.97 | 0.24 | 14.99 | 22.41 | 0.55 | | 99.24 | 44.3 | 41.2 | 12.5 | 77.0 |
| 89 | 15 | U | 50.84 | 0.44 | 1.93 | 0.04 | 9.41 | 0.31 | 14.53 | 21.40 | 0.38 | | 99.27 | 43.0 | 40.6 | 15.1 | 73.3 |
| 90 | 15 | U | 51.30 | 0.48 | 1.64 | | 9.34 | 0.21 | 14.94 | 21.69 | 0.29 | 0.00 | 99.90 | 43.0 | 41.3 | 14.7 | 74.0 |
| 91 | 16 | U | 51.23 | 0.55 | 2.09 | 0.03 | 9.27 | 0.29 | 14.78 | 21.87 | 0.44 | 0.01 | 100.59 | 43.2 | 40.6 | 14.6 | 74.0 |
| 92 | 16 | U | 50.64 | 0.26 | 1.75 | 0.04 | 8.62 | 0.21 | 14.64 | 22.48 | 0.46 | 0.01 | 99.11 | 44.5 | 40.3 | 13.5 | 75.1 |
| 93 | 16 | U | 51.31 | 0.33 | 1.46 | 0.05 | 9.56 | 0.24 | 14.60 | 21.96 | 0.36 | | 99.87 | 43.5 | 40.2 | 15.0 | 73.1 |
| 94 | 16 | U | 52.02 | 0.37 | 1.35 | 0.02 | 8.51 | 0.31 | 15.06 | 21.89 | 0.32 | | 99.84 | 43.6 | 41.7 | 13.6 | 75.9 |
| 95 | 17 | R | 51.45 | 0.42 | 1.43 | | 8.90 | 0.28 | 14.91 | 22.19 | 0.36 | | 99.93 | 43.8 | 40.9 | 14.0 | 74.9 |
| 96 | 17 | R | 51.21 | 0.46 | 1.44 | | 9.90 | 0.29 | 14.73 | 22.00 | 0.38 | | 100.41 | 43.1 | 40.2 | 15.4 | 72.6 |
| 97 | 17 | C | 51.04 | 0.39 | 1.49 | 0.01 | 9.53 | 0.31 | 14.55 | 21.93 | 0.43 | 0.01 | 99.70 | 43.4 | 40.1 | 15.0 | 73.1 |
| 98 | 17 | C | 51.02 | 0.39 | 1.40 | 0.06 | 9.50 | 0.32 | 14.24 | 22.27 | 0.42 | 0.01 | 99.62 | 44.2 | 39.3 | 15.1 | 72.7 |
| 99 | 17 | R | 51.44 | 0.43 | 1.40 | 0.01 | 9.08 | 0.30 | 14.89 | 22.09 | 0.28 | | 99.93 | 43.7 | 41.0 | 14.4 | 74.5 |
| 100 | 17 | R | 51.72 | 0.33 | 1.50 | 0.06 | 9.75 | 0.32 | 14.28 | 21.90 | 0.45 | | 100.31 | 43.5 | 39.4 | 15.5 | 72.3 |
| 101 | 17 | R | 50.98 | 0.34 | 1.42 | | 9.19 | 0.33 | 15.03 | 22.12 | 0.28 | | 99.71 | 43.5 | 41.1 | 14.5 | 74.4 |
| 102 | 17 | R | 51.23 | 0.46 | 1.41 | | 9.90 | 0.34 | 14.57 | 22.16 | 0.44 | 0.00 | 100.50 | 43.4 | 39.7 | 15.4 | 72.4 |
| 103 | 17 | R | 51.63 | 0.57 | 1.35 | 0.05 | 9.22 | 0.31 | 14.93 | 21.84 | 0.27 | 0.00 | 100.18 | 43.3 | 41.1 | 14.6 | 74.3 |
| 104 | 17 | C | 51.17 | 0.47 | 1.49 | | 9.42 | 0.27 | 14.37 | 21.89 | 0.42 | 0.01 | 99.51 | 43.7 | 39.9 | 14.9 | 73.1 |
| 105 | 17 | C | 51.78 | 0.31 | 1.16 | 0.03 | 9.08 | 0.21 | 14.30 | 22.73 | 0.36 | | 99.96 | 45.0 | 39.4 | 14.2 | 73.7 |
| 106 | 17 | C | 51.29 | 0.49 | 1.49 | 0.01 | 9.38 | 0.33 | 14.34 | 22.01 | 0.45 | | 99.78 | 43.8 | 39.7 | 14.9 | 73.2 |
| 107 | 17 | R | 51.53 | 0.51 | 1.43 | 0.03 | 9.30 | 0.29 | 14.66 | 22.21 | 0.38 | 0.00 | 100.33 | 43.8 | 40.2 | 14.6 | 73.7 |
| 108 | 17 | R | 51.76 | 0.35 | 1.43 | 0.02 | 9.10 | 0.30 | 14.63 | 22.40 | 0.43 | 0.02 | 100.43 | 44.1 | 40.1 | 14.3 | 74.1 |
| 109 | 17 | R | 51.72 | 0.37 | 1.43 | | 9.32 | 0.26 | 14.67 | 21.77 | 0.34 | | 99.88 | 43.3 | 40.7 | 14.8 | 73.7 |
| 110 | 18 | R | 51.29 | 0.50 | 1.35 | 0.03 | 9.67 | 0.26 | 14.85 | 21.80 | 0.27 | 0.01 | 100.02 | 43.1 | 40.8 | 15.2 | 73.2 |
| 111 | 18 | R | 51.50 | 0.23 | 1.24 | 0.01 | 8.71 | 0.28 | 14.86 | 22.12 | 0.37 | 0.00 | 99.32 | 43.9 | 41.0 | 13.8 | 75.3 |
| 112 | 18 | R | 51.68 | 0.27 | 1.87 | 0.18 | 6.87 | 0.20 | 15.33 | 22.96 | 0.37 | | 99.73 | 45.5 | 42.3 | 10.9 | 79.9 |
| 113 | 18 | R | 51.78 | 0.22 | 1.70 | 0.47 | 6.88 | 0.19 | 16.06 | 21.77 | 0.38 | 0.01 | 99.45 | 43.3 | 44.4 | 10.9 | 80.6 |
| 114 | 18 | R | 51.64 | 0.48 | 1.66 | 0.03 | 8.74 | 0.22 | 14.76 | 22.13 | 0.42 | | 100.06 | 44.0 | 40.8 | 13.8 | 75.1 |

Appendix 2 Continued

| Spot | Crystal | Zone | SiO2 | TiO2 | Al2O3 | Cr2O3 | FeO | MnO | MgO | CaO | Na2O | K2O | Total | Wo | En | Fs | Mg# |
|---|---|---|---|---|---|---|---|---|---|---|---|---|---|---|---|---|---|
| 115 | 18 | C | 51.17 | 0.29 | 1.49 | | 8.91 | 0.19 | 14.60 | 22.21 | 0.49 | 0.01 | 99.37 | 44.0 | 40.3 | 13.9 | 74.5 |
| 116 | 18 | C | 51.64 | 0.26 | 1.42 | 0.01 | 9.58 | 0.28 | 14.36 | 22.07 | 0.46 | | 100.07 | 43.7 | 39.6 | 15.1 | 72.8 |
| 117 | 18 | C | 51.58 | 0.31 | 1.34 | 0.02 | 9.42 | 0.34 | 14.54 | 22.27 | 0.51 | | 100.33 | 43.7 | 39.7 | 14.8 | 73.3 |
| 118 | 18 | C | 51.33 | 0.38 | 1.29 | | 9.95 | 0.34 | 14.25 | 21.83 | 0.43 | | 99.79 | 43.3 | 39.4 | 15.8 | 71.8 |
| 119 | 18 | C | 50.94 | 0.40 | 1.90 | | 9.90 | 0.22 | 14.18 | 21.64 | 0.41 | 0.00 | 99.59 | 43.3 | 39.5 | 15.7 | 71.8 |
| 120 | 18 | C | 50.94 | 0.39 | 1.93 | 0.00 | 10.05 | 0.29 | 14.42 | 21.50 | 0.35 | 0.01 | 99.87 | 42.8 | 40.0 | 15.9 | 71.9 |
| 121 | 18 | C | 51.43 | 0.38 | 1.96 | 0.03 | 9.56 | 0.29 | 14.36 | 21.24 | 0.35 | 0.03 | 99.63 | 42.9 | 40.4 | 15.4 | 72.8 |
| 122 | 18 | C | 51.99 | 0.33 | 1.28 | | 9.03 | 0.30 | 14.96 | 22.27 | 0.39 | | 100.53 | 43.7 | 40.8 | 14.2 | 74.7 |
| 123 | 18 | R | 52.01 | 0.17 | 1.68 | 0.58 | 6.70 | 0.20 | 16.11 | 21.55 | 0.45 | 0.01 | 99.46 | 43.0 | 44.7 | 10.7 | 81.1 |
| 124 | 18 | R | 51.66 | 0.25 | 1.73 | 0.48 | 6.73 | 0.20 | 15.67 | 21.99 | 0.41 | | 99.12 | 44.1 | 43.7 | 10.8 | 80.6 |
| 125 | 18 | R | 51.68 | 0.37 | 1.88 | 0.01 | 7.65 | 0.18 | 14.97 | 22.55 | 0.40 | 0.01 | 99.70 | 45.0 | 41.5 | 12.1 | 77.7 |

R-Rim; C-Core; U- Unzoned of small pyrocene grains; -below detection limit

Appendix 2 Continued

| Spot | | Zone | SiO2 | TiO2 | Al2O3 | Cr2O3 | FeO | MnO | MgO | CaO | Na2O | K2O | Total | An |
|---|---|---|---|---|---|---|---|---|---|---|---|---|---|---|
| 06XJ147 01 | P | R | 57.01 | | 26.67 | 0.06 | 0.36 | | 0.01 | 9.43 | 6.51 | 0.36 | 100.42 | 43.61 |
| 06XJ147 02 | P | C | 55.71 | 0.05 | 27.40 | | 0.35 | 0.02 | | 10.13 | 5.82 | 0.35 | 99.85 | 48.06 |
| 06XJ147 03 | P | C | 53.11 | 0.02 | 29.04 | | 0.39 | 0.02 | 0.02 | 12.41 | 4.48 | 0.23 | 99.72 | 59.68 |
| 06XJ147 04 | P | R | 58.38 | 0.05 | 25.52 | 0.04 | 0.36 | | 0.02 | 8.03 | 7.02 | 0.51 | 99.93 | 37.64 |
| 06XJ147 09 | P | R | 58.58 | 0.03 | 25.18 | 0.00 | 0.30 | | 0.02 | 7.84 | 7.37 | 0.51 | 99.84 | 36.00 |
| 06XJ147 10 | P | R | 57.01 | 0.02 | 26.43 | | 0.31 | 0.04 | 0.01 | 9.16 | 6.62 | 0.42 | 100.01 | 42.35 |
| 06XJ147 11 | P | R | 58.28 | 0.02 | 25.41 | 0.05 | 0.24 | 0.04 | 0.02 | 7.96 | 7.21 | 0.52 | 99.74 | 36.81 |
| 06XJ147 12 | P | R | 57.69 | 0.01 | 26.13 | 0.02 | 0.26 | 0.03 | 0.02 | 8.75 | 6.77 | 0.46 | 100.20 | 40.63 |
| 06XJ147 13 | P | R | 58.61 | 0.01 | 25.35 | | 0.23 | | 0.02 | 7.72 | 7.54 | 0.44 | 99.93 | 35.25 |
| 06XJ147 14 | P | R | 56.32 | 0.06 | 27.10 | 0.00 | 0.33 | 0.03 | 0.03 | 9.65 | 6.34 | 0.39 | 100.24 | 44.71 |
| 06XJ147 15 | P | R | 56.28 | | 26.88 | | 0.30 | 0.02 | 0.01 | 9.71 | 6.19 | 0.39 | 99.80 | 45.45 |
| 06XJ147 16 | P | C | 56.12 | 0.09 | 27.12 | | 0.29 | | 0.01 | 9.88 | 6.08 | 0.36 | 99.95 | 46.37 |
| 06XJ147 17 | P | C | 54.32 | 0.09 | 28.09 | 0.00 | 0.27 | 0.00 | 0.02 | 11.26 | 5.48 | 0.30 | 99.86 | 52.28 |
| 06XJ147 18 | P | C | 54.80 | 0.03 | 27.96 | 0.01 | 0.20 | 0.01 | 0.01 | 10.85 | 5.87 | 0.21 | 99.96 | 49.95 |
| 06XJ147 19 | P | C | 55.09 | 0.04 | 27.90 | | 0.24 | | 0.01 | 10.89 | 5.77 | 0.32 | 100.26 | 50.18 |
| 06XJ147 20 | P | R | 57.65 | 0.04 | 26.00 | 0.02 | 0.22 | | 0.02 | 8.63 | 6.79 | 0.46 | 99.88 | 40.21 |
| 06XJ147 22 | P | C | 54.75 | 0.00 | 28.16 | | 0.28 | | 0.03 | 11.08 | 5.68 | 0.29 | 100.30 | 51.05 |
| 06XJ147 23 | P | C | 54.64 | | 28.11 | 0.03 | 0.31 | 0.00 | 0.02 | 11.02 | 5.46 | 0.32 | 99.97 | 51.77 |
| 06XJ147 24 | P | R | 59.10 | 0.05 | 24.99 | | 0.28 | 0.05 | 0.01 | 7.24 | 7.73 | 0.47 | 99.92 | 33.22 |
| 06XJ153 01 | P | C | 56.08 | 0.02 | 26.84 | 0.01 | 0.47 | | 0.03 | 10.11 | 6.12 | 0.34 | 100.03 | 46.85 |
| 06XJ153 02 | P | C | 54.52 | 0.02 | 27.68 | | 0.49 | 0.04 | 0.03 | 10.82 | 5.70 | 0.30 | 99.60 | 50.35 |
| 06XJ153 03 | P | C | 53.59 | 0.03 | 28.74 | 0.02 | 0.35 | 0.01 | 0.03 | 12.04 | 4.98 | 0.25 | 100.06 | 56.39 |
| 06XJ153 04 | P | R | 55.86 | 0.02 | 26.88 | 0.01 | 0.41 | | 0.04 | 10.24 | 6.20 | 0.32 | 100.02 | 46.90 |
| 06XJ153 05 | P | C | 53.74 | 0.07 | 28.14 | | 0.55 | 0.00 | 0.07 | 11.72 | 5.22 | 0.21 | 99.72 | 54.73 |
| 06XJ153 06 | P | R | 56.01 | | 26.63 | | 0.48 | 0.03 | 0.05 | 9.76 | 6.44 | 0.31 | 99.74 | 44.80 |
| 06XJ153 07 | P | C | 52.93 | 0.10 | 26.60 | 0.01 | 1.21 | 0.01 | 0.73 | 11.92 | 4.72 | 0.22 | 98.51 | 57.51 |
| 06XJ153 08 | P | R | 55.03 | | 27.77 | 0.03 | 0.50 | 0.05 | 0.05 | 11.04 | 5.50 | 0.28 | 100.26 | 51.77 |
| 06XJ153 09 | M | | 58.53 | 0.03 | 24.58 | 0.01 | 0.39 | | 0.03 | 7.22 | 7.46 | 0.47 | 98.72 | 33.92 |
| 06XJ153 10 | M | | 63.80 | 0.03 | 22.31 | | 0.14 | 0.01 | 0.01 | 3.25 | 9.87 | 0.64 | 100.07 | 14.85 |
| 06XJ153 11 | M | | 55.47 | 0.02 | 26.70 | 0.04 | 0.45 | 0.01 | 0.04 | 9.68 | 6.20 | 0.26 | 98.94 | 45.64 |
| 06XJ153 12 | M | | 67.39 | 0.02 | 20.17 | | 0.25 | | 0.01 | 0.75 | 11.57 | 0.21 | 100.38 | 3.40 |
| 06XJ153 13 | M | | 65.09 | 0.03 | 21.67 | 0.01 | 0.03 | | | 2.42 | 10.83 | 0.13 | 100.22 | 10.92 |
| 06XJ153 14 | M | | 62.84 | 0.04 | 21.22 | 0.01 | 1.26 | 0.01 | 0.84 | 4.08 | 9.49 | 0.37 | 100.17 | 18.81 |
| 06XJ153 15 | M | | 65.71 | | 20.79 | 0.02 | 0.02 | | | 1.69 | 10.91 | 0.18 | 99.37 | 7.80 |
| 06XJ153 18 | M | | 57.08 | 0.05 | 26.26 | 0.04 | 0.30 | 0.00 | 0.05 | 8.57 | 6.04 | 1.62 | 100.01 | 39.99 |
| 06XJ153 19 | M | | 60.54 | | 24.25 | | 0.19 | 0.02 | 0.02 | 6.18 | 8.46 | 0.21 | 99.89 | 28.42 |
| 06XJ153 22 | M | | 66.03 | | 20.90 | 0.05 | 0.25 | 0.04 | 0.00 | 1.74 | 10.98 | 0.14 | 100.15 | 7.98 |
| 06XJ153 23 | M | | 64.67 | | 21.42 | | 0.06 | 0.01 | 0.01 | 2.49 | 9.80 | 0.94 | 99.46 | 11.67 |
| 06XJ153 24 | M | | 60.21 | 0.03 | 23.70 | | 0.28 | | 0.01 | 6.66 | 8.32 | 0.32 | 99.63 | 30.14 |
| 06XJ153 25 | M | | 62.43 | | 23.00 | | 0.06 | 0.03 | 0.03 | 4.39 | 9.56 | 0.17 | 99.68 | 20.06 |
| 06XJ153 26 | P | R | 56.74 | 0.06 | 26.20 | | 1.07 | 0.04 | 0.15 | 8.25 | 6.43 | 0.56 | 99.52 | 40.12 |

R-Rim; C-Core; M-Matrix; -below detection limit

# Appendix 3 Major (wt%) and trace (ppm) element compositions for the Baogutu ore-porphyries

| Sample | 06XJ-137 | 06XJ-138-1 | 06XJ-138-2 | 06XJ-139 | 06XJ-140 | 06XJ-141 | 06XJ-142 | 06XJ-143 | 06XJ-144 | 06XJ-145 | 06XJ-147 | 06XJ-148 |
|---|---|---|---|---|---|---|---|---|---|---|---|---|
| Position | | | | | WDH-No.2 | | | | | | WDH-No.5 | |
| SiO2 | 56.91 | 54.02 | 54.76 | 57.02 | 52.46 | 64.95 | 52.66 | 50.24 | 53.75 | 60.35 | 60.55 | 58.36 |
| TiO2 | 0.94 | 0.91 | 0.80 | 0.86 | 0.87 | 0.54 | 1.27 | 1.03 | 0.90 | 0.72 | 0.69 | 0.73 |
| Al2O3 | 18.32 | 17.33 | 17.62 | 17.02 | 16.35 | 15.96 | 16.57 | 15.73 | 16.26 | 17.75 | 16.08 | 16.03 |
| $FeO^{Total}$ | 6.51 | 6.75 | 6.23 | 6.26 | 7.44 | 4.28 | 8.38 | 8.56 | 7.00 | 3.21 | 3.44 | 3.50 |
| MnO | 0.08 | 0.10 | 0.09 | 0.09 | 0.12 | 0.04 | 0.15 | 0.14 | 0.11 | 0.06 | 0.06 | 0.07 |
| MgO | 3.39 | 5.01 | 4.72 | 4.20 | 7.20 | 2.23 | 6.10 | 8.46 | 7.28 | 3.93 | 4.78 | 5.84 |
| CaO | 5.80 | 7.83 | 7.36 | 6.84 | 6.83 | 3.84 | 6.65 | 8.01 | 7.27 | 6.24 | 7.13 | 7.37 |
| Na2O | 4.65 | 3.93 | 3.89 | 3.67 | 3.44 | 4.31 | 3.71 | 3.04 | 3.79 | 5.31 | 4.70 | 4.48 |
| K2O | 1.26 | 1.24 | 1.33 | 1.46 | 1.91 | 1.29 | 1.79 | 1.02 | 1.15 | 0.57 | 0.60 | 1.23 |
| P2O5 | 0.05 | 0.04 | 0.04 | 0.04 | 0.07 | 0.05 | 0.05 | 0.05 | 0.06 | 0.07 | 0.05 | 0.04 |
| LOI | 1.56 | 1.55 | 1.92 | 1.53 | 2.72 | 1.57 | 1.82 | 2.53 | 1.89 | 1.70 | 1.05 | 1.45 |
| Total | 100.19 | 99.48 | 99.47 | 99.70 | 100.23 | 99.53 | 100.08 | 99.77 | 100.23 | 100.27 | 99.51 | 99.49 |
| $Mg^{\#}$ | 48.1 | 56.9 | 57.4 | 54.5 | 63.3 | 48.2 | 56.5 | 63.8 | 64.9 | 68.6 | 71.2 | 74.9 |
| Sc | 8.38 | 18.4 | 17.2 | 18.0 | 14.7 | 5.10 | 12.8 | 22.2 | 16.0 | 12.2 | 13.2 | 15.0 |
| V | 109 | 175 | 151 | 129 | 173 | 93.3 | 189 | 187 | 153 | 97.2 | 127 | 149 |
| Cr | 22.7 | 77.6 | 87.7 | 88.2 | 274 | 39.6 | 138 | 353 | 291 | 57.5 | 152 | 171 |
| Co | 18.8 | 22.8 | 21.2 | 20.7 | 27.4 | 11.8 | 20.7 | 33.8 | 27.4 | 9.28 | 8.92 | 8.26 |
| Ni | 34.8 | 40.6 | 40.4 | 39.3 | 133 | 25.2 | 61.1 | 153 | 132 | 44.4 | 62.0 | 72.0 |
| Ga | 17.8 | 18.0 | 18.4 | 17.5 | 16.9 | 15.9 | 15.8 | 17.4 | 16.7 | 17.0 | 17.0 | 17.4 |
| Cs | 1.58 | 0.902 | 1.33 | 1.13 | 1.27 | 1.15 | 0.979 | 1.23 | 1.07 | 1.14 | 1.66 | 1.93 |
| Rb | 32.5 | 31.2 | 33.7 | 30.5 | 42.0 | 38.5 | 18.8 | 30.4 | 27.2 | 15.8 | 38.1 | 81.2 |
| Ba | 337 | 401 | 397 | 499 | 423 | 407 | 243 | 222 | 451 | 241 | 247 | 216 |
| Th | 1.70 | 1.35 | 1.81 | 2.60 | 1.07 | 4.96 | 0.715 | 1.03 | 1.43 | 2.58 | 3.21 | 2.72 |
| U | 0.410 | 0.370 | 0.481 | 0.539 | 0.341 | 1.15 | 0.439 | 0.256 | 0.348 | 1.01 | 1.07 | 0.822 |
| Pb | 3.00 | 4.18 | 4.69 | 4.06 | 3.13 | 3.33 | 1.40 | 1.60 | 2.18 | 2.58 | 2.16 | 1.33 |
| Nb | 1.91 | 2.95 | 2.96 | 3.32 | 2.32 | 3.01 | 2.50 | 2.78 | 2.39 | 2.71 | 3.35 | 2.64 |
| Ta | 0.172 | 0.208 | 0.204 | 0.251 | 0.164 | 0.267 | 0.187 | 0.205 | 0.224 | 0.228 | 0.244 | 0.210 |
| Sr | 623 | 603 | 614 | 581 | 508 | 487 | 401 | 445 | 575 | 716 | 561 | 540 |
| Y | 15.5 | 16.5 | 15.3 | 13.8 | 13.1 | 11.8 | 13.1 | 19.8 | 14.5 | 14.8 | 15.4 | 15.9 |
| Zr | 144 | 91.2 | 96.7 | 105 | 102 | 158 | 98.5 | 88.6 | 110 | 125 | 128 | 101 |
| Hf | 3.62 | 2.46 | 2.60 | 2.63 | 2.59 | 4.40 | 2.58 | 2.51 | 2.77 | 3.49 | 3.62 | 2.98 |
| La | 5.70 | 7.19 | 7.22 | 7.68 | 7.25 | 8.33 | 4.42 | 5.24 | 6.18 | 9.30 | 11.0 | 6.44 |
| Ce | 14.3 | 16.6 | 17.2 | 17.7 | 17.3 | 17.6 | 12.7 | 14.5 | 14.9 | 24.8 | 27.8 | 20.5 |
| Pr | 2.13 | 2.56 | 2.52 | 2.42 | 2.46 | 2.27 | 1.95 | 2.46 | 2.43 | 3.54 | 3.78 | 3.29 |
| Nd | 9.75 | 11.6 | 11.0 | 10.6 | 10.8 | 9.38 | 9.71 | 12.1 | 10.9 | 14.8 | 15.3 | 15.1 |
| Sm | 2.49 | 2.88 | 2.66 | 2.49 | 2.59 | 2.09 | 2.58 | 3.21 | 2.63 | 3.17 | 3.27 | 3.42 |
| Eu | 0.887 | 0.907 | 0.857 | 0.881 | 0.789 | 0.666 | 0.777 | 1.00 | 0.820 | 0.877 | 0.933 | 0.854 |
| Gd | 2.44 | 2.85 | 2.68 | 2.47 | 2.45 | 1.91 | 2.53 | 3.36 | 2.53 | 2.92 | 3.00 | 3.27 |
| Tb | 0.458 | 0.504 | 0.472 | 0.395 | 0.428 | 0.344 | 0.465 | 0.615 | 0.454 | 0.482 | 0.507 | 0.533 |
| Dy | 2.73 | 3.00 | 2.84 | 2.41 | 2.54 | 2.00 | 2.80 | 3.58 | 2.66 | 2.75 | 2.86 | 2.94 |
| Ho | 0.547 | 0.622 | 0.580 | 0.492 | 0.522 | 0.412 | 0.573 | 0.751 | 0.542 | 0.553 | 0.578 | 0.592 |
| Er | 1.52 | 1.64 | 1.63 | 1.39 | 1.48 | 1.22 | 1.63 | 2.05 | 1.49 | 1.59 | 1.56 | 1.62 |
| Tm | 0.222 | 0.235 | 0.237 | 0.203 | 0.203 | 0.177 | 0.229 | 0.284 | 0.221 | 0.229 | 0.226 | 0.233 |
| Yb | 1.48 | 1.60 | 1.49 | 1.42 | 1.41 | 1.24 | 1.49 | 1.95 | 1.43 | 1.55 | 1.48 | 1.59 |
| Lu | 0.232 | 0.247 | 0.235 | 0.216 | 0.209 | 0.207 | 0.230 | 0.284 | 0.209 | 0.239 | 0.231 | 0.233 |
| Sr/Y | 40.2 | 36.5 | 40.0 | 42.3 | 38.8 | 41.1 | 30.7 | 22.5 | 39.8 | 48.2 | 36.5 | 34.0 |
| Nb/Ta | 11.1 | 14.2 | 14.5 | 13.2 | 14.1 | 11.3 | 13.4 | 13.6 | 10.7 | 11.9 | 13.7 | 12.6 |

9

10 Appendix 3 Continued

| Sample | 06XJ-149 | 06XJ-150 | 06XJ-153 | 06XJ-154 | 06XJ-155 | 06XJ-156 | 06XJ-157 | 06XJ-158 | 06XJ-159 | Sanukitoid |
|---|---|---|---|---|---|---|---|---|---|---|
| Position | WDH-No.5 | | East KGSY | | | West KGSY | | | | |
| SiO2 | 60.45 | 58.20 | 59.78 | 57.77 | 59.51 | 65.66 | 65.31 | 58.92 | 54.87 | 56.53 |
| TiO2 | 0.74 | 0.67 | 0.71 | 0.77 | 0.68 | 0.44 | 0.43 | 0.67 | 0.85 | 0.66 |
| Al2O3 | 18.17 | 17.24 | 17.22 | 17.53 | 17.33 | 16.59 | 16.31 | 17.57 | 18.26 | 15.59 |
| $FeO^{Total}$ | 2.77 | 5.70 | 5.50 | 6.00 | 5.08 | 3.77 | 3.60 | 5.50 | 6.55 | 7.90 |
| MnO | 0.04 | 0.08 | 0.10 | 0.11 | 0.09 | 0.08 | 0.07 | 0.12 | 0.11 | 0.13 |
| MgO | 3.96 | 3.71 | 3.26 | 3.66 | 3.00 | 1.44 | 1.44 | 3.38 | 3.98 | 7.75 |
| CaO | 7.48 | 6.23 | 5.18 | 2.90 | 4.57 | 1.80 | 2.51 | 3.85 | 5.98 | 6.78 |
| Na2O | 4.52 | 3.78 | 3.82 | 4.36 | 4.56 | 4.61 | 4.00 | 4.23 | 3.46 | 2.91 |
| K2O | 0.76 | 1.82 | 1.74 | 1.61 | 1.81 | 2.07 | 2.02 | 1.75 | 1.16 | 1.72 |
| P2O5 | 0.04 | 0.04 | 0.08 | 0.11 | 0.07 | 0.09 | 0.12 | 0.14 | 0.19 | 0.15 |
| LOI | 0.98 | 1.38 | 2.03 | 4.09 | 2.30 | 2.86 | 3.45 | 3.24 | 4.02 | |
| Total | 100.23 | 99.49 | 100.03 | 99.57 | 99.56 | 99.83 | 99.67 | 99.96 | 100.16 | 100.57 |
| $Mg^{\#}$ | 71.8 | 53.7 | 51.3 | 52.1 | 51.3 | 40.5 | 41.6 | 52.3 | 52.0 | 68.8 |
| Sc | 14.0 | 14.3 | 11.7 | 12.7 | 10.6 | 1.91 | 3.46 | 10.1 | 12.9 | 21.7 |
| V | 155 | 145 | 134 | 143 | 115 | 65.0 | 59.5 | 126 | 171 | |
| Cr | 47.6 | 67.5 | 42.5 | 65.2 | 23.9 | 5.84 | 10.8 | 63.1 | 51.7 | 452 |
| Co | 5.87 | 18.7 | 17.5 | 20.4 | 16.3 | 4.64 | 4.30 | 15.5 | 21.6 | 36.1 |
| Ni | 41.8 | 55.8 | 33.5 | 42.8 | 32.0 | 9.07 | 6.38 | 42.4 | 51.6 | 176 |
| Ga | 17.6 | 18.5 | 18.3 | 18.0 | 17.7 | 16.6 | 16.9 | 18.1 | 18.3 | |
| Cs | 2.15 | 4.51 | 1.07 | 0.925 | 0.337 | 0.917 | 0.886 | 0.473 | 1.44 | 5.29 |
| Rb | 46.7 | 58.0 | 25.6 | 27.9 | 27.9 | 34.9 | 54.0 | 40.0 | 23.5 | 71.3 |
| Ba | 230 | 525 | 784 | 759 | 627 | 648 | 363 | 648 | 590 | 293 |
| Th | 2.18 | 2.84 | 2.47 | 1.76 | 2.33 | 2.31 | 2.96 | 1.45 | 2.24 | 4.61 |
| U | 0.850 | 0.664 | 0.755 | 0.666 | 0.914 | 0.679 | 0.781 | 0.468 | 0.575 | 2.21 |
| Pb | 2.37 | 3.54 | 5.77 | 2.46 | 2.91 | 7.94 | 4.21 | 3.56 | 2.49 | 15.2 |
| Nb | 2.47 | 2.41 | 2.26 | 1.99 | 2.27 | 2.36 | 2.31 | 1.50 | 2.15 | 4.93 |
| Ta | 0.182 | 0.188 | 0.171 | 0.148 | 0.171 | 0.209 | 0.186 | 0.128 | 0.141 | 0.447 |
| Sr | 628 | 577 | 769 | 523 | 624 | 346 | 387 | 637 | 841 | 297 |
| Y | 16.4 | 13.4 | 13.7 | 12.1 | 12.9 | 9.51 | 10.7 | 9.56 | 12.6 | 15.7 |
| Zr | 94.3 | 62.4 | 111 | 95.0 | 111 | 125 | 126 | 78.0 | 75.5 | 97.9 |
| Hf | 2.73 | 2.27 | 3.39 | 2.85 | 3.18 | 3.49 | 3.38 | 2.21 | 2.19 | 3.05 |
| La | 7.05 | 8.71 | 9.94 | 6.98 | 9.44 | 9.68 | 11.1 | 8.03 | 13.4 | 13.5 |
| Ce | 23.4 | 19.6 | 21.6 | 16.6 | 20.3 | 18.9 | 22.8 | 18.0 | 27.8 | 28.8 |
| Pr | 3.82 | 2.76 | 2.97 | 2.32 | 2.73 | 2.61 | 2.96 | 2.43 | 4.19 | 3.45 |
| Nd | 16.9 | 11.9 | 12.3 | 10.1 | 11.4 | 9.97 | 11.8 | 10.6 | 17.9 | 13.4 |
| Sm | 3.76 | 2.63 | 2.62 | 2.35 | 2.44 | 1.89 | 2.20 | 2.21 | 3.53 | 2.91 |
| Eu | 1.05 | 0.787 | 0.840 | 0.783 | 0.800 | 0.582 | 0.635 | 0.700 | 1.06 | 0.891 |
| Gd | 3.24 | 2.46 | 2.52 | 2.28 | 2.34 | 1.69 | 1.97 | 2.08 | 3.02 | 2.62 |
| Tb | 0.539 | 0.431 | 0.443 | 0.390 | 0.394 | 0.270 | 0.317 | 0.316 | 0.444 | 0.454 |
| Dy | 3.19 | 2.50 | 2.48 | 2.30 | 2.33 | 1.53 | 1.78 | 1.76 | 2.37 | 2.47 |
| Ho | 0.623 | 0.503 | 0.513 | 0.467 | 0.483 | 0.337 | 0.359 | 0.371 | 0.483 | 0.501 |
| Er | 1.71 | 1.42 | 1.45 | 1.29 | 1.42 | 1.00 | 1.07 | 0.947 | 1.29 | 1.46 |
| Tm | 0.241 | 0.206 | 0.211 | 0.201 | 0.211 | 0.156 | 0.163 | 0.147 | 0.179 | 0.211 |
| Yb | 1.59 | 1.38 | 1.46 | 1.28 | 1.36 | 1.08 | 1.14 | 0.927 | 1.15 | 1.57 |
| Lu | 0.239 | 0.199 | 0.215 | 0.198 | 0.219 | 0.172 | 0.193 | 0.143 | 0.171 | 0.240 |
| Sr/Y | 38.4 | 43.0 | 56.1 | 43.1 | 48.4 | 36.4 | 36.0 | 66.7 | 66.9 | 19.0 |
| Nb/Ta | 13.6 | 12.8 | 13.2 | 13.5 | 13.3 | 11.3 | 12.4 | 11.7 | 15.3 | 11.0 |

11 The value for a sanukitoid is the average of the high-Mg andesites from Setouchi

12 Volcanic Belt, Japan (after Tatsumi and Ishizaka, (1981; 1982); Shimoda et al., 2006)

13

## Appendix 4 Sr, Nd, Hf and Pb isotopic compositions of the Baogutu intrusive rocks

| Sample | T(Ma) | $^{87}Rb/^{86}Sr$ | $^{87}Sr/^{86}Sr$ | 2σ | $^{87}Sr/^{86}Sr_i$ | $^{147}Sm/^{144}Nd$ | $^{143}Nd/^{144}Nd$ | 2σ | εNd(t) | $T_{Nd2DM}$ | $f_{Sm/Nd}$ | $^{176}Lu/^{177}Hf$ |
|---|---|---|---|---|---|---|---|---|---|---|---|---|
| 06XJ-137 | 315 | 0.1510 | 0.703976 | 18 | 0.7033 | 0.1555 | 0.512978 | 8 | 8.3 | 402 | -0.21 | 0.00909 |
| 06XJ-138-2 | 315 | 0.1590 | 0.704403 | 11 | 0.7037 | 0.1473 | 0.512872 | 8 | 6.5 | 546 | -0.25 | 0.01283 |
| 06XJ-140 | 315 | 0.2394 | 0.705051 | 18 | 0.7040 | 0.1454 | 0.512873 | 10 | 6.6 | 538 | -0.26 | 0.01142 |
| 06XJ-141 | 315 | 0.2290 | 0.704566 | 14 | 0.7035 | 0.1358 | 0.512830 | 16 | 6.2 | 574 | -0.31 | 0.00666 |
| 06XJ-143 | 315 | 0.1973 | 0.704297 | 15 | 0.7034 | 0.1619 | 0.512965 | 15 | 7.8 | 445 | -0.18 | 0.01602 |
| 06XJ-145 | 315 | 0.0639 | 0.704146 | 17 | 0.7039 | 0.1301 | 0.512810 | 7 | 6.0 | 587 | -0.34 | 0.00969 |
| 06XJ-147 | 310 | 0.1964 | 0.704536 | 14 | 0.7037 | 0.1305 | 0.512824 | 9 | 6.3 | 566 | -0.34 | 0.00903 |
| 06XJ-148 | 310 | 0.4346 | 0.705599 | 17 | 0.7037 | 0.1374 | 0.512830 | 11 | 6.1 | 580 | -0.30 | 0.01109 |
| 06XJ-153 | 314 | 0.0961 | 0.704171 | 17 | 0.7037 | 0.020 | 0.512798 | 11 | 5.8 | 606 | -0.34 | 0.00897 |
| 06XJ-154 | 314 | 0.1544 | 0.704669 | 14 | 0.7040 | 0.032 | 0.512848 | 9 | 6.3 | 564 | -0.28 | — |
| 06XJ-156 | 307 | 0.2914 | 0.705185 | 14 | 0.7039 | 0.061 | 0.512828 | 8 | 6.9 | 512 | -0.41 | 0.00699 |
| 06XJ-158 | 307 | 0.1817 | 0.704943 | 18 | 0.7041 | 0.038 | 0.512862 | 8 | 7.1 | 493 | -0.35 | 0.00918 |

| Sample | $^{176}Hf/^{177}Hf$ | 2σ | εHf(t) | $f_{Lu/Hf}$ | $T_{HfDM2}$ | △εHf(t) | $^{206}Pb/^{204}Pb$ | $^{207}Pb/^{204}Pb$ | $^{208}Pb/^{204}Pb$ | $^{206}Pb/^{204}Pbt$ | $^{207}Pb/^{204}Pbt$ | $^{208}Pb/^{204}Pbt$ |
|---|---|---|---|---|---|---|---|---|---|---|---|---|
| 06XJ-137 | 0.28307 | 7 | 15.7 | -0.73 | 325 | 1.2 | 18.408 | 15.446 | 37.963 | 17.913 | 15.420 | 37.316 |
| 06XJ-138-2 | 0.28305 | 8 | 14.0 | -0.61 | 433 | 2.3 | 18.278 | 15.459 | 37.929 | 17.907 | 15.440 | 37.489 |
| 06XJ-140 | 0.28309 | 8 | 15.7 | -0.66 | 325 | 3.8 | 18.309 | 15.485 | 38.026 | 17.914 | 15.464 | 37.634 |
| 06XJ-141 | 0.28302 | 7 | 14.3 | -0.80 | 415 | 3.1 | | | | — | — | — |
| 06XJ-143 | 0.28310 | 7 | 15.0 | -0.52 | 365 | 1.4 | 18.518 | 15.486 | 38.223 | 17.964 | 15.466 | 37.521 |
| 06XJ-145 | 0.28304 | 8 | 14.3 | -0.71 | 409 | 3.5 | 19.351 | 15.534 | 38.574 | 17.899 | 15.457 | 37.405 |
| 06XJ-147 | 0.28304 | 7 | 14.5 | -0.73 | 396 | 3.3 | 19.833 | 15.533 | 39.378 | 17.975 | 15.435 | 37.608 |
| 06XJ-148 | 0.28304 | 7 | 14.1 | -0.67 | 425 | 3.1 | | | | — | — | — |
| 06XJ-153 | 0.28305 | 7 | 14.8 | -0.73 | 378 | 4.3 | 18.364 | 15.461 | 38.043 | 17.890 | 15.436 | 37.553 |
| 06XJ-154 | — | — | — | — | — | — | 18.744 | 15.463 | 38.331 | 17.753 | 15.411 | 37.503 |
| 06XJ-156 | 0.28304 | 9 | 14.8 | -0.79 | 376 | 2.5 | 18.365 | 15.471 | 38.052 | 18.055 | 15.455 | 37.720 |
| 06XJ-158 | 0.28302 | 8 | 13.5 | -0.72 | 456 | 0.9 | 18.317 | 15.456 | 37.962 | 17.842 | 15.431 | 37.497 |

The $^{147}Sm/^{144}Nd$ and $^{143}Nd/^{144}Nd$ ratios at the present time are 0.1967 and 0.512638 for chondrite, and 0.222 and 0.51315 for depleted mantle, respectively.$\lambda = 6.54\times10^{-12}$ $a^{-1}$ ; The $^{176}Hf/^{177}Hf$ and $^{176}Lu/^{177}Hf$ ratios at the present time are 0.282772 and 0.0332 for chondrite, and 0.28325 and 0.0384 for depleted mantle.

Appendix 5. (a) Histogram of plagioclase anorthite contents for the Baogutu adakitic rocks. (b) Back-scattered electron image of plagioclase. (c-d) Large plagioclase crystals may occasionally partly or totally enclose some clinopyroxene grains in the Baogutu adakitic rocks. Plag-Plagioclase; Cpx-clinopyroxene.